WATER AND CHEMICAL CYCLING IN PERMAFROST UNDERLAIN CATCHMENTS

WATER AND CHEMICAL CYCLING IN PERMAFROST UNDERLAIN CATCHMENTS

By: Arsh Grewal, MSA. BA.

A Thesis Submitted to the School of Graduate Studies in Partial Fulfillment of the Requirements for the Degree Doctor of Philosophy

McMaster University Doctor of Philosophy (2024)

Hamilton, Ontario, Canada (School of Earth, Environment and Society)

TITLE: Water and chemical cycling in permafrost underlain catchments.

AUTHOR: Arsh Grewal

Master of Spatial Analysis (Geography and Environmental Studies)
Toronto Metropolitan University, 2019

Honours Bachelor of Arts (Geography and Environmental Studies)
Toronto Metropolitan University, 2017

SUPERVISOR: Dr. Sean K. Carey, Professor

NUMBER OF PAGES: 166

ABSTRACT

Circumpolar watersheds are experiencing rapid environmental changes due to anthropogenic warming, impacting northern ecosystems through altered precipitation regimes, shifting runoff pathways, and changes in streamflow chemistry often linked to permafrost thaw. Additionally, northern hydrology is highly seasonal, with long cold winters and short dynamic summers where hydrological and geochemical fluxes are strongly influenced by active layer thawing.

This thesis presents unique hydrometric and hydrochemical data from multiple sites in Yukon Territory, Canada, employing new methods to understand the coupled movement of water and chemicals and the influence of cold region processes on their dynamics.

This thesis utilizes synoptic sampling across seasons in Wolf Creek Research Basin to assess the role of seasonality on spatial patterns of flow and chemistry. Results show consistent spatial patterns in flow and chemistry across seasons, with increasing production of major ions and dissolved organic carbon (DOC) during high spring flows. However, chemistry covariance between sites was low, indicating asynchronous biogeochemical and hydrological processes across subcatchments.

Stream chemistry across multiple seasons and diverse catchments in the Yukon Territory was also examined, where role of catchment characteristics on stream chemistry seasonality were assessed. Results reveal significant seasonal trends in major ions and DOC concentrations, driven by active layer thaw and soil organic carbon flushing during

freshet. Catchments with steep topography and less extensive organic soils had lower average DOC concentrations but greater seasonal changes.

Lastly, this thesis focuses on water storage, mixing, and release processes in two headwater catchments with continuous permafrost. A detailed hydrometric, meteorological, and stable isotope dataset was used to characterize water age dynamics. Mixing analysis and water balance results show that runoff was mostly snow water during freshet, with limited mixing with stored water. StorAge Selection frameworks indicate that evapotranspiration (ET) is composed of the youngest water, while discharge includes a greater proportion of previously frozen water during summer events.

This research highlights the complexity of hydrological and biogeochemical processes in permafrost environments. Novel approaches and extensive seasonal sampling provide fresh insights into water and chemical cycling in cold catchments, informing our understanding of permafrost hydrology and guiding predictions on how northern catchments will respond to environmental change.

ACKNOWLEDGEMENTS

I would like to thank Sean Carey for all the support over the years and his very timely feedback on my work, which allowed me to defend when I did. Thanks for providing me the opportunity to work in cool environments (no pun intended) and sending me to many conferences so I could establish my own network. I understand most grad students don't get to see so much of the world and meet so many new people so I'm grateful for that, even if it doesn't always seem like it.

I would like to thank the committee Mike Waddington, Alemu Gonsamo, and Chris Wellen for the insightful questions, suggestions, and discussions during the defence and also over the few years. I also thank Darren Scott for taking the time to chair the defence.

Special thanks to David Barrett and Tyler de Jong for all the field assistance over the years. None of this work (especially chapter 2) would be possible without you guys.

Thanks Calvin, Aliana, and Anna for letting me vent about the most random things during beers and answering all my biogeochemistry questions. Thank you, Erin, for showing me the ropes in the field in 2020 when no one else was around, and thanks for letting me play my music 95% of the time on those long drives. I hate country music.

Thanks Team B (you know who you are) for all the support over the past 5 years, I'm grateful to be friends with you all.

PREFACE

This Ph.D. dissertation is composed of five chapters. Chapter 1 provides a literature review of the thesis topics and presents key research gaps addressed in this thesis. Chapters 2, 3, and 4 constitute the main body of the dissertation; each of these three chapters is written as a journal article for peer-review. Chapter 2 assesses the role of seasonality on spatial patterns of stream discharge and chemistry. Chapter 3 utilizes multiple years of chemistry data across ten permafrost underlain catchments to assess the role of catchment characteristics on the seasonal variability of stream chemistry. Chapter 4 uses a variety of hydrological and meteorological data to characterize water age dynamics in two catchments underlain by continuous permafrost. Chapter 5 summarizes key findings from the thesis and suggests areas of focus for future research.

DECLARATION OF ACADEMIC ACHIEVEMENT

The main body of this thesis is contained in Chapters 2, 3, and 4 which each represent a journal article. Chapter 2 has been published. Chapter 3 is in preparation for submission to Journal of Hydrology. Chapter 4 is in preparation for submission to Water Resources Research.

Chapter 2:

Grewal A, Carey SK. 2024. Synoptic sampling reveals spatial stability in flow and chemistry patterns despite large seasonal variability in a subarctic mountain catchment. *Hydrological Processes* **38** (2): 1–11 DOI: 10.1002/hyp.15080

Arsh Grewal (dissertation author) is the main researcher, first author and corresponding author of this paper. Arsh Grewal collected and processed the field data. Winter data was collected by David Barrett and Tyler de Jong. Data analysis and writing was undertaken by Arsh Grewal with insight, guidance, and editing from Dr. Sean K. Carey.

Chapter 3:

Grewal, A., Nicholls, E.M., and Carey, S.K. (2024). The role of catchment characteristics and active layer thaw on seasonal stream chemistry across ten permafrost underlain catchments. In preparation for Journal of Hydrology.

Arsh Grewal (dissertation author) is the main researcher, first and corresponding author of this paper. Arsh Grewal collected the majority of the data. Data analysis and writing was undertaken by Arsh Grewal with insight, guidance, and editing from Dr. Sean K. Carey. Erin M. Nicholls collected 2018 and 2019 data, and established sampling protocols at several sites.

Chapter 4:

Grewal, A., Harman C.J., and Carey, S.K. (2023). Water storage and release in permafrost underlain catchments: Insights from end-member mixing and water age characterization. In preparation for Water Resources Research.

Arsh Grewal (dissertation author) is the main researcher, first and corresponding author of this paper. Arsh Grewal collected the majority of the data. Data analysis and writing was undertaken by Arsh Grewal with insight, guidance, and editing from Dr. Sean K. Carey and Dr. Ciaran J. Harman.

TABLE OF CONTENTS

CHAPTER 1

1.1 INTRODUCTION

High latitude regions are disproportionately warming due to polar amplification (Cohen et al., 2014). This warming is resulting in widespread permafrost thaw, shrub expansion, and changes in the timing, quantity, and phase of precipitation (Sillmann et al., 2013; McCrystall et al., 2021). Precipitation is projected to increase in northern catchments, transitioning from snowfall to rainfall, with greater frequency of heavy precipitation events (Sillmann et al., 2013; Kusunoki et al., 2015; McCrystall et al., 2021), potentially leading to greater summer runoff. Permafrost thaw is expected to increase groundwater-driven baseflow, and subsequently alter stream chemistry (Frey and McClelland, 2009; Walvoord and Kurylyk, 2016). Enhanced groundwater contributions to streams is expected to lead to an increase in major ion export, while changes in dissolved organic carbon (DOC) export caused by permafrost thaw are expected to be site specific (Frey and McClelland, 2009; Tank et al., 2023). For example, permafrost extent has been positively correlated with DOC export in Alaska, yet negatively correlated in West Siberia (Frey and McClelland, 2009). This contradiction is likely due to much deeper peat soils (~1-5 m) present in West Siberia but not in Alaska (Sheng et al., 2004; Frey and McClelland, 2009). Despite circumpolar regions rapidly changing and having highly complex biophysical processes, monitoring in the north has been steadily declining (Laudon et al., 2017). Vast distances, difficult and expensive logistics combined with the marginalized socioeconomic status of northern communities has created a situation where

our understanding of hydrological processes in these vulnerable systems is insufficient to appropriately mitigate future environmental challenges.

Seasonality plays a critical role in the rate, timing, and magnitude of hydrological and chemical transport in cold mountain catchments (Carey and Woo, 1999, 2000; Carey, 2003). Large volumes of water and solutes are exported in a span of a few weeks during snowmelt, and studies suggest that much of the water released during freshet is typically older water present in the basin before the onset of melt (Carey and Quinton, 2004). However, when ice rich frozen ground is present, there is limited infiltration and mixing with older water in storage (Metcalfe and Buttle, 2001). The onset of active layer thaw in spring results in the emergence of deeper flow paths, altering storage-discharge relationships and solute export (McNamara et al., 1998; Frey and McClelland, 2009; Hinzman et al., 2020). High latitude catchments typically have considerable seasonal differences solute concentrations. Typically, DOC concentrations are high during freshet and begin to decline shortly afterwards, whereas the opposite is true for major ion concentrations that peak in the fall (Carey, 2003; Shatilla et al., 2023). The mechanism most often cited for the seasonal nature of stream chemistry is that as the active layer expands following snowmelt, the water table descends from the surface through progressively deep soil horizons that shift from organic to mineral rich (Carey and Woo, 2001). In the spring when the saturated zone is confined to the near surface, organic material is rapidly flushed from shallow layers. As the active layer thickens, water tables decline into mineral horizons increasing the prevalence of weathering ions in solution (MacLean et al., 1999; Carey, 2003; Shatilla and Carey, 2019; Shatilla et al., 2023).

In addition to highly seasonal hydrological processes, cold mountain catchments have considerable spatial heterogeneity in biophysical characteristics due to aspect, slope, and elevation control on energy receipt, leading to distinct seasonal processes across space. For example (Carey and Woo, 1999) found ice rich permafrost-underlain north facing slopes promote greater lateral runoff than seasonally frozen slopes which promoted greater infiltration. Furthermore, there can be months-long differences in the onset of snowmelt due to energy and thermal differences across aspect and altitude. How the rate, timing and magnitude of fluxes in cold mountain regions combine to affect chemical export is largely unknown. Several studies have utilized high resolution synoptic sampling to elucidate runoff and chemical processes in more temperate environments (Abbott et al., 2018; Birkel et al., 2021; Gu et al., 2021) and even permafrost regions (Shogren et al., 2021a). However, the majority of high-resolution sampling in cold regions is restricted to the summer season (post freshet to first snow). How spatial patterns of runoff and chemical processes differ between spring, summer, and winter seasons in cold mountain catchments is not well understood.

The overall objective of this thesis is to understand how seasonal ground freeze thaw, discharge, and catchment characteristics alter storage and release, hydrological connectivity, and biogeochemical processes. In **Chapter 2**, mixing analysis and metrics such as spatial stability, subcatchment leverage, and temporal synchrony are used to quantify patterns in flow and chemistry in Wolf Creek Research Basin, Yukon. The aim of this chapter is to understand how runoff and chemical production across spatial scales are integrated and change seasonally in a heterogeneous subarctic mountain catchment.

Seasonal patterns in stream chemistry are ubiquitous in high latitude watersheds. Seasonal active layer thaw which leads to the activation of the deeper ion rich mineral layer, has been attributed as an important driver for explaining the seasonal trends in stream chemistry (MacLean et al., 1999; Carey, 2003). However, discharge is often negatively correlated with major ion concentrations and positively correlated with DOC concentrations. Additionally, discharge is typically much greater during freshet than later in the season leading to higher DOC concentrations and lower major ion concentrations, as stream chemistry often reflects the chemistry of the soil profile (Godsey et al., 2009; Stewart et al., 2022). Thus, both discharge and seasonal active layer thaw may be driving an increase in major ion and a decrease in DOC concentrations post freshet. The influence of seasonal active layer thaw and discharge on stream chemistry has not yet been disentangled in permafrost underlain catchments. Shifts in concentration-discharge (CQ) relationships can be used to identify changes in biogeochemical processes other than discharge. For example, Fork *et al.* (2020) examined changes in residuals of water flux versus DOC to infer changes in supply in terrestrial pools of DOC. Changes in CQ relationships have also been used to identify seasonal biogeochemical processes. For example, MacLean et al. (1999) compared CQ patterns between seasons in a permafrost underlain Alaskan catchment, however the authors classified each season and thus had to make the assumption that the transition between seasons is a discreet phenomenon. Although several potential drivers have been identified for seasonal patterns of chemistry in cold catchments, the relative importance of each factor and how it is influenced by permafrost extent and other catchment characteristics remains unresolved.

The objective of **Chapter 3** is to disentangle the influence of seasonal active layer thaw and discharge on DOC and major ion concentrations in permafrost underlain catchments. Generalized additive models are utilized, where a spline day of year term is added to the traditional concentration-discharge model to account for additional non-linear seasonal drivers of stream chemistry. Additionally, the role of permafrost extent on the strength of the seasonal trends of stream chemistry is examined.

The presence of permafrost and ground ice can have large influence on catchment storage, mixing, and transit times (Woo and Winter, 1993; Carey and Woo, 1999; Metcalfe and Buttle, 2001). The transit time of water (the time it takes water to leave the catchment after entering via precipitation or snowmelt) provides information about storage and flow pathways though a single descriptor (McGuire and McDonnell, 2006). However, much of our understanding of catchment storage, mixing, and release processes comes from hydrograph separation techniques. For example, Metcalfe and Buttle (2001) found melt intensity and ground ice content to be a major driver in the proportion of event water in the hydrograph. Transit time distributions can provide important information about storage and flow pathways. However, limited work has been conducted on characterizing water transit times in high latitude catchments, largely due to logistical challenges and high data requirements of traditional transit time modelling techniques. The introduction of more novel techniques such as StorAge (SAS) selection framework, can provide a more detailed representation of transit times in catchments and does not require consistent tracer sampling (Botter et al., 2011; Van Der Velde et al., 2012; Harman, 2015). Unlike traditional transit time distributions, the SAS framework

constrains transit times with the water balance. As such, the age distribution of fluxes is constrained by the amount of water that entered a catchment at a particular time (i.e. water cannot be 4 days old if it did not rain 4 days ago). Frameworks that characterize age dynamics of water in detail can provide critical information on transport processes in rapidly changing permafrost environments. Our understanding of the influence of seasonal processes on the age dynamics of water, and by extension water storage and release processes remains limited in high latitude systems. In **Chapter 4**, water age is characterized using a robust hydrometric dataset in two headwater catchments underlain with continuous permafrost to assess the role of seasonality on catchment storage, mixing, and release of water. End member mixing (snow and rain) is linked to the water balance to split different components of the water balance into rain and snow, and we use the SAS framework to simulate age dynamics of storage, evapotranspiration (ET), and streamflow. This chapter provides new insights on water storage, mixing, and release in rapidly warming cold high-latitude watersheds.

CHAPTER 2

SYNOPTIC SAMPLING REVEALS SPATIAL STABILITY IN FLOW AND CHEMISTRY PATTERNS DESPITE LARGE SEASIONAL VARIABILITY IN A SUBARCTIC MOUNTAIN CATCHMENT

ABSTRACT

Seasonality plays a critical role in cold mountain regions as variation in air temperature, ground thermal status, and precipitation phase alter the rate, timing and magnitude of hydrological and chemical transport. Additionally, cold mountain catchments can have highly variable topography, geology, permafrost, and landcover, which intrinsically add to this irregularity. Understanding how external and internal variability act to control mass fluxes requires sampling at a high spatial resolution over time, which rarely occurs in cold remote regions. In this work, we conduct five snapshot sampling surveys across 34 subcatchments during the ice-free period in Wolf Creek Research Basin (a mesoscale montane subarctic catchment) and two additional winter surveys across a subset of sites to assess the drivers of variability in stream chemistry and discharge. We sampled for specific conductance (SpC), major ions, and dissolved organic carbon (DOC) and used statistical metrics and Bayesian mixing analysis to quantify patterns of flow and chemistry across space and time. Our results indicate patterns in both flow and chemistry remain largely consistent across seasons for all solutes. However, there was weaker correlation of chemistry between sites, suggesting asynchronous behaviour within the catchment. There was evidence of increasing production of ions and

DOC along the stream network during high spring flows but not during low flows. Although concentrations and flows exhibit high seasonality in subarctic mountains, this seasonal variability does not alter spatial patterns that arise from highly variable catchment characteristics.

2.1 INTRODUCTION

Seasonality plays a critical role in the rate, timing and magnitude of hydrological and chemical transport in in subarctic mountain catchments (Carey and Woo, 2001b; Petrone et al., 2006; Boucher and Carey, 2010; Shatilla et al., 2023). During the spring, large volumes of water are delivered as snowmelt, yet infiltration is limited by the presence of frozen ground and shallow flow pathways rapidly deliver water to streams (Carey and Woo, 2000; Carey and Quinton, 2004). As thaw depth progresses during summer, there is an activation of deeper flow pathways and increasing soil water storage, altering rainfall-runoff response (Carey and Woo, 2000; Carey and Quinton, 2004) and chemistry (Boucher and Carey, 2010; Shatilla and Carey, 2019). This seasonal cycle leads to increasing non-linear storage-discharge relations as thaw progresses (Hinzman et al., 2020, 2022). In high latitude mountains, there exists a high degree of spatial heterogeneity in biophysical characteristics due to aspect and altitude-controlled energy receipt. This leads to distinct seasonal processes across space and challenges the application of simple two-dimensional concepts of runoff generation at larger scales. For example, Carey and Woo (1999) found north facing slopes to promote greater lateral runoff due to the presence of permafrost and ice-rich soils, whereas slopes with seasonal

permafrost promoted infiltration and groundwater recharge. Furthermore, there are ecosystem shifts with altitude whose vegetation assemblages strongly impact the partitioning of vertical and lateral fluxes (Nicholls and Carey, 2021; Nicholls et al., 2023). Linking our understanding seasonal controls with spatial heterogeneity to understand catchment scale runoff and chemical processes remains limited, largely due to the logistical challenges associated with sampling at a high spatial and temporal resolution in remote northern regions (Shogren et al., 2021a).

Several studies have attempted to bridge this gap between temporal and spatial resolution through synoptic snapshot sampling surveys. Birkel *et al.* (2020) utilized snapshot sampling and mixing analysis to assess hydrological contributions from headwaters in a large tropical catchment, finding an increase in proportional water contribution to the outlet in the dry season. Abbott *et al.* (2018) developed an analytical framework to quantify spatiotemporal variability of solutes across catchment scales. The authors introduced the concept of spatial stability, which measures the degree to which patterns in chemistry are reshuffled across space over time. Subcatchment synchrony was also introduced, which is a measure of covariance observed between sites. The authors observed high seasonal stability along with lower synchrony in solute concentrations in a mesoscale agricultural catchment in France. Gu *et al.* (2021) used similar methods in an agricultural catchment and found increased stability of spatial chemical patterns during high flows. Shogren *et al.* (2021a) assessed spatial stability of several solutes across multiple arctic watersheds over multiple years and found mixed results across watersheds and solutes. The authors found high stability of DOC in some catchments but not others,

and these differences were attributed to greater spatial shifts between early and late season thaw. A similar study by Shogren *et al.* (2019) assessed spatial patterns of solute concentrations in 3 arctic watersheds and the authors found higher spatial persistence in the more alpine catchment than the flatter lake dominated catchment. Significant work has been done to quantify the characteristics of spatial patterns of stream chemistry across catchments, however, the drivers of stability and synchrony of chemical patterns remains unresolved.

The objective of this research is to understand how runoff and chemical production across spatial scales are integrated and change seasonally in a heterogenous subarctic mountain catchment in Yukon Territory, Canada. We use grab samples from synoptic surveys during different flow conditions across 34 sites to assess the drivers of variability in hydrochemistry and longitudinal hydrological connectivity (defined as water contribution of subcatchments to the outlet) across space and time. We use mixing analysis along with metrics such as spatial stability, subcatchment leverage, and temporal synchrony to quantify patterns of flow and chemistry. Results from this work highlight the importance of spatial heterogeneity and processes at smaller scales and their relative influence in controlling patterns observed at the catchment outlet through time.

2.2 DATA AND METHODS

2.2.1 Study Area

Wolf Creek Research Basin (WCRB) is a 169 km^2 subarctic mountain watershed located southeast of Whitehorse, Yukon, Canada (60° 36′ N, 134° 57′ W) on the

traditional territories of the Kwanlin Dün, Ta'an Kwäch'än Council, and Carcross/Tagish First Nations (Figure 2.1). The elevation ranges from 720 – 2090 m.a.s.l. The watershed is largely covered by snow from mid-October to mid-May, with higher elevation areas covered with snow until late June. WCRB is underlain with discontinuous to sporadic permafrost at high elevations and on north-facing slopes (Bonnaventure et al., 2012). The catchment has a strong elevation-based ecotone gradient where much of the lowlands are covered with coniferous forests (25%), mid-elevation areas are dominated by shrub cover (46%), and high-elevation areas consists mainly of bare earth, grasses, mosses, and lichens (26%). Climate normals (1981-2010) reported at the Whitehorse airport shows the average air temperature at -0.1 °C and annual precipitation of 262.3 mm (161 mm as rain). Due to the large elevation gradient at WCRB, average temperatures in the headwater regions are several degrees lower, and precipitation volumes are larger, often exceeding 400 mm per year. Further details on physiography and geology of WCRB basin are described by Rasouli *et al.* (2014, 2019). WCRB has four subcatchments with hydrometric instrumentation; Coal Lake (CL), Granger Creek (GC), Buckbrush Creek (BB), and Wetland Outlet (WLO), with areas of 68 km^2, 7.25 km^2, 5.43 km^2, and 7.25 km^2 respectively. The CL stations is located at the outlet of a ~1 km^2 lake with a maximum depth of 12 m. GC and BB are alpine headwater catchments, covered with primarily with bare rock, tundra vegetation (mosses, lichens, and grasses), and shrubs. WLO is a wetland influenced headwater catchment, primarily covered with shrubs and partially fed by an alpine wetland. Detailed information on subcatchment characteristics can be found in Table A1.

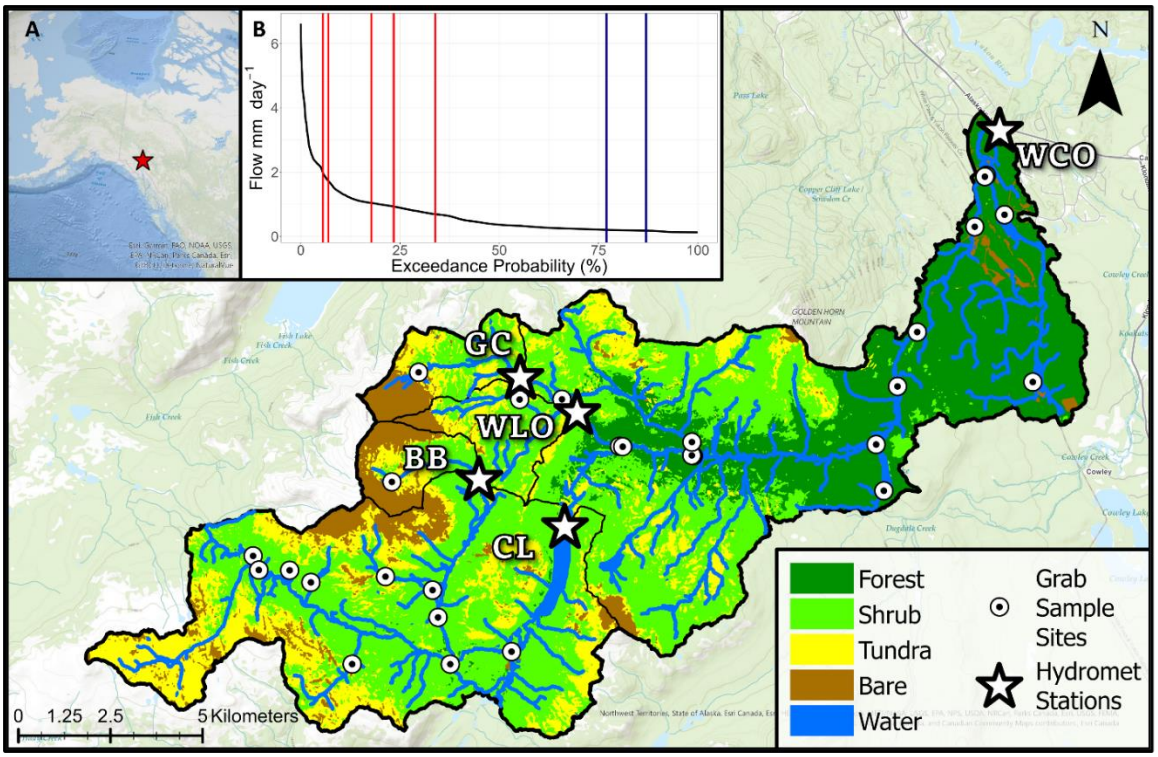

Figure 2.1. Land cover map of WCRB generated from Sentinel-2 imagery. Inset A shows the location of WCRB at the regional scale. Inset B is the flow duration curve of the outlet of WCRB from October 2019-October 2022. Winter flows were included in the creation of flow duration curves. Red vertical lines represent the flow state of each of the five ice-free snapshot surveys. From high flow to low flow the surveys were conducted on; July 4 2022, June 29 2021, August 3 2020, August 26, 2019, and September 15 2019. Blue vertical lines represent the two winter surveys conducted in the winter of 2021 and 2022.

2.2.2 Subcatchment characterization

All catchments were delineated using a 1 m DEM generated from a Lidar survey conducted in 2018. All topographic variables including aspect, slope, and mean elevation were calculated in SAGA GIS. Land cover was determined through a supervised classification using a resampled DEM and Sentinel-2 multiband imagery via the *RStoolbox* package in R (Leutner et al., 2023). An overall accuracy of 92% was achieved.

2.2.3 Continuous Data

Continuous flow data was collected at Wolf Creek outlet and all four subcatchments from late Spring to early Fall in 2021 and 2022. Continuous flow and SpC was collected at the outlet and two subcatchments (GC and CL) of WCRB from early Spring to late Fall from 2019 to 2022. Continuous Specific Conductance (SpC) data was collected through the use of HOBO U24 Freshwater Conductivity loggers. Level data was collected using Solinst leveloggers and compensated with proximal Solinst barologgers. Level data was collected at 15-minute intervals. Rating curves were generated from spot flow measurements and used to model continuous discharge.

2.2.4 Grab Sample Collection

Five open water snapshot sampling campaigns were conducted across 34 sites from late freshet to mid Fall from 2020-2022. The surveys represent a notable range of flow conditions (flow exceedance 6% to 34%; Figure 2.1b). All surveys were conducted within 56 hours, with the two high flow surveys completed within 36 hours. No precipitation occurred during any of the surveys. Each site was sampled for $\delta^{2}H$, $\delta^{18}O$, SpC, Dissolved Organic Carbon (DOC), and major ions. Two additional surveys were conducted over the winter at a subset of the sites at low flow conditions (flow exceedance 77% and 87%; Figure 2.1b), which were selected based on accessibility and availability of water under ice. Isotope samples were collected in 20 mL scintillation vials and stored in room temperature. Major ions and DOC samples were filtered through a 0.45 µm syringe filter, collected in 60 mL HDPE bottle (DOC samples stored in a brown HDPE bottle). After collection, major ion and DOC samples were kept cool and dark in the field

via icepacks and immediately refrigerated at 4 °C for storage. SpC was determined in the field using a multiparameter sonde (YSI proPlus or proDSS).

$\delta^{2}H$ and $\delta^{18}O$ analysis was conducted at multiple laboratories (University of Saskatchewan McDonnell Isotope Lab, University of Toronto Scarborough WATER Group, and Toronto Metropolitan University Watershed Hydrology Research Group). All analysis was conducted on a Los Gatos Research Liquid Water Isotope Analyzer. All labs used similar procedures with 6-8 injections scaled relative to Vienna Standard Mean Ocean Water (VSMOW) and Standard Light Antarctic Precipitation (SLAP) scale. Major ions analysis was conducted by using ion chromatography (DIONEX ICS 6000, IonPac AS18 and CS12A analytical columns), all major ion analysis was conducted by the University of Waterloo Biogeochemistry Lab. All DOC analysis was conducted on Shimadzu TOC-5000A Total Organic Carbon Analyzer by the Biogeochemical Analytical Service Laboratory in the University of Alberta. The US Environmental Protection Agency Test Method 415.1 was followed (EPA, 1974).

2.2.5 Quantifying Spatial Patterns of Longitudinal Hydrologic Connectivity

We determined variance thresholds in concentrations using the pruned exact linear time (PELT) method (Killick et al., 2012). This technique takes a sequence of ordered values (concentrations ordered by subcatchment area in this case), and clusters the data into statistically distinct variances (Killick et al., 2012; Abbott et al., 2018). Variance threshold for each solute in WCRB was determined using the ‘changepoint’ package in R (Killick et al., 2022; R Core Team, 2022). All catchments below the threshold area were

included in a Bayesian mixing model to assess the stability of hydrological contributions of various subcatchments of WCRB. Bayesian mixing models are implicitly probabilistic and allow for direct accounting of uncertainties (Parnell et al., 2013). We applied k-means clustering analysis using mean chemistry and catchment characteristics as inputs to create three distinct groups that serve as the sources for the mixing model similar to Birkel *et al.* (2020). We used MixSIAR, a flexible Bayesian tracer mixing model framework in R (Stock et al., 2018) to quantify hydrological contributions of each group as determined from the PELT method and k-means clustering analysis. δ^2H and DOC were used as tracers and raw values of tracers were used (instead of using means and standard deviations) to account for covarying tracers (Stock et al., 2018). δ^2H and $\delta^{18}O$ were largely covarying and therefore not ideal for mixing analysis so δ^2H and DOC were used. MixSIAR was run separately for each of the five surveys to detect changes in proportion of contribution from each group between surveys. Methods similar to Hooper (2003) were used to determine the tracers which would be ideal for the mixing analysis. Residuals between the projected tracers via principal component analysis (PCA) and the original tracer values were analyzed for structure. The tracers with the smallest residuals and random structure in the residuals were selected. Due to the limited number of surveys, we utilized chemistry data taken from WCO from our long-term sampling campaign at our gauged stations to determine the ideal tracer set for the mixing analysis. The mixing analysis was run for each survey to identify changes in relative contributions from each group to the outlet. Although this analysis primarily focuses on the ice-free season, MixSIAR was also applied with winter surveys included (Appendix A.2).

To determine the degree of similarity between the posterior distribution of surveys for each source, pairwise overlap was used via the 'overlapping' package in R (Pastore and Calcagnì, 2019; Pastore et al., 2022). Overlap provides the integral of the overlapping area of two distributions. A value of one indicates the two distributions are identical and a value of zero signifies the two distributions do not overlap at all. The overlap function describes the total area of the intersection of two distributions. The mean overlap value for each of the three groups was determined from the mean of pairwise overlaps of the MixSIAR posterior distributions for all survey combinations. Sites that were not present in all seven surveys were removed to enable better comparison of contributions between surveys. MixSIAR analysis with the addition of winter surveys is further discussed in Appendix A.2.

2.2.6 Quantifying Spatiotemporal Variability of Solutes

2.2.6.1 Leverage

Subcatchment leverage (Equation 1) is a spatially distributed mass balance for a particular solute (Abbott et al., 2018).

$$Leverage = (C_S - C_O) \times \frac{A_S}{A_O} \times \frac{Q_S}{Q_O} \quad (1)$$

Where the concentration of a solute at a subcatchment (C_S) and the outlet (C_O) is multiplied by the subcatchment:outlet ratio of; area (A) and specific discharge (Q). The mean leverage of all subcatchments for a particular survey can be used to determine whether there is net production or removal of a solute (Abbott et al., 2018; Shogren et al., 2021a). Negative mean leverage represents increased production of solute along the

stream network. Leverages were normalized to the outlet concentration and reported as a percent. The assumption of uniform specific discharge is sometimes made to quantify leverage (Abbott et al., 2018; Shogren et al., 2021a), however this assumption is rarely satisfied, particularly in heterogeneous catchments (Karlsen et al., 2016b; Floriancic et al., 2019). We utilize flows from continuous hydrometric stations, spot discharge measurements, mixing model outputs, and the assumption of uniform specific discharge of proximal subcatchments with similar catchment characteristics to estimate discharge at all sample sites to better estimate subcatchment leverage (See Appendix A.3 for details).

2.2.6.2 Spatial Stability and Synchrony

Spatial stability and temporal synchrony were determined as the pairwise Spearman rank correlation between sites (temporal synchrony) and surveys (spatial stability) as described in Gu et al. (2021). High spatial stability indicates the spatial patterns of chemistry remain consistent between surveys and is determined by the median pairwise Spearman's rank correlation (rcorr) of concentrations between a particular survey C_t to four other surveys ($C_{t_i \neq t}$; Equation 2). For example, a correlation test was conducted for concentrations for survey 1 $C_{t=1}$ against the concentrations of survey 2 $C_{t=2}$ and so on until survey 5 $C_{t=5}$. This results in 4 correlations for survey 1$C_{t=1}$, the median of these values is the the spatial stability value for a particular survey (survey 1 in this example). The spatial coefficient of variation (CV) of a particular solute for each survey was determined by equation 3, where *t* is the sampling date, σ is the standard deviation, and μ is the mean of concentrations for all sites at a particular date.

$$Spatial\ Stability = median\left[rcorr\left(C_t, C_{t_i \neq t}\right)\right] \quad (2)$$

$$Spatial\ CV = \frac{\sigma_t}{\mu_t} \quad (3)$$

Temporal synchrony quantifies correlation between sites among sampling events (Gu et al., 2021). High synchrony represents strong positive correlation between subcatchments over time. Synchrony is determined by the median pairwise rcorr of concentrations C_s between a particular site to all other 33 subcatchments ($C_{s_i \neq s}$; Equation 4). The median was used instead of the mean to limit large values from skewing the results. Although out of phase hydrological signals can be considered synchronous (Seybold et al., 2022), our metric of synchrony does not consider such signals to be synchronous. Thus, this synchrony in this case is defined by the correlation of signals, since phase is difficult to estimate with discrete data. The temporal coefficient of variation (CV) of a particular solute for each site was determined by equation 5, where *s* is a sampling site, σ is the standard deviation, and μ is the mean of concentrations for all dates at a particular site.

$$Temporal\ Synchrony = median\left[rcorr(C_s, C_{s_i \neq s})\right] \quad (4)$$

$$Temporal\ CV = \frac{\sigma_s}{\mu_s} \quad (5)$$

Although spatial stability and synchrony are related, they are distinct measures of spatio-temporal catchment processes. Stability is a measure of the consistency of spatial patterns and synchrony is a measure of the correlation between subcatchments. Thus, catchments may have uncorrelated patterns but may display high stability if the

differences in mean concentrations/flows is greater than the range of concentrations/flows. The opposite can also be true if the patterns in flow/chemistry are highly correlated between subcatchments but the mean values in flow/chemistry are similar, in this scenario the catchment may have high synchrony but low stability (See figure A1 for a visual depiction).

2.3 RESULTS

2.3.1 Discharge

Specific discharge for 2020 to 2022 displayed characteristic patterns for northern mountain catchments (Figure 2.2). All catchments had peak flows during mid-June in both years, reflecting the snowmelt driven freshet signal which typically began at the beginning of June and ended early July. BB was missing spring data for 2021 and WLO station was missing spring data for both 2021 and 2022 due to access limitations. No reliable flow data exists for WLO and BB for 2020. 2022 was the wettest year out of the three years included in this study, with an average flow of 1.67 mm d^{-1} at WCO, whereas 2020 was the driest year with an average flow of 1 mm d^{-1} at WCO. The higher elevation headwater stations typically had higher specific discharge than the larger catchments (WCO and CL). WCO had the lowest specific discharge over the study period (1.23 mm d^{-1}), whereas GC had the highest mean specific discharge (2.97 mm d^{-1}). GC had the highest peak flow for all three years, with peak annual flow ranging from ~25 to ~27 mm d^{-1}. Results from a snow pillow located within WCRB show 2022 with the highest peak SWE at (326 mm), followed by 2021 (322 mm), and 2020 (202 mm). Peak flow during

summer events was typically lower than freshet at all sites. Event peaks from rainfall were much smaller than snowmelt at all sites. The streams were gauged until early October, as formation of channel ice begins to alter stage-discharge relationships.

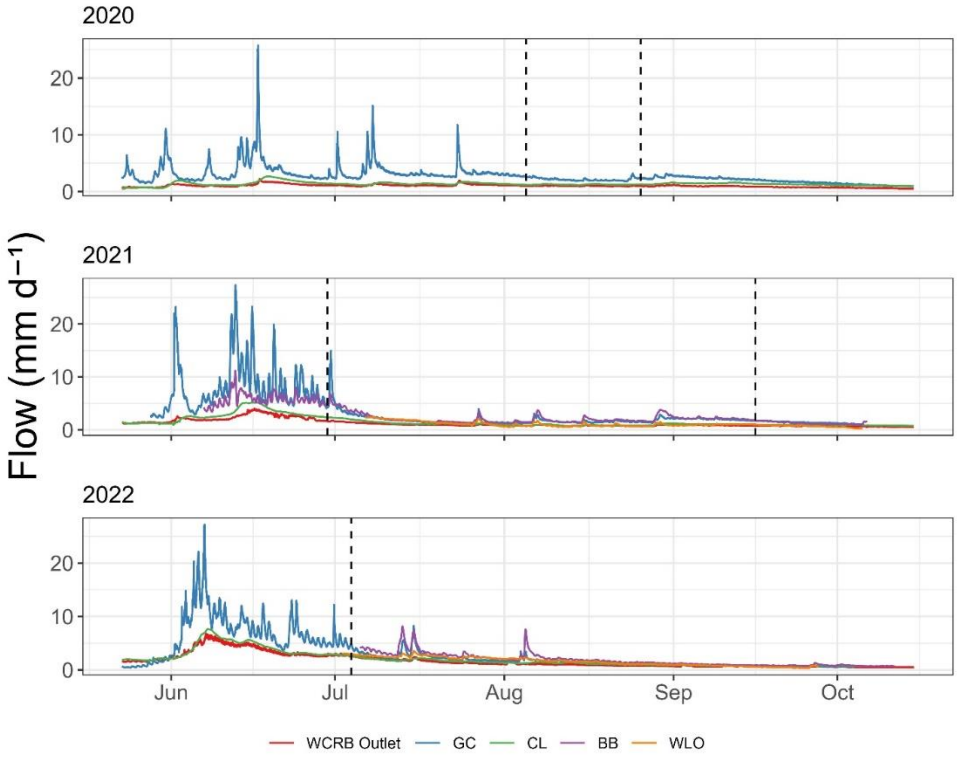

Figure 2.2. Hydrographs for all gauged sites in WCRB for 2020, 2021, and 2022. Colours represent gauged sites. Flows are in mm d^{-1}. Vertical lines indicate the timing of the five surveys.

2.3.2 Spatial Patterns of Longitudinal Hydrologic Connectivity

Changepoint analysis showed variance collapse at ~16 km^2 for DOC, and ~23 km^2 for SpC and major ions (Figure 2.3). Variability was relatively low between the ice-free surveys, indicating the variance collapse is constant throughout this period for the solutes analyzed, and was not affected by the time of sampling during the ice-free period. 22 of the 33 sites had an area less than 23 km^2 and were included in K-means cluster analysis.

K-means results for the 22 sites indicated the presence of three distinct groups that we labelled as: i) Alpine Catchments (n=7-9), ii) Lowland Lakes and Wetlands (n=4), and iii) Wetland Influenced Catchments (n=9). We did not sample two of the Alpine Catchment sites that were in the 3 August 2020 survey. Alpine Catchments are defined as having a high slope (18.33 deg) and low concentrations in all solutes. Wetland Influenced Catchments are flatter (13.75 deg) and have a lower mean elevation than alpine headwater catchments (1678 m.a.s.l to 1465 m.a.s.l). Lowland Lakes and Wetlands have a lower slope (6.88 deg) and elevation (956 m.a.s.l) than the other groups. Lowland Lakes and Wetlands had the highest mean concentrations for all solutes including DOC (13.7 ± 4.77 [SD] mg L^{-1}), Wetland Influenced Catchments had lower mean DOC concentrations (3.49 ± 2.31 [SD] mg L^{-1}), and Alpine Headwater Catchments had the lowest mean DOC concentrations (1.71 ± 0.5 [SD] mg L^{-1}). Detailed information about catchment characteristics along with the mean and standard deviation of solute concentrations for each survey is presented in Appendix A (Table A1; Table A2).

Although the mixing results in this case cannot be used to explicitly quantify the total contribution to the outlet due to high uncertainties in posterior distributions, they were used as a tool to detect changes in relative contributions of sources to the outlet. This is because we are not capturing variability from the source waters. Mixing results showed the highest contributions from Alpine Catchments, Wetland influenced Catchments, and Lowland Lakes and Wetlands, respectively, for all surveys (Figure 2.4). There was a high degree of similarity in source contributions, with a mean pairwise overlap of 92% for Lowland Lakes and Wetland, a mean pairwise overlap of 92% for

Wetland Influenced Catchments, and a mean pairwise overlap of 94% for Alpine Catchments (Table 2.1). Including the two winter surveys showed similar mean overlap values to the ice-free surveys for Alpine catchments but resulted in lower values for Wetland Influenced Catchments and Lowland Lakes and Catchments (Table A5). This is likely due to poor separation of sources in the mixing space due to a smaller sample size.

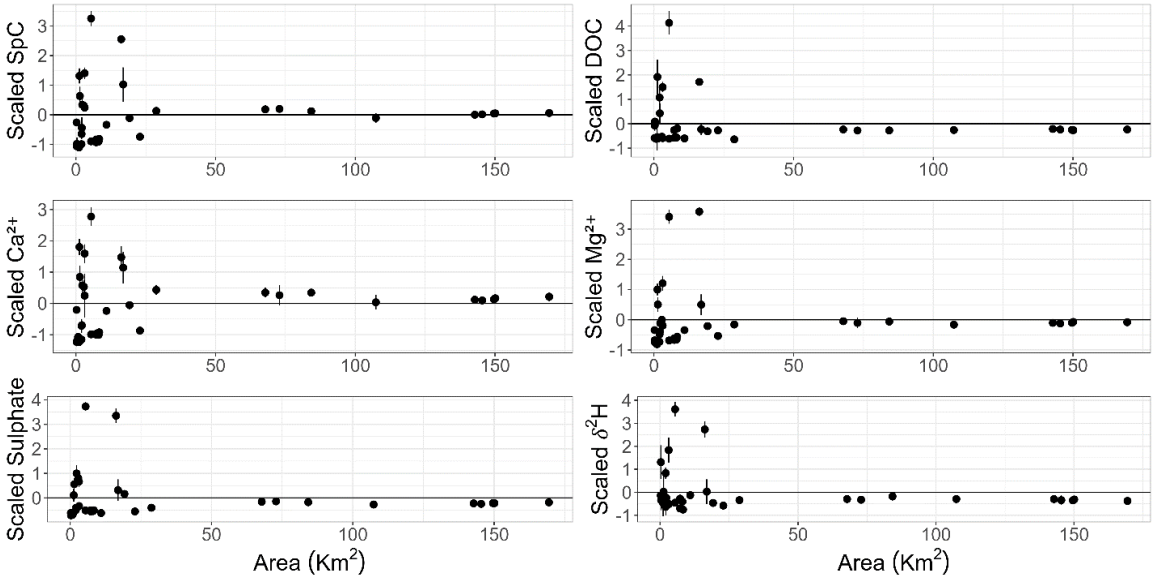

Figure 2.3. Standardized concentrations vs subcatchment area. Error bars indicate standard deviations of the standardized concentrations for solutes.

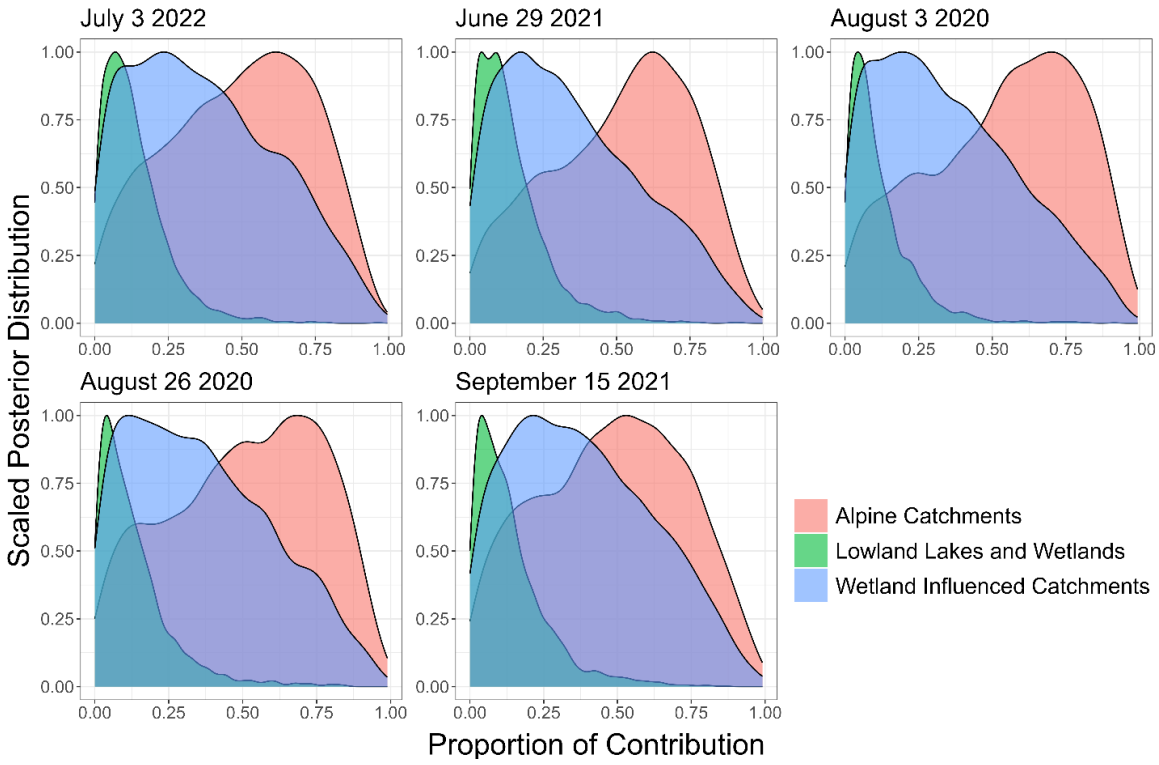

Figure 2.4 MixSIAR results showing the proportion of contribution of each group as a density. δ^2H and DOC were used as tracers. x-axis represents proportion of contribution to the outlet and y-axis is the rescaled (0-1) density of probability.

Table 2.1. Overlap results from all possible survey combinations for each of the three sources. An overlap of 1 indicates the distributions are the same. Overlap is a measure of the intersecting area of two probability distributions.

Survey Combinations	Alpine Catchments	Lowland Lakes and Wetlands	Wetland Influenced Catchments
3 Jul 2022 - 29 Jun 2021	0.96	0.97	0.97
3 Jul 2022 - 3 Aug 2020	0.94	0.86	0.86
3 Jul 2022 - 26 Aug 2020	0.96	0.92	0.92
3 Jul 2022 - 15 Sept 2021	0.94	0.94	0.94
29 Jun 2021 - 3 Aug 2020	0.92	0.88	0.88
29 Jun 2021 - 26 Aug 2020	0.95	0.93	0.93
29 Jun 2021 - 15 Sept 2021	0.96	0.94	0.94
3 Aug 2020 - 26 Aug 2020	0.95	0.93	0.93
3 Aug 2020 - 15 Sept 2021	0.89	0.90	0.90

26 Aug 2020 – 15 Sept 2021	0.93	0.96	0.96
Mean	0.94	0.92	0.92

2.3.3 Spatiotemporal Variability of Solutes

2.3.3.1 Leverage

Concentrations fell below the analytical detection limits for several solutes at several sites. Thus, subcatchment leverage was only calculated for DOC, SpC, Ca^{2+}, Mg^{2+}, and Sulphate. Student's t-test indicated significant ($p \leq 0.05$) negative mean leverage values for all solutes except Sulphate for the 4 July 2022 survey (Figure 2.5). SpC and DOC also had significant negative mean leverage values for the 29 June 2021 survey. Sulphate showed a significant negative mean leverage value for the 26 August 2021 survey.

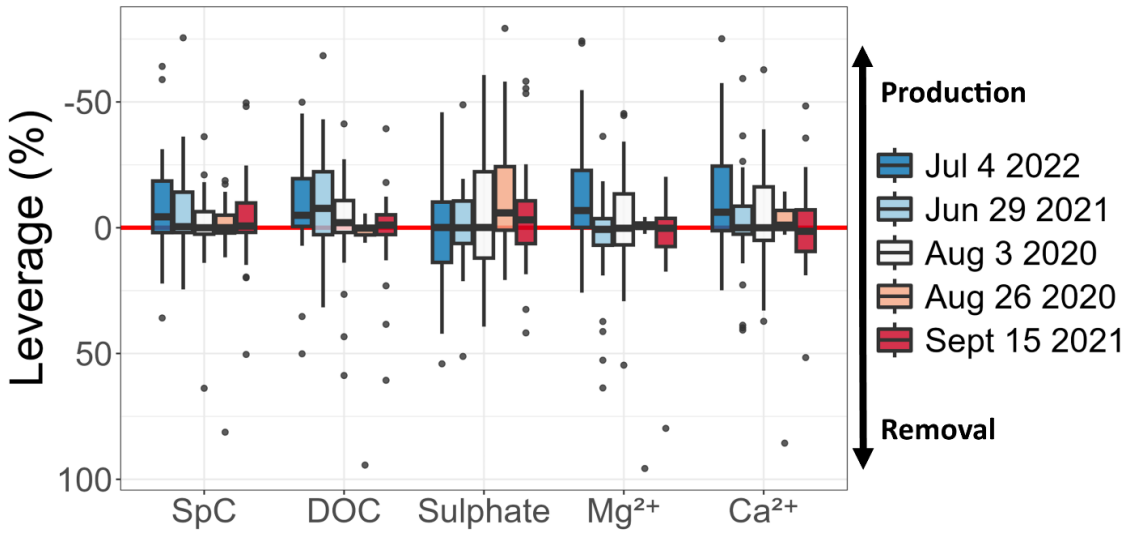

Figure 2.5 Boxplots showing distribution of subcatchment leverage of each survey. Leverage is normalized to the outlet and represented as a percent. Surveys are ordered from high flow (dark blue) to low flow (dark red) at the outlet of WCRB.

2.3.3.2 Spatial Stability and Synchrony

Spatial stability was higher than 0.89 for all five solutes, and spatial CV ranged from 0.56 (Ca^{2+}) to 1.5 (Sulphate; Figure 2.6). The standard deviation of spatial stability and spatial CV was generally low (<0.05 and <0.12 respectively) for all solutes (Table A3). These results indicate there was high variation in chemistry across space and spatial patterns remained relatively stable for all solutes during the ice-free period in WCRB. Temporal synchrony of water quality parameters ranged from 0.38 (DOC) to 0.70 (Mg^{2+}), indicating the DOC concentrations were largely asynchronous between sites over time compared to other solutes (Table A4). The degree of temporal synchrony varied significantly between sites, as the standard deviation of temporal synchrony was relatively high for all solutes, ranging from 0.12 (Mg^{2+}) to 0.27 (SpC). These results show that variability in concentrations was much greater across space than across time, as temporal CV was lower than spatial CV for all solutes. Results after including the two winter surveys lead to no significant differences in synchrony or stability (Appendix A.2).

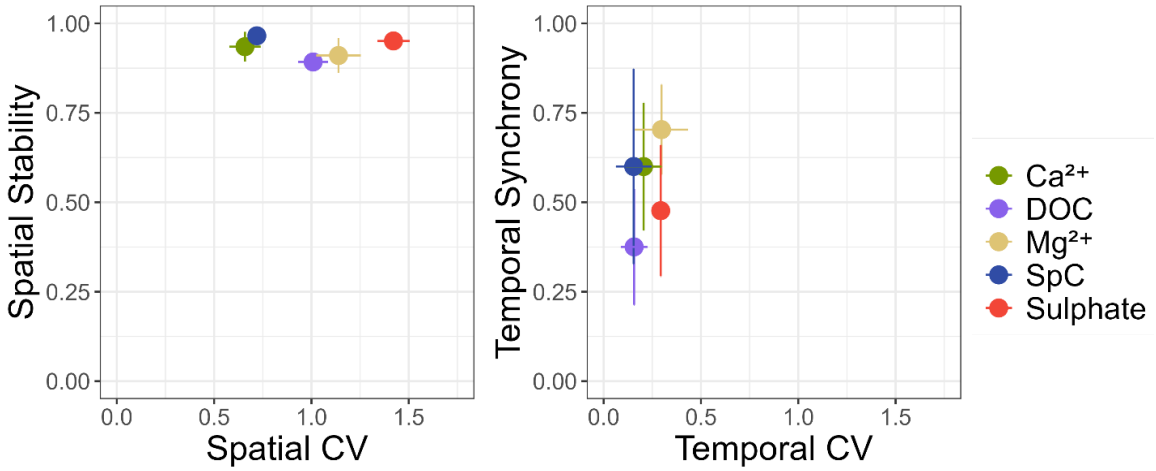

Figure 2.6. Left panel shows Spatial Stability plotted against Spatial CV. Right panel

shows Temporal Synchrony plotted against Temporal CV. Error bars represent standard deviation.

2.4 DISCUSSION

Although seasonality is well documented as a major driver of hydrological and hydrochemical variability in high latitude alpine catchments (Carey and Woo, 1999; Wang et al., 2009; Shatilla and Carey, 2019; Shogren et al., 2021b), there remains limited understanding of how seasonality affects spatial patterns across watersheds. The scales at which runoff and chemical signatures change, and how these vary with time, is critical to understand intra-catchment hydrological and chemical functions of larger watersheds. Tools such as subcatchment leverage, mixing analysis, and metrics of spatial stability and temporal synchrony aid our understanding of the processes that drive hydrochemical patterns across space.

2.4.1 Drivers of Spatial Patterns of Longitudinal Hydrological Connectivity

Although streamflow exhibited strong seasonality in WCRB, our results suggest the relative proportion of flow contributions of various subcatchments was not notably influenced by seasonal processes. Mixing results showed a high consistency in spatial patterns of flow throughout the ice-free period in WCRB and the addition of the two winter surveys in the analysis did not significantly alter our interpretation. However, it is important to note that peak freshet and summer event flows were not captured in this analysis. Our results are in contrast to Birkel *et al.* (2020) who found seasonality and catchment wetness to have a significant influence on source contributions in a

heterogeneous tropical catchment and that more proximal catchments to the outlet were an important source of tracer during wetter months. In WCRB, the Lowland Lakes and Wetland catchments, which were the more proximal catchments to the outlet, consistently had the lowest tracer contributions. This discrepancy can potentially be explained by the size difference between the two catchments, as the area of the tropical catchment (~1,500 km^2) in Birkel *et al.* (2020) was an order of magnitude greater than WCRB. At this larger scale, atmospheric forcing may be much more variable, leading to more intra-catchment variability in discharge and by extension chemistry. The high seasonality in tracer contributions could also be explained by the lowland subcatchment in the tropical basin exceeding a threshold during the wet season leading to significantly greater connectivity, whereas the headwater catchments in the basin may not have to exceed the same thresholds. In WCRB, the lack of seasonality in relative flow contributions implies the thresholds for the lowland subcatchments were either similar to the headwater catchments or were never exceeded during our surveys. Our results also somewhat contradict the early work of Wood *et al.* (1988), where they showed higher variability in hydrological response for smaller subcatchments. The higher spatial heterogeneity along with the exclusion of summer events and peak freshet flows in our analysis can explain the high spatial stability of flow contributions.

2.4.2 Drivers of Spatial Hydrochemical Patterns

Our results are largely in agreement with Gu *et al.* (2021) and Abbott *et al.* (2018), who found high stability but lower synchrony for a majority of the more conservatively behaving solutes. High spatial CV relative to temporal CV results in

greater spatial stability (Gu et al., 2021). The average spatial CV in WCRB was significantly higher than what was reported in Gu *et al.* (2021) and Abbott *et al.* (2018). A higher spatial CV indicates greater chemical heterogeneity, as high heterogeneity in catchment characteristics can lead to high variability in flow and chemistry (Floriancic et al., 2019). In WCRB, spatial CV is significantly greater than temporal CV (Figure 2.6), indicating greater variability in concentrations across space than time. Heterogeneity in catchment characteristics had a greater influence on spatial stability of flow and chemistry than seasonality in WCRB. This was evidenced by the high spatial stability, greater spatial CV than temporal CV, and high overlap in MixSIAR posterior distributions (Table 2.1) between surveys. When spatial heterogeneity is high and seasonal differences in chemistry are less than differences between subcatchments across space, we may observe a scenario similar to the one shown in Figure A1 (bottom left). In this case, the high variability in subcatchment characteristics leads to high variability in mean solute concentrations and low covariance between sites, as both the magnitude and timing of flows and chemistry are influenced by catchment characteristics (Ali et al., 2012; Karlsen et al., 2016a, 2016b; Birch et al., 2021; Shogren et al., 2021b), but seasonal differences are relatively muted. The high variability across space could lead to differences in mean concentrations which are too great to be overcome by seasonal processes, thus maintaining rank order of concentrations across seasons.

Our results are in contrast Shogren *et al.* (2019) who analyzed stability for DOC in three arctic catchments and found lower stability in the more heterogeneous lake catchment. However, the lake catchment was relatively flat and homogeneous in terms of

topography compared to WCRB. Additionally, DOC production (inferred from mean subcatchment leverage) along with connectivity of headwater lakes may be highly seasonal in a low gradient lake dominated catchment, indicating that seasonal processes were more important to DOC concentrations than heterogeneity in this basin. Whether the net increases in DOC concentrations were driven by greater terrestrial inputs on an increase in stream production could not be determined via subcatchment leverage. Studies have shown changes in connectivity and dominant flow paths to be an important driver in DOC export in high latitude systems (Shatilla and Carey, 2019; Spence et al., 2019). WCRB has multiple small lakes, including the 1 km^2 central Lake (CL). However, preliminary analysis has shown that CL is well mixed and is not particularly productive in terms of DOC (unpublished data).

Temporal synchrony was much lower in WCRB compared to stability and had much higher standard deviation for all solutes. This indicates that subcatchments generally had low covariance with each other and the degree of covariance varied strongly between sites. This can partly be explained by the low number of surveys (n=5) in WCRB. However, high heterogeneity in chemistry and specific discharge suggests that the subcatchments have distinct storage-discharge relationships. Catchment characteristics can often be a first order driver in CQ relationships (Musolff et al., 2015; Creed et al., 2015; Carroll et al., 2018). Thus, high heterogeneity in catchment characteristics will lead to high heterogeneity in chemical response across flows, leading to less correlation between subcatchments. Mountain subcatchments typically store larger amounts of snow and generally release it later as snowmelt than lowland catchments due

to elevational differences in air temperature. Additionally, catchments underlain with permafrost typically have higher linearity in storage-discharge relationships (Lyon and Destouni, 2010; Hinzman et al., 2020). Thus, permafrost underlain headwater catchments in WCRB will have distinct responses to external forcing (i.e. precipitation) compared to lowland areas, and lead to greater asynchrony.

2.4.3 Drivers of Subcatchment Leverage

Leverage results indicate that an increase net production occurs for DOC and major ions along the stream network during late freshet high flows. DOC concentrations have shown to rapidly decline in GC during late freshet as organic matter can quickly be flushed from soils and lead to source limited behaviour of DOC in the headwaters of these systems (Shatilla and Carey, 2019). The presences of greater available organic matter in soils in lowland areas may lead to greater lateral transport of DOC during late freshet. Weathering derived ions typically display source limited behaviour in the headwaters of WCRB during late freshet, leading to lower concentrations during high flows. All ions displayed greater production in the spring but not during lower flows. Sulphate was the only exception to this, as it showed greater production in lower flows but not during high flows. Greater microbial activity later in the season may result in high sulphate concentrations via sulfide oxidation (Van Stempvoort et al., 2023). Another explanation for this is a greater contribution from sulfide rich groundwater downstream which has negligible influence during high flows. Sulfide rich groundwater has been shown to be a dominate source of sulphate in Yukon streams (Van Stempvoort et al., 2023).

2.4.4 Future Directions and Limitations

All of our surveys were conducted during baseflow or during late freshet and the study only utilized seven surveys (two winter surveys are discussed in Appendix A.2). This captures a range of wetness conditions in WCRB, with flow exceedance ranging from 5% to 85% at WCO. However, the flows at WCO can be several times that amount. Quantifying how summer event flow and peak freshet alters spatial patterns is a natural next step to advance our understanding on spatial patterns of flows and chemistry in these regions.

Although this study was conducted at the seasonal scale, there is a need to evaluate spatial patterns at shorter temporal scales (i.e. event and diel scale). This is becoming increasingly viable with the advent of lower-cost high frequency hydrochemical monitoring instruments. However, very few catchments (particularly in high latitude regions) have a dense nested monitoring network with high resolution flow and chemistry measurements. Considering that high latitude catchments are warming fast with strong changes to the rate, timing, and magnitude of all hydrological processes along with decreases in frozen ground, these results present an interesting case, suggesting that there is some inherent stability and resilience in hydrochemical response to changing flows, yet altered flow paths and emergent processes may eventually override previous system states.

2.5. CONCLUSIONS

By utilizing snapshot synoptic sampling along with new metrics such as stability, synchrony, and leverage, we disentangled the relative influence of seasonality and heterogeneity on subcatchment variability in flow and chemistry in a cold, mountainous catchment. Additionally, we conducted snapshot sampling during the winter, which is rarely done in these regions due to various logistical challenges. Our results showed high similarity in relative flow contributions, and high spatial stability for stream chemistry across seasons and flow conditions. We found higher intrinsic variability across space than across time, and high spatial stability in both flow and chemistry. These results indicate the highly seasonal patterns in flow and chemistry do little to alter the spatial patterns of flow and chemistry in Wolf Creek. The high spatial variability suggests that catchment biophysical heterogeneity is critical in understanding and characterizing flows and chemistry in Wolf Creek and presumably catchments in similar environments. This study highlights the role of synoptic sampling in revealing new insights on catchment function and integrated responses. Considering that northern mountains such as Wolf Creek are experiencing rapid change from global heating (e.g. Leipe and Carey, 2021), focussing process research at headwater scales where variability is large remains critical.

ACKNOWLEDGEMENTS

We would like to thank David Barrett and Tyler de Jong for field assistance and winter data collection. We thank Lauren Bourke, Aliana Fristensky, Anna Grunsky, Erin Nicholls, Calvin Newbery, and Ryan Benson for field assistance. We would like to thank Global Water Futures and National Science and Engineering Council of Canada for

providing financial support for this project. We acknowledge the continued support of the Water Resources Branch, Government of Yukon, for the operation of Wolf Creek Research Basin. We also thank our two anonymous reviewers for their feedback, which greatly improved the clarity of this paper.

DATA AVAILABILITY

Data is available upon request.

CHAPTER 3

THE ROLE OF CATCHMENT CHARACTERISTICS AND ACTIVE LAYER THAW ON SEASONAL STREAM CHEMISTRY ACROSS TEN PERMAFROST UNDERLAIN CATCHMENTS

ABSTRACT

High latitude catchments are rapidly warming, leading to altered precipitation regimes, widespread permafrost degradation and observed shifts in stream chemistry for major arctic rivers. At headwater scales, stream discharge and chemistry are seasonally variable, and the relative influence of catchment characteristics, climate and active layer thaw on this seasonality has been poorly addressed. To provide new insight into mechanisms driving changes in streamflow chemistry withing permafrost watersheds, we measured discharge and sampled major ion and dissolved organic carbon (DOC) concentrations across ten permafrost underlain catchments. We incorporated concentration-discharge relationships within generalized additive models to resolve the influence of discharge and seasonal active layer thaw on stream chemistry and identify the role of watershed characteristics on the magnitude and seasonality of solute concentrations. Results indicate both major ions and DOC were highly seasonal across all catchments, with DOC declining and major ion concentration increasing post freshet after accounting for seasonal variations in discharge. Seasonal variability in major ions concentrations were primarily driven by seasonal active layer thaw, whereas seasonality for DOC by flushing of soil organic carbon during freshet. Although major ion

concentrations were likely driven by surficial geology, greater permafrost extent led to greater relative seasonality in major ion concentrations. Mountainous catchments, which generally have higher specific discharge and a thin organic layer, had lower DOC concentrations but greater relative seasonality in DOC. Our results highlight the important role of catchment characteristics play on shaping both the seasonal variations and magnitude of solute concentrations in permafrost underlain watersheds.

3.1 INTRODUCTION

High latitude catchments are experiencing rapid warming due to polar amplification (Cohen et al., 2014), and are highly sensitive as thawing permafrost and altered precipitation regimes strongly affect their hydrological and biogeochemical cycles (Walvoord and Kurylyk, 2016; McKenzie et al., 2021). Frozen ground and permafrost act as impeding layers to water movement, restricting flow and separating supra, intra and sub-permafrost aquifers (Woo 1986, Carey and Woo, 1999; Quinton and Marsh, 1999; McKenzie *et al.*, 2021). Where present, permafrost enhances runoff by restricting deep percolation and encouraging flow through more hydraulically conductive near-surface pathways (Steer and Woo, 1983; Carey and Woo, 1999). Permafrost degradation, which includes deepening of the seasonal thawed zone (termed the active layer) and wholesale loss, also influences stream chemistry. Dissolved solutes are expected to increase due to greater contact with mineral surfaces as flow pathways lengthen. Vast stores of frozen organic material are thawing, yet dissolved organic carbon (DOC) concentration projections are uncertain due to potential increased adsorption and in-stream processes

(Frey and McClelland, 2009; Tank et al., 2023). Studies from large arctic rivers show increase exports of weathering products such as Ca, Mg and DOC (Tank et al., 2016), yet results are varied across circumpolar regions (Tank et al., 2023), and long-term studies are limited to extremely large rivers that cross multiple ecozones and permafrost extent, confounding interpretation.

Seasonal active layer thaw along with seasonal precipitation (phase and magnitude) play a critical role in runoff and solute export processes (Woo and Winter, 1993; McNamara *et al.*, 1998). During spring, large volumes of meltwater infiltrate the soil yet are restricted to near surface layers that are often organic in nature, exporting large volumes of water rich with dissolved organic matter (DOM; Woo and Steer, 1986; MacLean *et al.*, 1999; Carey, 2003; Shatilla *et al.*, 2023). As the frost front descends, mineral layers thaw and catchment storage increases resulting in greater concentrations of weathering solutes and reduced dissolved organic matter (Carey, 2003; Petrone *et al.*, 2006). Concentrations of weathering derived solutes generally increase from spring to fall, whereas DOM concentrations typically decrease (MacLean et al., 1999; Carey, 2003; Frey and Smith, 2005). The position of the water table with respect to different soil horizons in the active layer has largely been used to explain seasonal patterns of dissolved solutes in permafrost literature. Permafrost extent is also identified as a key driver of hydrological and biogeochemical processes. For example, Petrone *et al.* (2006) and Webster *et al.* (2022) attributed lower yield of NO_3^- and higher yield of fluorescent dissolved organic matter (fDOM) to greater permafrost extent in Alaska. Webster *et al.*

(2022) found evidence of greater seasonality of NO_3^- in high permafrost catchments compared to catchments with lower permafrost extent.

Changes in hydrological connectivity across the landscape can alter streamflow chemistry and solute export (Creed et al., 2015; Zhi et al., 2019; Li et al., 2024). During wet periods, water tables are near the surface in highly conductive organic soils and areas distal to the stream can be connected. During drier conditions, flow is primarily through deeper mineral pathways and landscape connectivity declines (Zhi et al., 2019; Stewart et al., 2022). The presence and disposition of permafrost strongly affects the interaction between solute sources, water pathways and the stream network. Direct observation of these interactions is particularly challenging in northern watersheds as permafrost extent is often difficult to assess and logistics are typically challenging. Concentration-Discharge (CQ) relations have increasingly been used to characterize flow-solute coupling to infer catchment processes (Hall, 1971; Godsey et al., 2009; Wymore et al., 2023). By comparing the log-log slope between the two, it is possible to characterize whether a solute is transport limited (positive slope) or source limited (negative slope). Other metrics such as CV_C/CV_Q ratios can be used to determine whether a solute is chemostatic or chemodynamic even when there is no clear directionality (Thompson et al., 2011; Musolff et al., 2015). Positive/negative slopes can indicate spatial and vertical heterogeneity within a catchment, whereas slopes close to zero can indicate homogeneity in vertical and spatial distribution of solute stores or dominance of instream biogeochemical processes (Creed et al., 2015).

Both solute concentration and streamflow are highly seasonal in permafrost catchments, making it difficult to ascertain the relative influence of different factors driving seasonal solute dynamics. For example, low major ion concentrations during snowmelt occurs due to greater connectivity within the mineral poor organic layer. This increased connectivity occurs due to high water tables often present during snowmelt in mountain catchments, and/or the lack of activation of deep mineral rich flowpaths due to frozen ground. The potential influence of these two factors influencing solute dynamics in cold regions are rarely addressed. However, shifts in CQ relationships can be used to detect changes in solute export driven by processes other than discharge, such as changes in the internal structure of the catchment (i.e. ground freeze-thaw) or in the quantity/mobility of solute stores. For example, Fork *et al.* (2020) examined changes in residuals of water flux versus DOC to infer changes in supply in terrestrial pools of DOC. Biagi *et al.* (2022) and Ross *et al.* (2022) utilized generalized additive models (GAMs), which are flexible models that allow for the addition of spline terms to model non-linear behaviour, to quantify changes in CQ relationships over time in agricultural environments. CQ relationships are often highly seasonal in northern catchments, particularly between snowmelt and summer periods (MacLean et al., 1999; Shatilla et al., 2023). At the event scale, Shogren *et al.* (2021) found both seasonality and landscape drivers to be important for the relations between DOC, NO_3^- and flow. The authors determined that landscape drivers were more important to CQ relationships than seasonality for DOC and NO_3^- in Arctic catchments post freshet.

In cold catchments, seasonal patterns of freeze-thaw, discharge, and solute stores have been identified as drivers for seasonal variability in stream chemistry (Boyer et al., 1997; MacLean et al., 1999; Carey, 2003; Petrone et al., 2006). However, the relative importance of each factor and how it is influenced by permafrost extent and other catchment characteristics remains unresolved. To address this, we characterize CQ relationships using discrete major ion and DOC data across ten permafrost influenced catchments. We utilize GAMs with an additional spline Day Of Year (sDOY) term to the traditional CQ approach to test two hypotheses:

1. As active layer thaws post freshet, concentrations will increase for major ions and decrease for DOC at all sites (irrespective of seasonality in discharge), due to seasonal ground thaw induced activation of deeper mineral rich flow paths.
2. Seasonal changes in concentrations will be the largest in catchments with greater permafrost extent (irrespective of seasonality in discharge) for both major ions and DOC due to greater connectivity of subpermafrost water to streams in catchments with lower permafrost extent.

Testing these hypotheses will provide new insights on the role of catchment characteristics and permafrost extent on the seasonality major ion and DOC export. By disentangling different drivers of seasonal solute export in northern environments, we can make more informed predictions of stream biogeochemistry in a rapidly changing north.

3.2 DATA AND METHODS

3.2.1 Study Area

Our study consists of 10 catchments with areas ranging from ~5 Km^2 to ~170 km^2, all located in Yukon Territory, Canada. Four of the catchments are part of the Wolf Creek Research Basin (WCRB; 60° 36' N, 134° 57' W; Figure 3.1), with Wolf Creek outlet (WCO) being the largest. Coal Lake (CL) is a ~70 km^2 subcatchment of WCRB that has a ~ 1 Km^2 mixed lake near the outlet. Two alpine headwater subcatchments, Granger Creek (GC) and Buckbrush Creek (BB), have areas less than 10 Km^2. WCO and CL are underlain with sporadic permafrost (Lewkowicz and Ednie, 2004; 10%-50%). Low elevation areas of WCRB consist of primarily coniferous forests, whereas high elevation areas consist of shrub taiga and alpine tundra vegetation. High elevation subcatchments (BB, GC) are estimated to be underlain by discontinuous permafrost (Lewkowicz and Ednie, 2004; 50 %-90 %) and are typically colder and wetter than low elevation areas of WCRB. Near surface geology consists of mostly sedimentary rocks such as limestone, sandstone, and siltstone capped by a till mantle and glaciofluvial/glaciolacustrine deposits (Rasouli et al., 2014). WCRB is part of the traditional territories of the Kwanlin Dün, Ta'an Kwach'an Council, and Carcross/Tagish First Nations. More detailed description of WCRB can be found in Rasouli *et al.* (2014, 2019). Climate normals (1981-2010) reported near WCRB at the Whitehorse airport shows the average air temperature at -0.1 °C and annual precipitation of 262.3 mm (161 mm as rain). Due to the large elevation gradient at WCRB, average temperatures in the headwater regions are several degrees lower, and precipitation volumes are larger, often exceeding 400 mm per year.

Six of our study catchments are a part of the Tombstone Waters Observatory (TWO; Figure 3.2), which is part of the traditional territory of Tr'ondëk Hwëch'in First Nation. All TWO catchments have areas less than 35 km^2 and intersect the Dempster highway, a critical north-south road, and are named after the kilometer marker. The six catchments are called Km 44, Km 71, Km 99, Km 104, Km 175, and Km 185. Km 44 (64° 19' N, 138° 31' W) and Km 71 (64° 31' N, 138° 8' W) are the most mountainous catchments, with a high average slope. Km 44 primarily consists of bare earth whereas Km 71 is primarily overlain with shrub cover. Km 99 and Km 104 (64° 41' N, 138° 28' W) contain no trees and are overlain by a thick layer of peat except for the high elevation areas with steep slopes. Km 104 is largely flat, whereas Km 99 has mountainous uplands with more mineral soils. Km 175 (65° 12' N, 138° 26' W) and Km 185 (65° 16' N, 138° 18' W) are primarily covered by open coniferous forests and are a part of the Ogilvie Mountain range. Although there is some discrepancy between various permafrost mapping products in regard to permafrost extent, the general consensus is that the WCRB sites have less permafrost than the TWO sites (Bonnaventure et al., 2012; Obu et al., 2019; Ran et al., 2022; Yukon Geological Survey, 2023). Surficial geology maps in TWO indicate that Km 71, Km 99, Km 104, and Km 185 are underlain with continuous permafrost (>90%), whereas Km 44 is underlain with sporadic permafrost and Km 175 is underlain with discontinuous permafrost (Thomas and Rampton, 1982a, 1982b; Yukon Geological Survey, 2023). Climate normals (1981-2010) from Dawson City, the nearest Environment Canada weather station to TWO, reports annual precipitation of 324 mm of

which 201 mm is rainfall. The annual air temperature is -4.1 ℃. However, local climate can be quite variable amongst study catchments in TWO.

Bedrock geology across TWO is diverse (Colpron, 2022). Km 44 is primarily underlain by thick-bedded quartz arenite. Km 71 is primarily underlain by two geological units; the first is described as dark grey argillite, slate, and phyllite, commonly graphitic and the second is described as black graptolitic shale and black chert. Km 99 and 104 are underlain by black shale and chert, dolomitic siltstone, calcareous shale, and buff platy limestone in the low-lying areas. The uplands of the basins are underlain by interbedded maroon and apple-green slate, siltstone, and sandstone. Km 175 and 185 are primarily underlain by grey and buff-weathering dolostone, limestone, black graptolitic shale,

minor chert shale, siltstone, and sandstone.

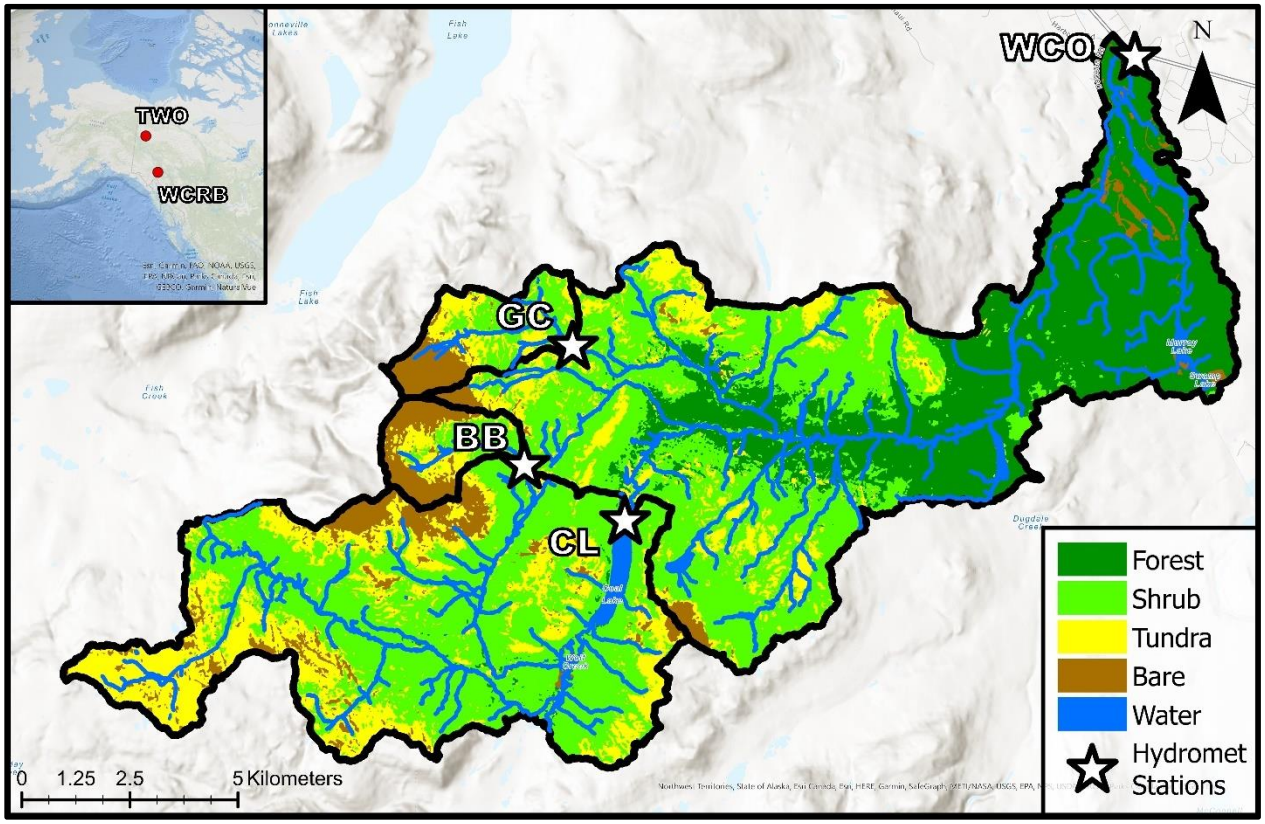

Figure 3.1. Study area map of Wolf Creek Research Basin and its subcatchments.

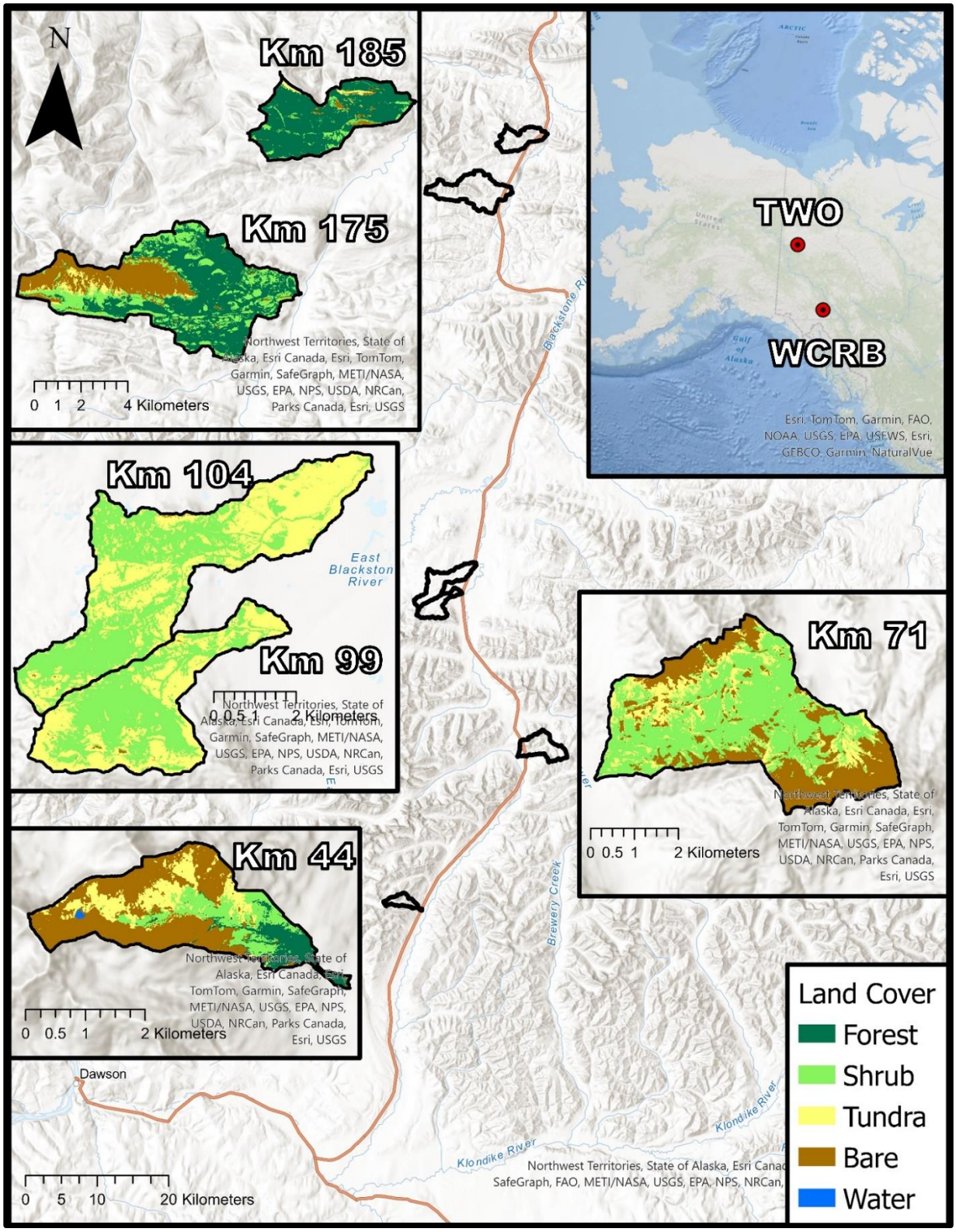

Figure 3.2. Study area map of all Tombstone Waters Observatory catchments.

3.2.2 Catchment characterization

All TWO catchments were delineated using the 2 m resolution ArcticDEM product, whereas WCRB catchments were delineated using a 1-m DEM generated from a 2018 LiDAR scan. All topographic parameters including aspect, slope, and mean elevation were calculated in SAGA GIS. Land cover was determined through a supervised classification using a resampled DEM and Sentinel-2 multiband imagery via the *RStoolbox* package in R (Leutner et al., 2023). Catchment characteristics are reported in Table 3.1.

Table 3.1. Table of catchment characteristics for WCRB and TWO catchments.

Site	Area (Km^2)	Forest (%)	Shrub (%)	Tundra (%)	Bare (%)	Water (%)	Elevation (m.a.s.l)	Slope (deg)	Permafrost
Km 44	5.54	12.4	17.2	18.5	51.6	0.3	1413.9	26.7	Sporadic
Km 71	16.48	0.0	48.4	17.7	33.9	0.00	1429.5	25.1	Continuous
Km 99	10.97	0.0	50.7	48.3	0.9	0.1	1401.5	10.9	Continuous
Km 104	17.77	0.0	50	49.6	0.4	0	1251.2	6.8	Continuous
Km 175	35.86	48.2	25.6	3.4	22.8	0	1003.2	19.2	Discontinuous
Km 185	14.68	84.3	8.8	3.5	3.4	0	916.2	18.9	Continuous
BB	5.43	0	29.7	23	46.8	0	1678	17.5	Discontinuous
GC	7.25	0	40.5	31.5	26.6	0	1618.7	11.1	Discontinuous
CL	67.78	0.4	55.4	29.7	11.8	2.7	1464	15.4	Sporadic
WCO	169.39	25.3	46	19.3	7.5	1.9	1303.7	12.3	Sporadic

3.2.3 Stream chemistry

Grab samples for major ions and DOC were collected across flow states at all sites over multiple years. Major ions and DOC samples were filtered through a 0.45 µm syringe filter and collected in 60 mL HDPE bottle (DOC samples stored in a brown HDPE

bottle). After collection, samples were kept cool and dark in the field via icepacks and immediately refrigerated at 4 °C for storage. Specific conductance (SpC) was determined in the field using a multiparameter sonde (YSI proPlus or proDSS). Only one year of samples were included for Km 104. The number of observations varied among sites and ranged from 24 (SpC at CL) to 92 (major ions at WCO). The number of samples for each solute and site can be found in table B1.

Major ions analysis was conducted via ion chromatography (DIONEX ICS 6000, IonPac AS18 and CS12A analytical columns) at the University of Waterloo Biogeochemistry Lab. All DOC analysis was conducted on Shimadzu TOC-5000A Total Organic Carbon Analyzer by the Biogeochemical Analytical Service Laboratory in the University of Alberta. The US Environmental Protection Agency Test Method 415.1 was followed (EPA, 1974). Out of all the ions measured, only Ca, Mg, and Sulphate had concentrations consistently over the detection limit, and were the only major ions considered for analysis. Continuous SpC was measured using HOBO Conductivity loggers. The loggers were calibrated in post using the YSI ProDSS handheld multiparameter sonde.

3.2.4 Runoff

All ten catchments were instrumented with Solinst level loggers to determine continuous volumetric flow rate via stage-discharge relationships. Flow measurements were generally conducted in association with a chemistry grab sample. In the event that samples were collected without a flow measurement, we used discharge determined from

stage-discharge relationship and continuous level loggers. The majority of the catchments had very low or zero discharge over the winter and often have channel ice which makes winter stage-discharge relationships highly uncertain and as such there was limited winter data available. Additionally, discharge measurements during freshet for BB were limited due to logistical access constraints during the snowmelt period. Discharge data is available from 2017-2022 at the WCRB sites, and from 2019-2022 at the TWO sites. Km 104 was instrumented in late 2021 and only had data from 2022.

3.2.5 Generalized Additive Models

Generalized Additive Models (GAMs) extend traditional linear models by allowing the addition of terms that are a sum of smooth functions (Hastie and Tibshirani, 1986). The additional terms can be linear or non-linear spline terms, and the flexibility of the spline terms can be set by the user to prevent overfitting. In this study, we use GAMs to extend the traditional concentration-discharge models by adding day of year as a spline term to the linear CQ model.

$$log(C) = b * log(Q) + log(a) + sDOY \quad (1)$$

Where DOY is the day of year of the sample, Q is discharge, C is the concentration of the solute, and b and a are constant coefficients. This equation can also be expressed:

$$C = e^{s(DOY)} a Q^b \quad (2)$$

GAMs provide the effective degrees of freedom (edf) for the spline term, and provide p-values for both the sDOY term and the log-log slope. The standard error for the spline term can also be extracted from the model, however the standard error is not constant. In this case, standard error for the sDOY term may be higher during freshet than mid summer due to high interannual difference in discharge. The mean standard error for sDOY can be used to determine the average uncertainty in the seasonality of a model. The range of the sDOY fit can be used to quantify the degree of seasonality in a CQ model, where a greater sDOY range means greater relative change in concentrations across seasons at a constant discharge.

We fit a GAMs model for all five reported solutes across all ten sites, where each model was fit using the restricted maximum likelihood (REML) estimation. The mgcv package in R was used for all analyses involving GAMs (Wood, 2023). GAMs provides a partial effect plot, which is the measure of the influence a particular term has on the model. We extracted the *b* term, the R^2 value, sDOY range, p-values for both the *b* term and the sDOY term, and the mean sDOY standard deviation from each model.

The presence of heterogeneity in sources within the catchment and changes in connection to these sources due to ground thaw will be indicated by statistical significance in both the log-log slope and the sDOY term. A non-significant log-log slope with significant seasonality suggests other processes (i.e. in stream biogeochemical processes) are driving seasonality. A greater sDOY range in catchments with greater permafrost extent will support the second hypothesis, suggesting a greater relative change

in concentrations due to ground thaw. Other factors, such as greater stratification of solute sources within the soil profile, may also influence sDOY range.

3.2.6 Coefficient of Variation Ratios

Ratios of coefficient of variation of concentrations (CV_C) and of runoff (CV_Q) were used to quantify chemodynamic behaviour for solutes even when there was no directionality with runoff (Thompson et al., 2011; Musolff et al., 2015). We calculated CV_C:CV_Q for all solutes at all sites and the CV ratios were plotted against the log-log term as shown in Equation 1 and 2. CV ratios can be a useful tool to broadly compare chemodynamic behaviour across catchments and solutes, particularly in situations where multiple distinct drivers influence stream chemistry.

3.3. RESULTS

3.3.1. Discharge and Concentrations across basins

We determined the median of specific discharge estimates of grab samples from each site as opposed to the mean to account for missed sampling at extreme low and high flows at certain sites. Median specific discharge was the greatest at Km 44 and Km 71 (2.2 mm d^{-1} and 2.03 mm d^{-1} respectively). The lowest median specific discharge occurred at Km 99, WCO, and Km 104 (0.57 mm d^{-1}, 0.64 mm d^{-1}, and 0.65 mm d^{-1} respectively). Of note, Km 44 and 71 were adjacent sites and had the highest average slopes (most mountainous), whereas Km 99 and Km 104 were adjacent and had the lowest average slopes (least mountainous).

Solute concentrations were generally lower at all WCRB sites compared to TWO sites (Figure 3.3). Km 71 typically had the highest concentrations of major ions, particularly Mg (median concentration of 87.6 mg L^{-1}). Km 175 and Km 185 also had relatively high concentrations of major ions across both seasons (Figure 3.4). Km 104 and Km 99 had the highest mean concentrations of DOC, with median concentrations of 15.2 mg L^{-1} and 8 mg L^{-1} respectively. In contrast, the lowest DOC concentrations generally occurred at the WCRB sites and Km 44. Concentrations in spring were typically more variable than late season across sites, likely due to high variability in discharge (Figure 3.2).

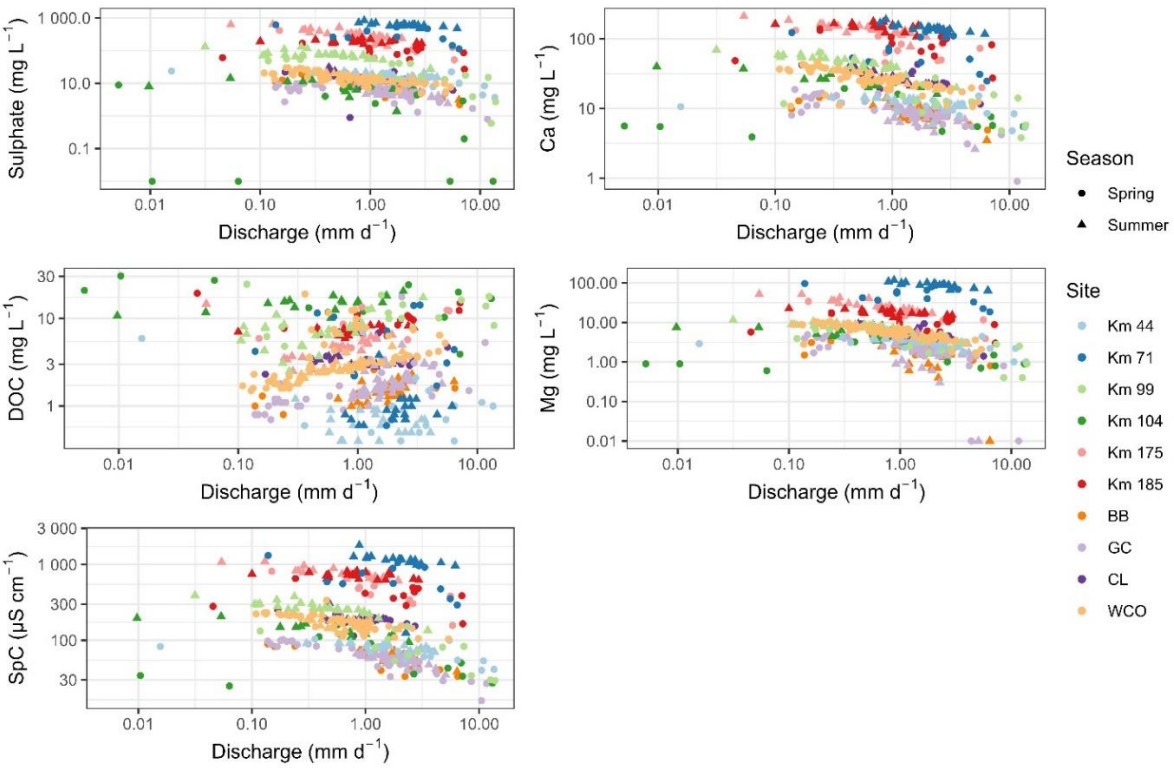

Figure 3.3. Solute concentrations plotted against flow for all sites. Winter samples were lumped in with spring.

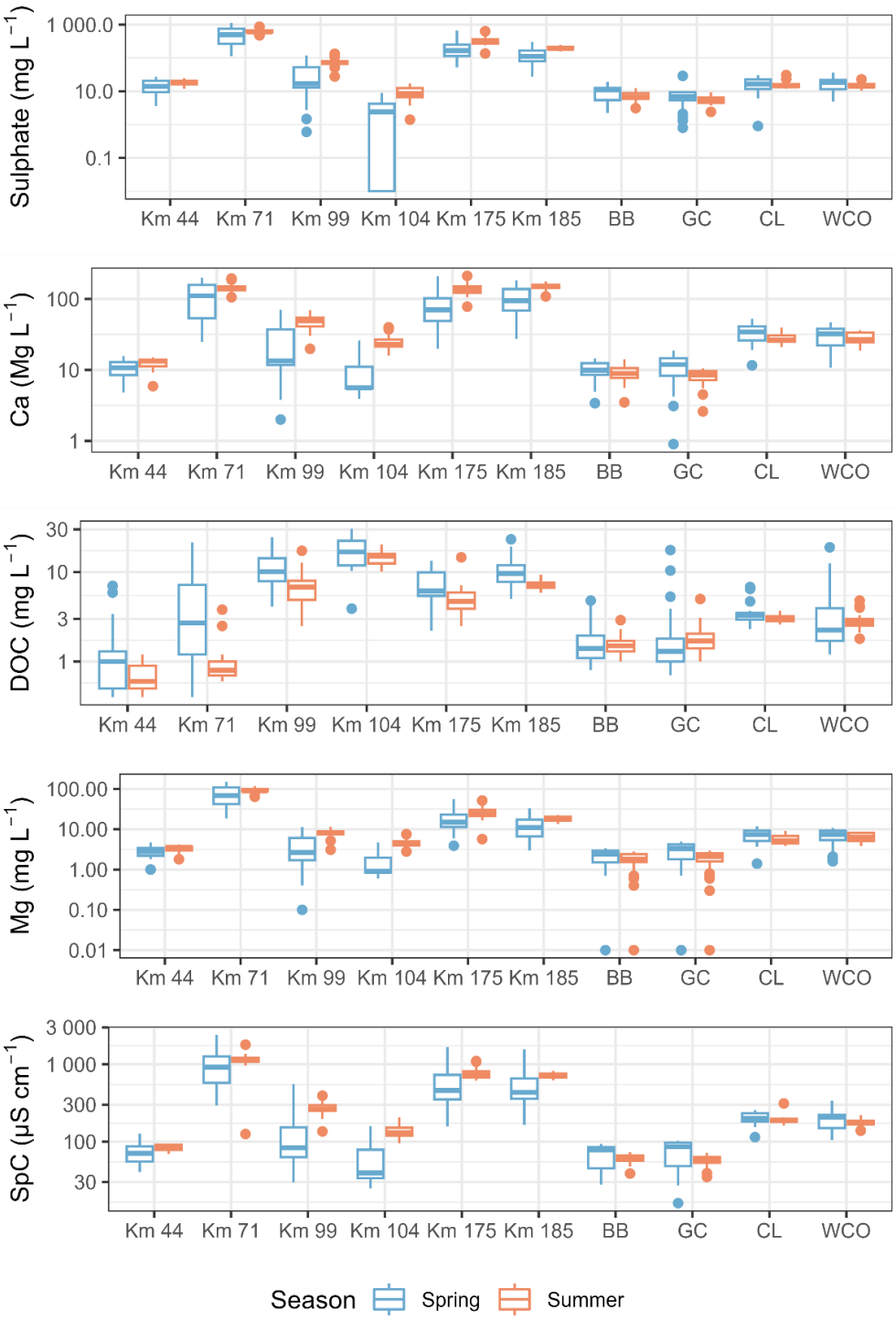

Figure 3.4. Boxplots depicting log solute concentrations for Spring and Summer for all catchments. Winter values were grouped into spring and grab samples where flow was not available are also included in the boxplots.

3.3.2 GAMs

Results from the GAMs indicate that not all sites had a significant seasonality for all solutes (Figure 3.5), which was defined by a p-value lower than 0.05 in the sDOY term. The degree of seasonality, defined as sDOY range, is reported in Appendix B (Table B3). In general, sDOY increased as the season progressed post freshet for major ions but decreased as the season progressed for DOC (Figure 3.5). Thus, concentrations for DOC decrease over time but increase for major ions at most sites after accounting for changes in flow. The WCRB sites exhibited less seasonality (lower sDOY range) for major ions than the TWO sites. Model performance was generally lower for DOC than other solutes, particularly for CL, Km 175, and Km 104, which had an R^2 less than 0.2. The models exhibited poor performance (R^2<0.25) in predicting Sulphate and SpC in CL, as well as in predicting Mg in BB (Figure 3.6).

DOC had significant seasonality at all sites with the exception of CL, Km 104, and Km 175. Among the sites with significant seasonality, BB and Km 99 had the least pronounced seasonality for DOC, characterized by sDOY ranges of 0.52 and 0.76 respectively. Conversely, Km 44 and Km 71 had the most pronounced seasonality, with sDOY ranges of 1.60 and 2.35 respectively. In general, the standard error for sDOY was notably higher for DOC compared to other solutes, particularly at sites exhibiting wider sDOY ranges.

Sulphate exhibited significant seasonality (sDOY p-values) at across all sites. The site with the least pronounced seasonality was WCO, with an sDOY range of 0.42. In

contrast, Km 104 had the greatest seasonality (sDOY range: 4.99) coupled with a relatively large mean standard error (0.64) for the sDOY term. Km 185 had the second highest sDOY range (1.87) for sulphate with a lower mean standard error (0.1).

WCO and CL were the only catchments that did not have significant seasonality for the sDOY term for Ca (p-values: 0.051 and 0.16, respectively). Km 104 and Km 185 had the greatest seasonality for Ca, with sDOY ranges of 2.14 and 1.41 respectively. Granger and Km 44 had the weakest significant seasonality for Ca, with sDOY ranges of 0.39 and 0.4 respectively.

Mg exhibited significant seasonality only at WCO among the WCRB sites, and Km 175 was the only site to not exhibit significant seasonality for Mg among the TWO sites. Km 104 and Km 185 had the largest significant seasonality for Mg, with sDOY ranges of 2.23 and 1.73 respectively, while WCO had the lowest significant seasonality for Mg (sDOY range: 0.43).

SpC had significant seasonality across all sites with the exception of CL (p-value: 0.37). Km 104 and Km 185 exhibited the highest seasonality for SpC, with sDOY ranges of 1.69 and 1.48 respectively. In contrast Granger and WCO, had the lowest significant seasonality for SpC with sDOY ranges of 0.32 and 0.28 respectively. Complete GAMs results are reported in table B.1.

3.3.3 CV ratios and log-log slopes

Log-log slopes from the GAMs were generally negative for major ions and positive or close to zero for DOC (Figure 3.6). The standard errors of the log-log slopes

were typically higher for sulphate and DOC than any other solute among sites. BB and GC for Mg had the strongest negative slopes, approaching -0.7. WCO and Granger had the strongest positive slopes for DOC (0.20 and 0.31 respectively). Km 71, CL, and Km 104 had negative or near zero log-log slopes. All other sites had weak but positive log-log slopes for DOC close to 0.1. CV ratios for all major ions were lower than 0.75 at all sites, however the majority of sites had CV ratios of less than 0.5. DOC was generally more chemodynamic than the major ions, this was particularly true for Km 71, Km 44, and GC, which had CV ratios close to or greater than one. Chemodynamic behaviour for DOC was influenced by high seasonality, as Km 71, Km 44, WCO, and GC had higher sDOY and CV ratios for DOC than any other site.

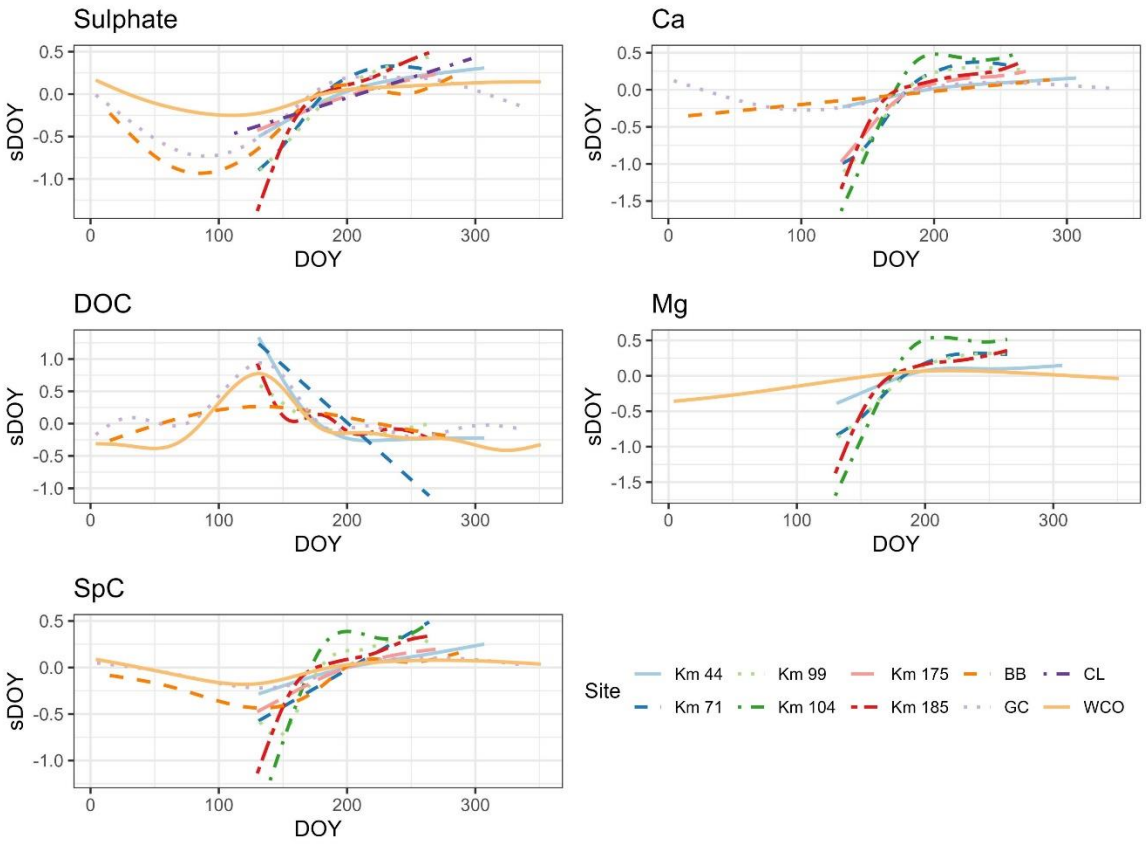

Figure 3.5. sDOY for all solutes and sites where the sDOY was significant (p-value < 0.05) and had a mean SE less than 0.5.

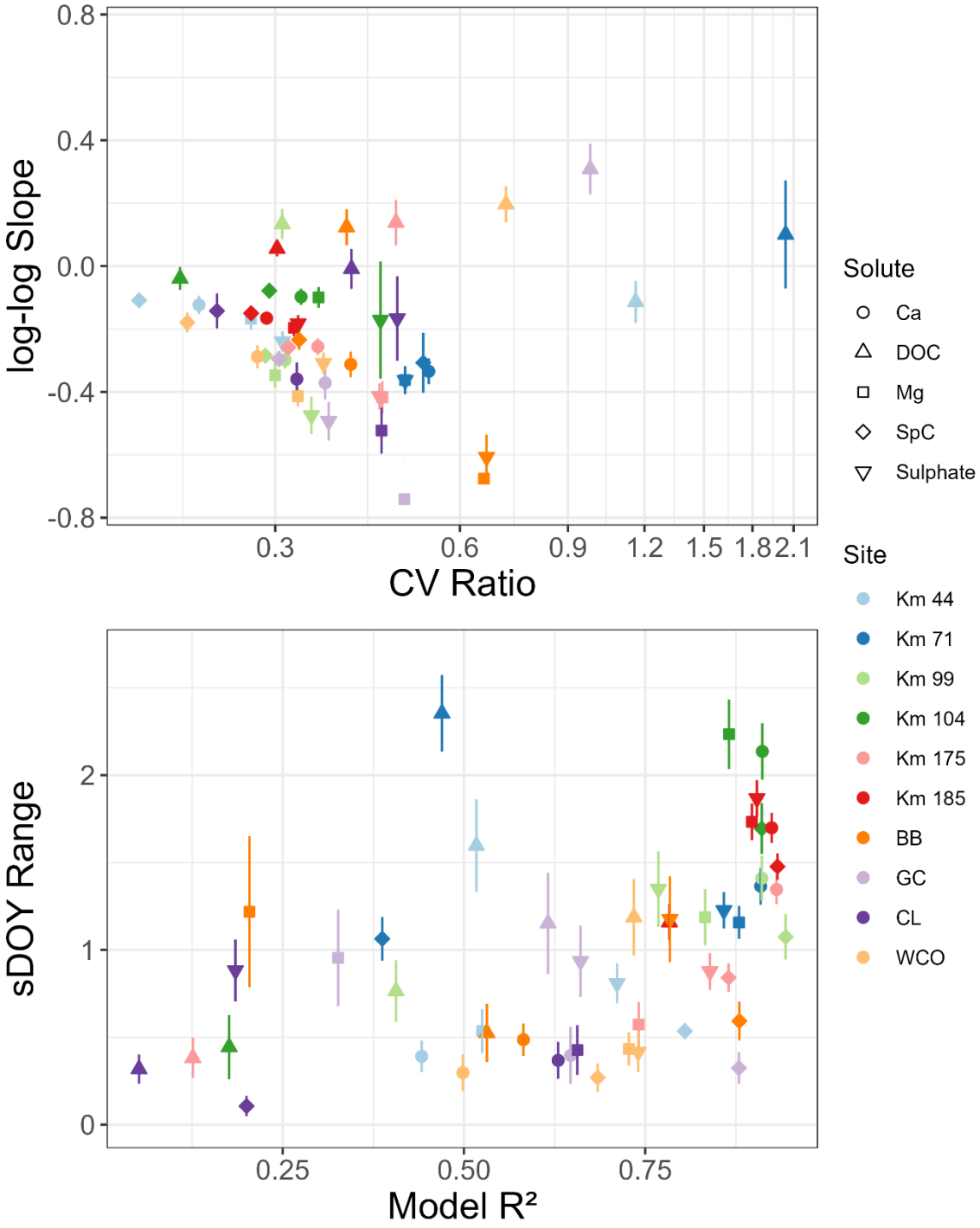
log-log Slope
0.8
0.4
0.0
-0.4
-0.8
0.3
0.6
0.9
1.2
1.5
1.8
2.1
CV Ratio
sDOY Range
2
1
0
0.25
0.50
0.75
Model R²
Solute
Ca
DOC
Mg
SpC
Sulphate
Site
Km 44
Km 71
Km 99
Km 104
Km 175
Km 185
BB
GC
CL
WCO

Figure 3.6. CV ratio plotted against log-log slopes from GAM models (top). Gam R^2 plotted against sDOY range (bottom). Error bars indicate standard error of sDOY range and the log-log slope from GAMs models. The sDOY range for Sulphate for Km 104 was large and was not included in this plot for visualization purposes.

3.4 DISCUSSION

In permafrost influenced catchments, solute concentrations are typically highly seasonal (MacLean et al., 1999; Carey, 2003; Townsend-Small et al., 2011; Shatilla and Carey, 2019; Shogren et al., 2021b; Koch et al., 2021). Concentrations of DOC generally decrease, and concentrations of weathering derived ions generally increase over the course of the ice-free season. Depleting solute stores, seasonal active layer dynamics, and seasonality in discharge have been use to explain these patterns previously (Carey, 2003; Shatilla and Carey, 2019). However, little work has been done to attempt to resolve the relative influence of these drivers of variability. Here we provide insights on the mechanisms of solute export in permafrost underlain catchments by assessing changes in CQ relationships.

Results largely confirm our first hypothesis, which states concentrations for DOC would increase and the concentrations for major ions would decrease post freshet due to seasonal ground thaw after accounting for the seasonality in discharge. However, our results also indicate that depletion of soil organic matter during spring, not ground thaw, is the primary driver for seasonality in DOC concentrations.

Our second hypothesis states that greater permafrost extent would lead to greater seasonality for major ions and DOC. Although we found evidence to support this

hypothesis for major ions, our results indicate that permafrost is less important than other catchment characteristics when considering seasonality of DOC.

3.4.1 Seasonal drivers for DOC and major ions

3.4.1.1 Spatial/vertical heterogeneity in soil chemistry is evident in most catchments

Log-log C-Q slopes were predominantly negative for all major ions and positive or with no significant slope for DOC. This corresponds to work of others who reported log-log slopes as typically positive for DOC (MacLean et al., 1999; Skierszkan et al., 2024) and negative for major ions (MacLean et al., 1999; Shatilla et al., 2023) in permafrost underlain catchments. The negative log-log slopes for major ions indicates the presence of greater mineral rich soils at depth. The log-log CQ slopes were closest to zero for Km 104 (a relatively flat catchment with homogenous catchment characteristics) for all major ions, indicating high homogeneity in terms of the spatial and vertical distribution of solute sources within the catchment.

Although many catchments had significant positive log-log slopes for DOC; CL, Km 44, Km 71, Km 104, and Km 175 all had non-significant log-log DOC slopes. A near zero log-log slope suggests that mobile organic carbon (OC) may be homogeneous vertically/spatially, or in-stream/near-stream biogeochemical processes drive variability in DOC concentrations (Creed et al., 2015; Zhi and Li, 2020). CL is the second largest catchment in this study with a ~1 km^2 lake just above the sampling outlet. The non-significant log-log slope at CL is likely due to greater dominance of in-stream processes (i.e. photosynthesis, respiration, photo-oxidation). Previous work also suggests that DOM

CQ relationships move towards chemostasis as catchment scale increases due to dominance of instream biogeochemical processes (Creed et al., 2015). Km 104 has a largely homogeneous vertical/spatial soil profile spatially and has a low catchment slope, leading to log-log slopes which are close to zero. Additionally, the stream is slow moving and instream processes may be more important in this catchment than the other TWO catchments. Km 44 and Km 71 have high catchment slopes, a thin organic layer along with a high proportion of bare ground; particularly upslope of the riparian area. Thus, as the source area expands during high flows, low DOC concentration water from upslope areas (which do not have a defined organic layer) move quickly through the organic layer near riparian areas (limiting contact time) due to the steep gradients and dilute the stream DOC signal. The high seasonality of Km 44 and Km 71 for DOC (see section 3.3.3.) suggest that despite near zero log-log slopes near-stream/in-stream processes likely do not dominate in this catchment.

3.4.1.2 Seasonal depletion of soil stores is important for DOC export

High seasonality in GAMs at most sites for DOC along with log-log slopes that were not significantly different than zero indicates changing flow paths due to active layer thaw is likely not the primary driver in the seasonality of DOC concentrations. The seasonality term in GAMs accounts for changes in flow, and the presence of non-significant log-log slopes indicate a lack of vertical heterogeneity in soil OC concentrations or dominance of in/near-stream processes. Thus, seasonality in CQ relationships for DOC must be driven by processes other than changing flow paths. Previous work in snow dominated mountains has shown the flushing of organic matter in

soils during freshet can reduce the soil reservoir of DOC (Hornberger et al., 1994; Boyer et al., 1997). For example, Boyer *et al.* (1997) attributed declines in DOC as melt progressed to source depletion in the upper soil horizons in a mountain headwater catchment in Colorado, USA. Certain sites (GC, WCO, BB, Km 99, and Km 175) did have positive log-log slopes for DOC, suggesting that depletion of DOC stores and thawing active layer may have a combined effect in controlling DOC concentrations. The strong decline of the sDOY term during freshet at several sites indicates that flushing of DOM in soils during freshet rapidly deplete finite labile OC stores within catchment soils. This phenomena has been directly observed in other snow dominated mountains as well (Hornberger et al., 1994; Boyer et al., 1997). Previous work at GC (one of the WCRB sites included in this analysis), attributed a strong hysteresis of DOC concentrations during freshet and summer events to both a rapid decline in organic matter and greater emphasis on deeper flow pathways (Carey, 2003; Shatilla and Carey, 2019). Townsend-Small *et al.* (2011) compared DOC concentrations at the same discharge level and saw a decrease in DOC concentrations in the upper Kuparuk River in Alaska, suggesting seasonality is at least partially driven by active layer thaw and/or depleting solute stores. Skierszkan *et al.* (2024) used a mixing model and found seasonality in DOC concentrations to primarily be driven by changing flowpaths in the Dawson range, Yukon, Canada. In contrast, our analysis suggests that depletion of organic matter is likely the primary driver for seasonal declines in DOC, yet active layer thaw may be secondary driver depending on the spatial/vertical distribution of organic matter concentrations in soil.

3.4.1.3. Seasonal ground freeze-thaw is important for major ion export

CQ relationships are variable among seasons for major ions in permafrost underlain catchments (MacLean et al., 1999; Shatilla et al., 2023). The negative log-log slopes and strong seasonality at multiple sites for multiple major ions suggest that activation of different flow paths from seasonal thaw and changing discharge influence export in these regions. Thawing of the active layer leads to greater flow from the deeper mineral rich soil horizons and bedrock and consequently higher ion concentrations. GAM results indicate seasonality causes an increase in solute concentrations for major ions, suggesting the seasonality in CQ patterns is not primarily driven by changes of ion stores. Our study largely is in agreement with others in permafrost environments that attributed the seasonality of major ions to seasonal active layer thaw. Shatilla *et al.* (2023) attributed ground thaw and increasing connectivity of deep groundwater to seasonal increases in solute concentrations in GC. Lehn *et al.* (2017) attributed a seasonal increase of major ion concentrations in Alaskan watersheds to seasonally thawing active layer and cryoconcentration in soils during later fall and winter of the previous years.

3.4.2 Seasonality and permafrost extent

3.4.2.1 Permafrost extent is not important for DOC seasonality

Although permafrost extent has a strong influence on DOC export (MacLean et al., 1999; Petrone et al., 2006; Frey and McClelland, 2009), greater permafrost extent did not necessarily lead to greater seasonality (sDOY range) in CQ relationships for DOC. For example, DOC was highly seasonal in WCO (sporadic permafrost) but had relatively

low seasonality for Km 99 (continuous permafrost). Although DOC concentrations were generally higher in the TWO sites, they did not necessarily exhibit a greater relative change in concentrations than the sites in WCRB, which generally have a lower permafrost extent than the TWO sites. Our results are in contrast to MacLean *et al.* (1999) and Petrone *et al.* (2006) who observed stronger seasonality for DOC/DOM in catchments with greater permafrost extent. MacLean *et al.* (1999) reported stronger CQ relationships and greater model performance for DOC in the high permafrost catchment compared to the low permafrost catchment in central Alaska during the summer. However, CQ relationships were similar between the catchments during snowmelt. The authors attributed this to a lower variability in discharge during the summer for the low permafrost catchment. Petrone *et al.* (2006) observed a larger increases of DOC export in catchments with greater permafrost extent. However, Petrone *et al.* (2006) did not account for relative changes in DOC export or seasonality in discharge, where connectivity to DOC changes with changing catchment wetness.

In our study sites, catchment characteristics related to slope and specific discharge were more important for DOC seasonality than permafrost extent. For example, the two most mountainous sites (Km 44 and Km 71) had the highest seasonality for DOC, indicating the relative seasonal changes in concentrations were the greatest after accounting for discharge. Both Km 44 and Km 71 had high specific discharge, limited organic soils and the lowest average concentrations for DOC, supporting the idea that organic matter stores were limited. Non-significant log-log slopes imply that nearly all of the seasonality at these sites was due to the depletion of solute stores and not due to active

layer thaw. The limited DOC supply and rapid flushing due to high flows presumably led to a more rapid depletion in DOC stores in these catchments. Conversely, Km 99 and Km 104 had high average DOC concentrations and high permafrost extent, yet exhibited lower seasonality than Km 71 and Km 44. Additionally, the CV ratio at Km 104 was also very low, indicating DOC is chemostatic in this catchment. Km 99 and Km 104 had much lower catchment slopes and specific discharge, indicating the abundance of organic matter within the catchments and limited flushing of soils (low specific discharge) played an important role in the weak seasonality of DOC. One caveat is that Km 104 had a very low R^2 value (<0.2) for DOC and did not have significant seasonality or log-log slopes, potentially due to the lack of multi-year sampling. Km 99 is similar to Km 104 but had significant seasonality and a positive log-log slope. Unlike Km 104, Km 99 is not entirely overlain with peat in the active layer as mineral soils are present in the headwaters. The significant seasonality in Km 99 may be driven by thawing of the active layer, leading to activation of deeper mineral-influenced flow paths, as the log-log slopes were significant at this site. However, we cannot disentangle the influence of depletion of solute stores and thawing of the active layer on seasonality of DOC in catchments that do have significant log-log slopes.

Low seasonality in BB relative to GC is likely a function of limited sampling during freshet at BB. Seasonality was also low in Km 175 and CL. High median Fe concentrations (1.8 mg L^{-1}) in Km 175 (unpublished data) indicate the dominance of instream processes in Km 175 as Fe interacts strongly with DOM (Gu et al., 1994; McKnight and Duren, 2004). The presence of a lake near the outlet of CL can lead to

dampening of the terrestrial DOC signal and may be dominated by in-lake biogeochemical processes.

3.4.2.2 Permafrost extent is important for major ion seasonality

Unlike DOC, permafrost extent and winter groundwater contributions do influence the seasonality of major ions along with overall export. In general, catchments in WCRB had lower seasonality than TWO catchments for major ions. Km 44 and Km 175 were the only exception to this, as these sites generally had low seasonality for major ions. This may be explained by significant surface-groundwater connection throughout the ice-free season as neither of these catchments are underlain with continuous permafrost. Our results are similar to Webster *et al.* (2022) who observed seasonal increases in NO_3 in Alaska, which the authors attributed to thawing active layer in a high permafrost extent catchment but not in low permafrost catchments. The authors argued that dominance of ground water was responsible for the lack of a seasonal trend in the low permafrost catchments. This supports our hypothesis for major ions, where the presence of deep groundwater contributions in low-permafrost catchments can dampen seasonality of CQ relationships for major ions. However, these results should be interpreted with caution as estimating permafrost extent in mountain headwater catchments can be uncertain. BB and GC had relatively high seasonality in Mg concentrations compared to other ions, yet these catchments also had highly negative log-log slopes, indicating considerable heterogeneity in soil Mg concentrations in solution. The high heterogeneity in soil concentrations may offset the dampening of seasonality due to lower presence of permafrost. The seasonality metrics for Mg at BB and GC

should be interpreted with caution, as low R^2 with high log-log slopes suggests another variable not accounted for in GAMs is driving variability in Mg (i.e. stream temperature, contact time with substrate, weathering rates, etc). Additionally, the sampling scheme among the sites was not consistent, although freshet was generally captured at most sites. Nevertheless, due to the vast distances among such remote catchments, sampling intervals and the number of observations vary. This is particularly true for Km 104 where only one year of sampling was included, and for BB, where discharge measurements were often not available during freshet.

3.5 CONCLUSION

In this study, we assessed the role of catchment characteristics, seasonal active layer thaw, and depletion of solute stores in controlling solute export in permafrost underlain watersheds. We obtained new insights on chemical transport through hydrochemical data collected across multiple catchments and seasons, a task scarcely undertaken in remote permafrost underlain environments. We utilized GAMs to assess changes in connectivity to solute sources after accounting for seasonally changing discharge. We largely confirmed our first hypothesis, where ion concentrations increased, and DOC concentrations decreased (irrespective of seasonality in discharge). However, we found that the majority of seasonality in DOC was caused by flushing of OC from soils stores during freshet, whereas our results indicate seasonal active layer thaw to be the primary driver of seasonality in major ions. Our second hypothesis suggesting permafrost extent drove variability in chemical concentrations was found to be largely

true for major ions. However, although permafrost extent was important for the average concentrations of DOC, topography was a more important driver in terms of seasonality as mountainous catchments with thin organic soils and high specific discharge lead to rapid flushing of limited soil OC stores.

Our results suggest climate change induced increases in active layer thickness and greater connectivity of subpermafrost, inter-permafrost, and suprapermafrost water will lead to elevated concentrations of weathering derived ions, reduced concentration of DOC and a decrease in seasonality of major ions in high latitude catchments. The role of permafrost extent on the seasonality of DOC concentrations remains unclear. This work highlights the need for long-term stream chemistry sampling across a biogeophysical range of high latitude watersheds. Greater sampling resolution could provide a means of quantifying the influence of secondary drivers (i.e. stream temperature) on stream chemistry in these environments. Currently, the majority of the literature assesses the role of catchment characteristics on solute exports, but limited work has been done on the drivers of seasonality in permafrost underlain catchments, largely due to the lack of sampling in the shoulder seasons. This study is one of the few to assess the drivers of seasonality of stream chemistry in permafrost underlain catchments.

ACKNOWLEDGEMENTS

We would like to thank David Barrett, Tyler de Jong, Lauren Bourke, Aliana Fristensky, Anna Grunsky, Calvin Newbery, and Andras Szeitz for field assistance. We would like to thank Global Water Futures and National Science and Engineering Council

of Canada for providing financial support for this project. We acknowledge the continued support of the Water Resources Branch, Government of Yukon, for the operation of Wolf Creek Research Basin.

DATA AVAILABILITY

Data is available upon request.

CHAPTER 4

WATER STORAGE, MIXING, AND RELEASE IN PERMAFROST UNDERLAIN CATCHMENTS: INSIGHTS FROM END-MEMBER MIXING AND WATER AGE CHARACTERIZATION

ABSTRACT

Seasonality plays a critical role in the rate, timing and magnitude of hydrological and chemical transport in permafrost underlain mountain catchments. During spring, large volumes of water are delivered as snowmelt, yet infiltration is limited by the presence of frozen ground and shallow flow pathways rapidly deliver water to streams. As thaw progresses, catchment storage capacity increases, runoff pathways lengthen, and previously frozen soil water becomes mobile. Changing storage capacity and activation of deeper flow paths can alter the degree of mixing in storage and alter transit time distributions of outgoing fluxes. Water age can reveal vital information about catchment storage and flow pathways however, limited work has been conducted on characterizing water age dynamics in permafrost underlain catchments due to logistical challenges associated with working in cold and remote catchments. Here we characterize the age dynamics of two headwater catchments underlain with continuous permafrost located in Tombstone Territorial Park in Yukon, Canada. Considering the lack of hydrological characterization in this environment, our objectives are to; (1) evaluate the rate, timing, and magnitude of all hydrological fluxes, (2) utilize Bayesian mixing analysis to partition runoff into rain and snow contributions, and (3) apply StorAge Selection (SAS) functions

to characterize water age dynamics in both catchments. The SAS framework can characterize variability in transit times and characterize preferential movement of water through storage, as it can assess age dynamics of water at the catchment scale by age tagging all parcels of water stored within and moving out of a hydrological system. We utilized snow survey, discharge, meteorological and eddy covariance data to quantify the inputs and outputs of the basins. Additionally, we utilized frost surveys and continuous soil moisture/temperature data to estimate active layer thickness across the basin and potential mobilization of previously frozen water. We used Isosnow, a spatially distributed parsimonious model, to simulate isotopic evolution of snow and snowmelt. A total of 410 mm precipitation entered the basin, 45% of which was snow, which melted over 4 weeks. Evapotranspiration (ET) approximately equaled discharge and increased in magnitude as summer progressed. Mixing results suggest nearly all (> 90%) of runoff during freshet was snow water in both catchments, indicating very little mixing with old water during this period. In contrast, the majority of rain left the basin as ET. The water balance and SAS framework indicate significant contributions of melting ground ice to discharge post freshet, highlighting the importance of late season rains for a particular year on discharge in the following year. The SAS framework also indicates that ET is composed primarily of very young water, likely due to high storage capacity of organic soils and shallow root depth of tundra vegetation. High discharge led to a more uniform SAS function for discharge, indicating greater mixing of storage during high flows.

4.1 INTRODUCTION

High latitude regions are experiencing rapid environmental change due to accelerated warming and declines in the cryosphere (Kaplan and New, 2006; Bekryaev et al., 2010; Cohen et al., 2014). Permafrost degradation, shifts in the timing, phase and amount of precipitation, along with rapid vegetation change are all influencing hydrological, biogeochemical and thermal processes across circumpolar regions (Walvoord and Kurylyk, 2016). Rapid change in northern environments is also occurring at time of decreasing monitoring capacity (Laudon et al., 2017), particularly at headwater scales where process understanding is generated, creating the potential for unseen impacts on aquatic ecosystems and societies.

In permafrost environments, which cover approximately 15% of the northern hemisphere, there is a strong seasonality to the hydrological cycle in driven by large annual variations in energy and air temperature. Over-winter, snowpacks accumulate and during snowmelt a large fraction of the annual precipitation is released. This meltwater interacts with frozen ground and restricted storage promotes rapid near-surface movement of water to the stream network (Quinton and Marsh, 1999; Carey and Woo, 2001a). Following snowmelt, frozen ground thaws and the active layer above permafrost gradually expands throughout the summer, encouraging deeper flow paths and increasing available water storage while changing catchment connectivity. Runoff responses to rainfall become increasingly dampened, and the emergent flow paths alter stream chemistry (Carey, 2003; Petrone et al., 2006). As temperature declines in fall, soils

rapidly freeze and the movement of water in the subsurface declines depending upon the extent of permafrost and active layer thickness. While there has been over a half century of research examining the interaction of permafrost on water movement, our understand of storage and release processes is still nascent as observations are relatively scarce and confined to limited geographical domains.

Storage dynamics in permafrost catchments are distinct as the annual freeze thaw cycle imparts a strong temporal component to mobile water and available storage, which characterizes hydrological states (McNamara et al., 2011). Approaches such as hydrograph recession analysis and physically based models have been used to identify increases in dynamic storage from spring to fall, and changes in storage as related to thawing permafrost (McNamara et al., 1998; Carey and DeBeer, 2008; Wang et al., 2009; Hinzman et al., 2020). However, research on mobile storage, which typically requires tracers, is rare (Staudinger et al., 2017; Tetzlaff et al., 2018; Piovano et al., 2019) and most studies have relied on techniques such as End Member Mixing Analysis (EMMA) and hydrograph separation that do not explicitly quantify age, but provide results that are implicitly a function of catchment transit time distributions. There have been several studies that have employed stable isotopes for hydrograph separation in permafrost-influenced catchments with varied results. For the snowmelt freshet period, some have identified the majority of water to be composed of snowmelt during freshet (Cooper et al., 1991; Metcalfe and Buttle, 2001) whose fraction relates to melt intensity and frost table dynamics, whereas others have reported near or over half of the water to be composed of pre-event or 'old' water. Spence *et al.* (2014) in a discontinuous permafrost environment

found winter runoff to be composed mostly of event water but freshet water to be composed mostly of pre-event water. For summer rainfall events, McNamara *et al.* (1997) and Carey and Quinton (2005) found that pre-event water dominated at two catchments in northwestern North America. While there is considerable variability in the values reported, one common aspect of these findings is that the presence of frozen ground is a first order control on mixing and its presence can immobilize and store considerable volumes of water over-winter.

The transit time of water (the time it takes water to leave the catchment after entering via precipitation or snowmelt) provides information about storage and flow pathways though a single descriptor (McGuire and McDonnell, 2006). Mean transit times have been used as a metric to quantify catchment storage properties in various settings (Dinçer et al., 1970; Maloszewski et al., 1992; Morales and Oswald, 2020) whereas transit time distributions (the distribution of water ages within the outflow) provide a more detailed representation of age dynamics within a catchment. To adequately characterize transit times, comprehensive tracer data is typically required to be combined with analytical techniques including newer frameworks such as young water fractions (F_{yw}) and StorAge Selection (SAS) functions (Botter et al., 2011; Van Der Velde et al., 2012; Harman, 2015; Kirchner, 2016). Kirchner (2016) proposed F_{yw}, a metric quantifying the fraction of water younger than a certain threshold age, as a more robust alternative to mean transit times due to aggregation bias. Since its establishment, there have been many applications of F_{yw} in the literature, with Jasechko *et al.* (2016) summarizing that approximately 1/3 of global runoff consists of water less than 2-3

months old; with the proportion of young water decreasing in steeper catchments due to longer flow pathways. Application of young water fractions to permafrost-underlain watersheds has occurred on the Tibetan Plateau. Song *et al.* (2017) showed that the young streamflow ranged from 9% to 21% and that the young water threshold ages ranged from 35 to 52 days. The proportions of young water varied with catchment characteristics, particularly vegetation cover. Wang *et al.* (2023) for the large 4586 km^2 Buqu catchment that is dominated by glaciers and permafrost reported MTT of 107 days, with 15 % of the stream water younger than 41 days. Estimated water age showed significant spatial heterogeneity with shorter water ages in high-elevation and glacier catchments and longer water ages in low-elevation and non-glacier catchments.

Another recent tracer-guided approach is the StorAge Selection (SAS) framework, which assigns an age to all parcels of water stored within and moving out of a catchment or defined system (Botter et al., 2011; Van Der Velde et al., 2012; Rinaldo et al., 2015). Unlike traditional transit time distributions, the SAS framework accounts for temporal variability and can reveal changes in transit times and characterize preferential movement of water through storage (Rinaldo et al., 2015; Kim et al., 2016; Smith et al., 2020). Storage is typically age ranked at the catchment scale, which sorts stored water from youngest to oldest, allowing the utilization of the SAS framework when the total amount of water in storage is unknown or highly uncertain (Harman, 2015). More recently, SAS functions have been utilized to characterize transport processes in highly complex basins (Fang et al., 2019; Rodriguez and Klaus, 2019) and have been directly observed in a controlled experimental catchment (Kim et al., 2022). Frameworks that seek to assign

ages to water provide critical information on transport processes and in rapidly changing permafrost environments, this information may provide information on the nature and consequences of future hydrometric and geochemical responses. While F_{yw} and SAS frameworks have been utilized in temperate regions, their application in permafrost underlain systems is rare and presents distinct challenges: (1) snow tracer information and snow melt processes are difficult to resolve and quantify across scale; (2) permafrost underlain catchments are often remote and difficult to access compared to their more temperate counterparts; and (3) the presence of channel ice can make discharge measurements difficult during certain periods of a given water year.

Our knowledge of seasonality (freeze-thaw dynamics and rain vs snow) on the age dynamics of water and by extension storage and release processes in in permafrost underlain systems is limited. To address this, we utilize hydrometric data, along with stable isotope measurements of rain, snow, and streamflow to identify water sources and quantify water age dynamics in two adjacent permafrost underlain headwater catchments in Yukon, Canada. Specifically, we (1) use end-member mixing analysis to quantify the proportion of runoff composed of rain vs snow water; (2) quantify young water fractions of both catchments; and (3) utilize StorAge Selection functions to simulate age dynamics of storage, ET, and streamflow. Through the application of these frameworks, this work provides new insights on water storage, mixing and release in cold high-latitude systems that are rapidly warming.

4.2 METHODS

4.2.1 Study sites

The Tombstone Waters Observatory (TWO) is located in Tombstone Territorial park, Yukon Territory, Canada and lies within the traditional territory of the Tr'ondëk Hwëch'in First Nation. TWO consists of several monitored catchments that intersect the Dempster Highway, which cuts through the park and connects Dawson City, YT to Inuvik in Northwest Territories. Km 99 (Slavin Creek) and Km 104 (unnamed) are two headwater catchments located in TWO (64°42'46.8"N 138°27'03.6"W) in the Blackstone Uplands that intersect the Dempster highway at those kilometer markers, respectively. Both catchments are underlain with continuous permafrost and are primarily overlain with short shrubs and other tundra vegetation. Km 99 is smaller (11 km^2) than Km 104 (18 km^2) and more mountainous. Km 99 is primarily north facing, particularly the upland areas. Climate normals (1981-2010) from Dawson City, the nearest Environment Canada weather station ~85 km away (Euclidian distance), shows annual precipitation of 453.2 mm of which 307.2 mm is rainfall. The annual air temperature is -4.1 ℃, yet air temperature at Km 99 is typically lower. Air temperature data from a tower at Km 95 along the Dempster Highway had an average air temperature of -7.1 ℃ in 2022, which was 3.2 ℃ colder than Dawson City. The surficial material of the basins primarily consists of moraine till and colluvium. The basins are primarily underlain by Paleozoic black shale, dolomitic siltstone, carbonaceous sandstone, and limestone and are part of the Selwyn Basin. Both of the catchments are primarily overlain by a thick organic soil. Both basins have a maximum active layer thickness of ~40 cm.

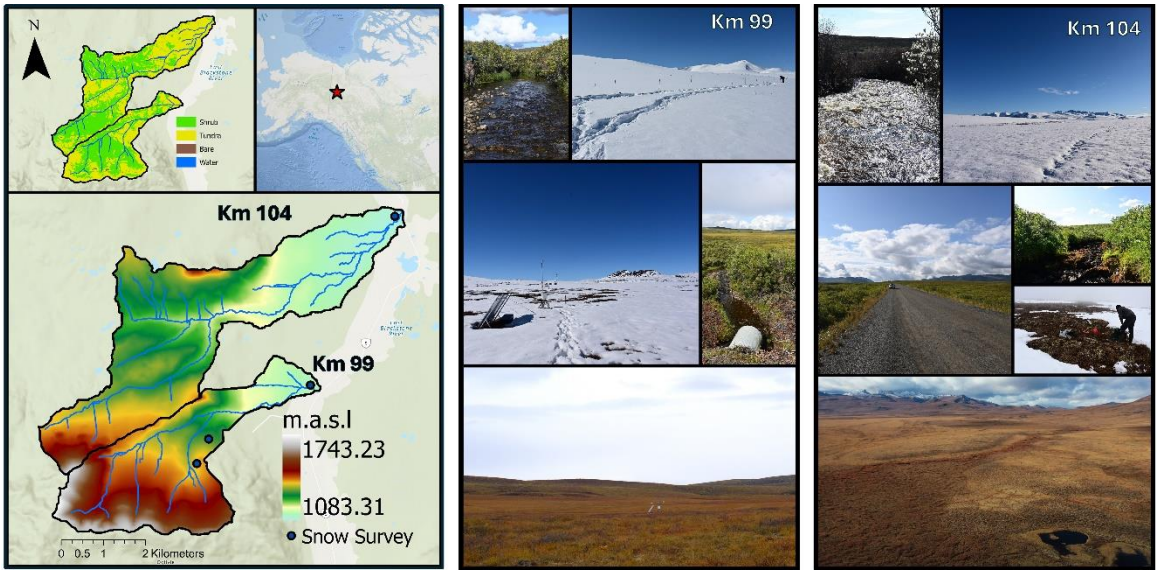

Figure 4.1. Map of Km 99 and Km 104. The elevation data was obtained from ArcticDEM (version 3). Inset on the left is a land cover map generated using Sentinel-2 imagery and the inset on the right is the general location of the catchments.

4.2.2 Meteorological

The study period was from 20 April 2022 to 21 September 2022. Meteorological data from 2022 was obtained from a tower installed near the outlet of Km 99. Air temperature, wind speed, longwave and shortwave radiation, soil moisture and temperature, humidity, along with rainfall were measured at an hourly timestep. Rain data was collected using a HOBO tipping bucket located near the outlet of Km 99 and was assumed to be largely uniform across both basins. Evapotranspiration (ET) was directly measured using an open-path eddy-covariance system.

Evapotranspiration was measured using an eddy covariance tower located on the permafrost tundra in Km 99 watershed (Figure 4.1). Instrumentation included a LI7500-

and a Gill R3-50 sonic anemometer, both installed at a height of 2.6 m. High frequency measurements were processed in Eddypro. Density fluctuations were compensated using the Webb, Pearman, and Leuning correction (Webb et al., 1980). Covariance maximization was used to detect and compensate for time lags. Spike detections and removal were computed according to Vickers and Mahrt (1997). Analytical correction for high-pass filtering effects were computed according to Moncrieff *et al.* (2004) and low-pass filtering effects evaluated using methods by Moncrieff *et al.* (1997).

ET measured at the flux tower was scaled across the catchment using the Penman-Monteith (P-M) method. All components of the P-M equation were measured at the flux tower with the exception of surface resistance, which was determined by inverting the P-M equation with measured latent heat. The catchments were then segmented into 10 hydrological response units (HRUs) based on elevation, slope and cosine transformed aspect. Average slope and aspect were used to estimate clear sky downwelling radiation for each HRU using the Cold Regions Hydrological Model (CRHM; Pomeroy *et al.*, 2007). Theoretical downwelling radiation was compared to measurements at the tower and then converted and scaled across the HRUs based on this predicted to observed ratio. Net radiation was determined for the HRUs by assuming longwave components and albedo were uniform across the catchment. Basin scale ET was then determined via P-M for each HRU. ET was assumed to be zero when snow was present.

4.2.3 Discharge

We collected continuous discharge data using stage-discharge rating curves. Stream stage was obtained via Solinst Levelloggers at both catchments. During early freshet, when there was significant channel ice, multiple spot measurements of discharge were taken, and values linearly interpolated between measurements.

4.2.4 Snow Water Equivalence

SWE was measured via four snow survey transects (25 points per transect) using a Mount Rose snow sampler. Three of the transects were in Km 99 and one in Km 104. SWE was measured in 5 of the 25 stations in each transect to estimate snow density. We used the snow density along with the depth measurements at all 25 stations to estimate the average SWE for each transect. To track the progress of melt, SWE at each of the four transects was measured four times during the melt period.

4.2.5 Stable Isotope Collection

Rain and Stream isotopes were collected at least weekly in 2022, with a shorter collection interval during rain and melt events. Autosamplers were deployed in both catchments, however the autosampler at Km 99 worked more consistently than at Km 104 providing greater sample depth. Three δ^2H samples were taken from the snowpack at each transect for the initial April survey. We took 1-3 δ^2H samples at approximately the same locations at each transect in following surveys. If one or more locations at a transect did not have enough meltwater to fill a 20 mL vial with no head space, a bulk sample was taken, combining snow from all stations. If one or more locations at a transect (where a

δ^2H sample was taken in the initial survey) had no snow, that transect was considered to have no δ^2H data for that particular survey. If the transect had zero snow, it was assigned a value of zero for δ^2H. This was done to account for the spatial variability in δ^2H within a transect. Over the course of this study, we ended up with a total of 16 SWE and 13 δ^2H observations across our four transects during the melt period. Bulk snow samples were allowed to melt at room temperature in a sealed plastic bag and were transferred to a 20 mL vial after it was completely melted.

4.2.6 Snowmelt Model

We used Isosnow, a spatially distributed parsimonious model that can simulate isotopic evolution of a snowpack and snowmelt (Ala-aho et al., 2017a), to estimate snowmelt input in Km 99 and Km 104. Isosnow utilizes the PCRASTER PYTHON framework, and the calculations are conducted at a pixel level. The model requires a DEM, incoming solar radiation, air temperature, relative humidity, initial SWE, precipitation, and the isotopic composition of precipitation. In this study, Isosnow was used to model snowmelt starting mid-April until the end of snowmelt at an hourly timestep. All inputs were assumed to be spatially uniform with the exception of the DEM, incoming solar radiation, SWE, and air temperature. Air temperature was estimated using an established lapse rate for the two basins, and incoming solar radiation was estimated using CRHM and measured incoming radiation as previously discussed. Isosnow was run for each basin separately at a 30 m resolution. Isosnow calibration was conducted using 2,500 Monte Carlo simulations at a 300 m resolution for both basins simultaneously. Details on Isosnow calibration can be found in Appendix C.1.

4.2.7 End-Member Mixing

End-member mixing was conducted for both Km 99 and Km 104 using MixSIAR, a Bayesian mixing framework (Stock et al., 2018) and the hydrograph was separated into rain and snow. The mean δ^2H and $\delta^{18}O$ volume weighted values along with their standard deviations were included as source data in MixSIAR. A uniform distribution was implemented as the prior distribution. Mixing analysis was performed for each stream sample. The results were then linearly interpolated to estimate the snow and rain fractions of the hydrograph.

4.2.8 StorAge Selection

We applied the age-ranked SAS framework (Harman, 2015) to both catchments using mesas.py (Harman and Xu Fei, 2024) in Python at a daily timestep for both Km 99 and Km 104 to characterize age dynamics in both basins for 2022. We assumed a functional form for a weighted SAS function and calibrated its parameters using δ^2H observations. The conservation equation for bulk transport of both catchments was described by

$$\frac{d}{dt}s_T(T,t) = J(t)\delta(T) - \sum_Q Q(t)p_Q(T,t) - \sum_{ET} ET(t)p_{ET}(T,t) \quad (8)$$

where $s_T(T,t)$ is an incremental volume of storage of age *T* at time *t* and has units of volume per time. *J(t)*, *Q(t)*, and *ET(t)* are the input (snowmelt + rain), runoff, and evapotranspiration fluxes at time *t* respectively. $p_Q(T,t)$ and $p_{ET}(T,t)$ are PDFs of transit time distribution of water of age T or younger leaving storage volume at time *t* as Q or

ET. Integrating $s_T(T,t)$ over all ages up to age T leads to age-ranked storage $S_T(T,t)$ (Equation 9).

$$S_T(T,t) = \int_0^T s_T(T,t)dT \quad (9)$$

We can also apply the conservation equation on a conservative solute.

$$\frac{d}{dt}m_T(T,t) = J(t)C_J\delta(T) - \sum_Q m_Q(T,t) - \sum_{ET} m_{ET}(T,t) \quad (10)$$

where $m_T(T,t)$ is the incremental tracer mass of age T in storage, $\delta(.)$ is the dirac delta distribution, $m_Q(T,t)$ and $m_{ET}(T,t)$ are the incremental tracer mass of age T leaving storage as runoff or ET. m_Q and m_{ET} can be determined by

$$m_Q(T,t) = Q(t)C_T(T,t)p_Q(T,t) \quad (11)$$

$$m_{ET}(T,t) = ET(t)C_T(T,t)p_{ET}(T,t) \quad (12)$$

where $C_T(T,t)$ is the age rank concentration in storage. The outflow tracer concentration can be determined by

$$C_Q(t) = \frac{1}{Q(t)}\int_0^{T_{max}} m_Q(T,t)dT + C_{old} * (1 - P_Q(T_{max},t)) \quad (13)$$

where $C_Q(t)$ is the tracer concentration in runoff and C_{old} is the tracer concentration assigned to all water older than T_{max}. $p_Q(T,t)$ and $p_{ET}(T,t)$ can be expressed as

$$\Omega_Q(S_T,t) = P_Q(T,t) \quad (14)$$

$$\Omega_{ET}(S_T, t) = P_{ET}(T, t) \quad (15)$$

where $P_Q(T, t)$ and $P_{ET}(T, t)$ are the cumulative transit time distributions, and $\Omega_Q(S_T, t)$ and $\Omega_Q(S_T, t)$ are the cumulative SAS functions. The density form can be written as

$$p_Q(T, t) = \omega_Q(S_T, t)s_T \quad (16)$$

$$p_{ET}(T, t) = \omega_{ET}(S_T, t)s_T \quad (17)$$

where ω_Q and ω_{ET} are the SAS functions for Q and ET in density form.

We were able to estimate the amount of total mobile storage in both of our basins via frost surveys and soil moisture data (See Appendix C.2 for details), thus we utilized a beta distribution to fit SAS functions for Q and ET. The CDF of the beta distribution is represented as

$$Beta(x; \alpha, \beta) = \frac{B(x;\alpha,\beta)}{B(\alpha,\beta)} \quad (18)$$

where α ands β are parameters that have a value > 0, $x = \frac{S_T}{S_0}$, and $S_0 = S(t)$. The SAS function for ET was constant but the SAS function for Q varied with flow rate using a weighted sum of M components similar to Rodriguez and Klaus (2019)

$$\omega_Q(S_T, t) = \sum_{m=1}^{M} f_{Q,m}(t)\omega_{Q,m}(S_T, t) \quad (19)$$

where $f_{Q,m}(t)$ is a time varying weight at time *t*. We used a two component SAS function with weights defined as

$$f_{Q,m=1}(t) = \frac{Q_C}{Q(t)+Q_C} \quad (20)$$

$$f_{Q,m=2}(t) = 1 - f_{Q,m=1}(t) \quad (21)$$

where Q_C is a parameterized value representing the discharge at which the weights for both components would be 0.5. We used the downhill simplex algorithm from Scipy package in Python to determine the values for $\alpha_{m=1}$, $\alpha_{m=2}$, $\beta_{m=1}$, $\beta_{m=2}$, and Q_C that lead to the lowest RMSE between observed tracer observations in discharge and the ones simulated from equation 13 for each basin. Since tracer concentrations are difficult to measure from ET fluxes, we performed this fitting with several ET SAS functions to determine the sensitivity of the SAS function of Q to the ET SAS function for Km 99. We assumed that the ET SAS function would be similar in both basins.

We considered all water stored in the basin before data collection for 2022 to be old water. The tracer concentration for old water (C_{old}) in storage was assumed to be the same as the tracer concentration of discharge during late Fall. We assume that practically all the water in storage was frozen (immobile) and mobile storage was zero at the start of the simulation, as mixing results indicated that much of the discharge during freshet is snow water. Mobilization of previously frozen water can make transit time estimation difficult (Tetzlaff et al., 2018). We estimated the amount of water that mobilized from thawing active layer via frost surveys and soil moisture data and added that to storage for the SAS framework (See Appendix C.2). It is important to note that water added via thaw mobilization was not considered to be an input but instead was old water already present in the basin that gradually mobilizes over time. Due to the presence of ice-rich permafrost

and the lack of deep groundwater contributions to runoff in either basin, we assume that all old water is melting ground-ice in both basins.

4.2.9 Young Water Fractions

F_{yw} were calculated from Km 99 and Km 104 using the methods of Stockinger *et al.* (2016). Iteratively reweighted least squares (IRLS) regression was used for sine-wave fitting (Kirchner, 2016). Equations outlining the procedure are presented in Appendix C.3.

A frequency of 170 days was used to calculate F_{yw}, as the catchment has virtually zero input and output fluxes during the winter. Both discharge weighted young water fractions (F^*_{yw}) and non-discharge weighted fractions (F_{yw}) were calculated for both sites. The young water fractions from the SAS framework were extracted for comparison with young water fractions determined from sine-wave fitting as depicted in Kirchner (2016). The young water fractions from SAS were the mean of young water fractions across all timesteps, where the threshold age was determined from the sine-wave fitting approach for an accurate comparison. The SAS young water was also discharge weighted for comparison with the sine-wave fitting approach.

4.3 RESULTS

4.3.1 Water Balance

During the start of the study period on April 20, both catchments were largely hydrologically inactive. Evaporation was very close to zero as the basin was snow-covered (sublimation and evaporation losses from the snowpack were accounted for by

Isosnow), both basins had zero flow conditions, and no snowmelt was occurring Table 4.1. Results from the cumulative water balance (Figure 4.2) show the change in storage by the end of the study period was +25 mm and -3 mm for Km 99 and Km 104 respectively.

At Km 99 from 20 April (when the basins were still snow covered with zero flow) until 21 September (when stream icing began and flows were very low), 193 mm of snowmelt and 247 mm of rainfall entered the catchment. Approximately half of this occurred during May and June, and rainfall gradually declined each month. Evapotranspiration totaled 187 mm and followed the typical growing season progression and rapid onset during peak radiation in June as the catchment became snow free and gradually declined through senescence in late August and into September. A total of 206 mm was recorded as runoff, with over half leaving the basin in June. The overall runoff ratio was 0.47. While there were no groundwater fluxes considered due to the presence of continuous permafrost, soil moisture profiles and thaw depth suggested 200 mm of water became mobile in storage by the end of August. Cumulative storage shows a large increase during freshet, which becomes negative in July despite continued flows and then fluctuates around zero responding to rainfall events.

The water balance was similar in terms of magnitude and timing at Km 104. SWE was 190 mm and rainfall was assigned the same value (217 mm). Evapotranspiration was slightly greater (199 mm) largely due to aspect considerations and a slightly longer snow-free period. Overall, 220 mm of runoff occurred, giving a runoff ratio of 0.53. The most

notable difference from Km 99 is that flows began earlier at Km 104 from advanced onset of melt, resulting in less runoff in June. Km 104 was slightly more responsive to summer rainfall events, yet both catchments required large precipitation to initiate a stormflow runoff response. Cumulative storage again quickly increased beginning in May and declined in June to values slightly below zero throughout the remainder of the study period. Approximately 204 mm of frozen water was released gradually as the active layer expanded.

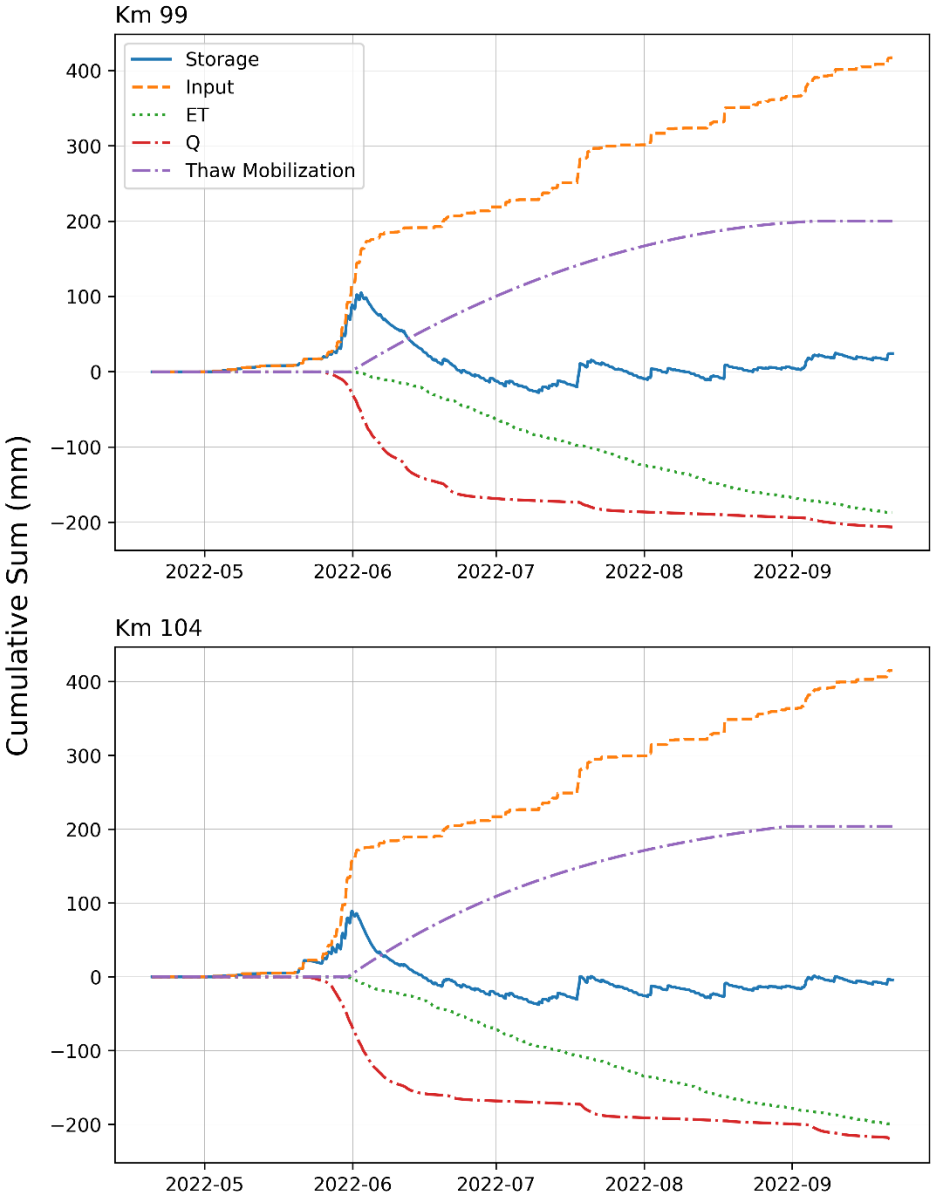

Figure 4.2. Cumulative water balance of Km 99 and Km 104 for 2022. Thaw mobilization values estimated using frost surveys from 2022 and soil moisture just before freeze up in 2020. Storage does not include thaw mobilization and was determined by the cumulative sum of J, Q, and ET. S = J – Q–- ET.

Table 4.1. Monthly fluxes for Km 99 and Km 104 for 2022. September only includes dates up to 21 September. Table includes monthly change in storage (not cumulative) determined via water balance (dtS).

Site	Month	Q (mm)	Rain (mm)	Snowmelt (mm)	ET (mm)	dtS (mm)
Km 99	April	0	0	0.1	0	0.1
	May	30	9	109.7	0.1	88.5
	June	138.3	40.5	59.7	62.9	-101
	July	17.8	82.4	0	61.4	3.2
	August	7.3	64.2	0	42.8	14.1
	September	12.5	51.4	0	19.6	19.4
Km 104	April	0	0	0	0	0
	May	69	9	150.8	2.5	88.3
	June	98.9	40.5	16.8	69.5	-111.2
	July	22.8	82.4	0	62.4	-2.8
	August	8.6	64.2	0	43.9	11.7
	September	21.1	51.4	0	20.7	9.7

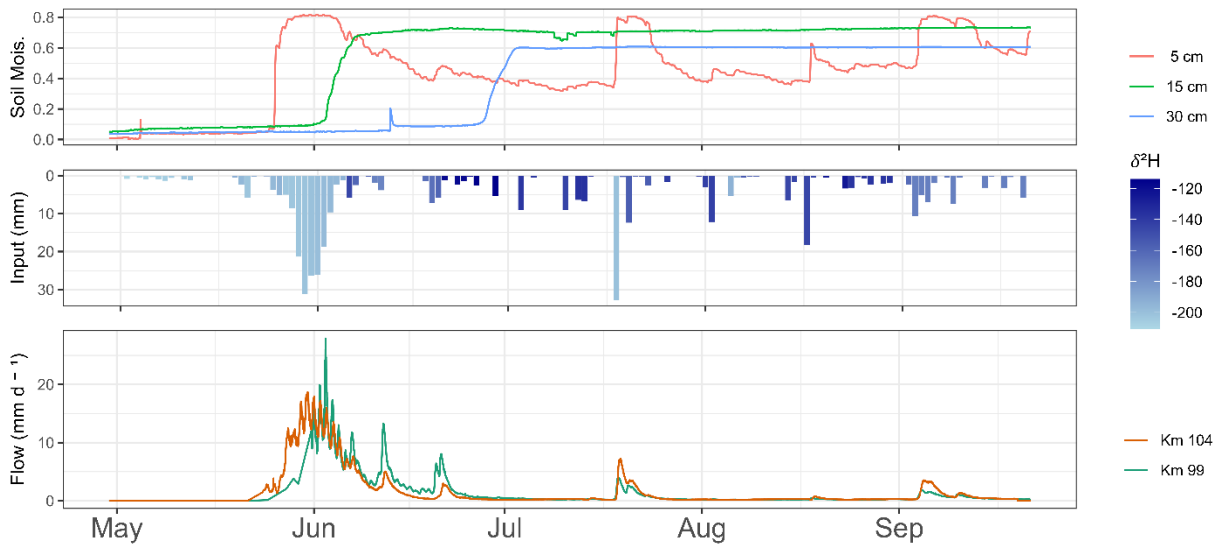

Figure 4.3. Time series of Runoff, Soil Moisture, and Input (Rain + Snowmelt) data used at Km 99. The hydrograph from Km 104 is also included in this plot. Soil moisture was measured at the Met tower. A near zero soil moisture indicates the soil was frozen.

4.3.2 Mixing Analysis

Mixing analyses were performed using volume weighted δ^2H and $\delta^{18}O$ values from 2022, which were similar to previous years. Results indicate over 90% of discharge was snow water during freshet for both basins (Figure 4.4). Streamflow became rain dominant in both catchments by July, contributing over 75% of flows by September (Figure 4.5). During summer and fall event flows, the hydrograph had a greater proportion of rainwater than during pre-event baseflow in both basins. The uncertainty in the proportion of end member contributions were generally lower during freshet when compared to later in the year. Peak SWE was approximately 190 mm for both basins, and Km 99 had 157 mm +/- 17 mm leave as runoff compared to and 153 mm +/- 21 mm at Km 2014, suggesting approximately three quarters of snowmelt water exited as runoff. Conversely, less than 70 mm of runoff (<30%) was composed of rain water in both basins. Considering nearly 250 mm of rain fell on each basin in 2022, the mixing results indicate that most rainwater left as ET and/or entered soil storage.

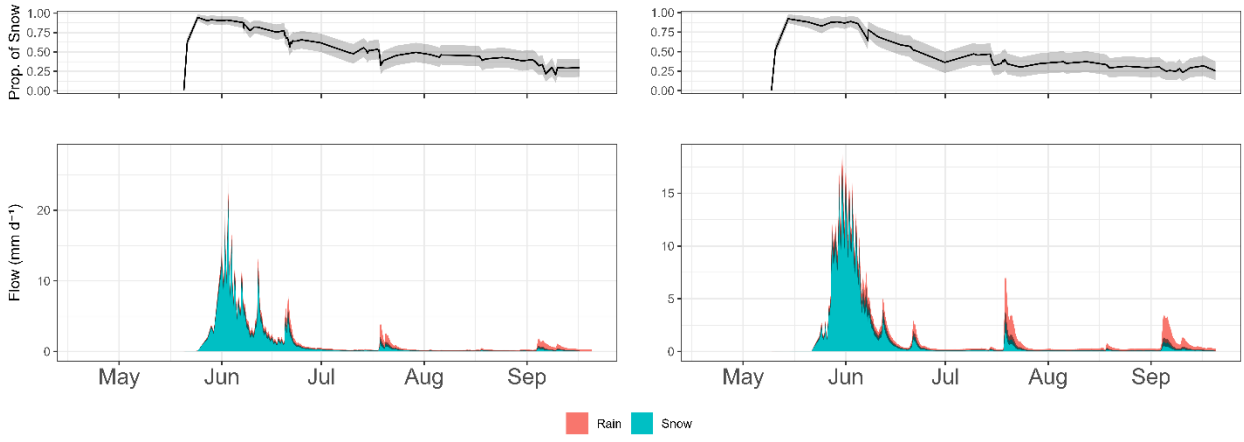

Figure 4.4. End-member mixing results from Km 99 (left), and Km 104 (right).

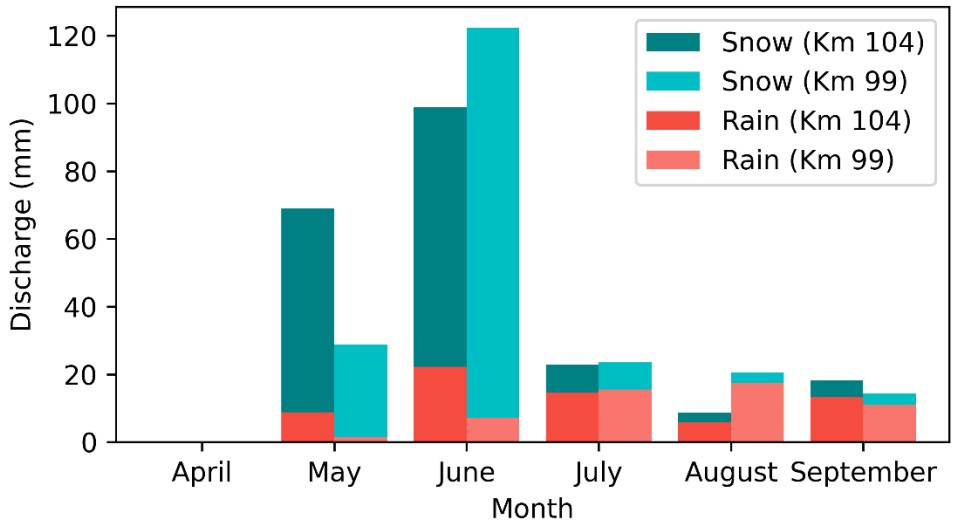

Figure 4.5. Monthly estimates of total volume of snow and rain components of discharge in both Km 99 and Km 104.

4.3.3 SAS Framework

As we did not measure the tracer concentrations of ET, we estimated parameters for the ET SAS function and calibrated the Q SAS function using stream tracer data. The downhill simplex algorithm was used to find the parameter set for the SAS function for Q, for which the simulated tracers from the SAS framework best match the observed stream tracer data. This process was repeated for several plausible parameters sets for the ET SAS function (Table 4.2).

The RMSE for the SAS function of Q was the lowest for Km 99 when $\alpha_{ET} = 0.03$ and $\beta_{ET} = 10$ was assumed for the ET SAS function, a distribution that approached the last in first out (LIFO) distribution, indicating the youngest water was preferentially

selected by ET from storage. Model performance declined as the SAS function for ET moved away from LIFO and increased again as it approached a First In First Out (FIFO) distribution, although RMSE was still greater than LIFO. Additionally, newer water was often found near the surface, where it was more subject to evaporation, particularly in regions where vegetation typically has shallow root depth. Thus, we assume the LIFO SAS function for ET is reasonable in our catchments. This means that ET will be composed of the youngest water available in storage at a given time.

When the SAS function for ET was set as LIFO, the weighted SAS function for Q that best simulated observed stream tracer data in Km 99 had parameters $\alpha_1 = 7.38$, $\beta_1 = 36.09$, $\alpha_2 = 1.45$, $\beta_2 = 2.18$, and $Q_C = 0.22$ (RMSE=3.99). The RMSE for Km 104 was the lowest (4.28) when the weighted SAS function for discharge had parameters $\alpha_1 = 3.86$, $\beta_1 = 11.63$, $\alpha_2 = 7.71$, $\beta_2 = 2.51$, and $Q_C = 5.23$. The simulated tracer values generally fit the observed data at both sites (Figure 4.6).

Table 4.2. RMSE for the best fitting SAS function for discharge using a downhill simplex algorithm with several SAS functions for ET. As the α increases and/or β decreases, greater proportion of old water is selected. When both α and β are 1, the distribution would be uniform.

α_{ET}	β_{ET}	RMSE
0.03	10	3.99
0.5	10	5.05
1	10	6.48
1	5	7.5
1	1	6.84
10	0.03	5.43

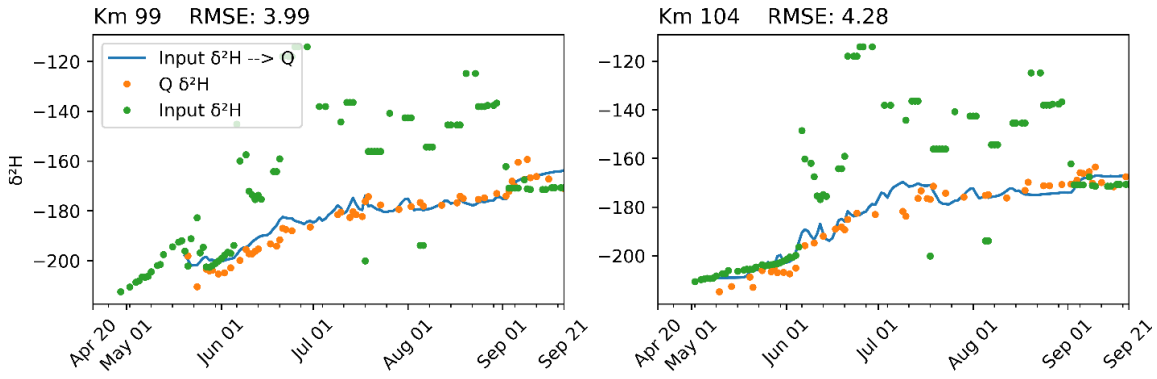

Figure 4.6. Points indicate the observed deuterium concentrations for J and Q, while the blue line indicates the simulated tracer concentrations from the SAS fit with the lowest RMSE.

The contribution of old water, defined as water stored in the basin over-winter, to the hydrograph was considerable in both basin after freshet (Figure 4.7b). Nearly 100% of discharge was composed of old water in Km 104 in early July. The contributions from old water generally increased during summer events for both basins. SAS functions for both basins indicated that much of the youngest water in storage was not selected for discharge (Figure 4.7c; Figure 4.7d). During high flows discharge was selected from a greater range of ages for both basins. During low flows, neither the youngest nor the oldest flows from 2022 were selected for discharge at Km 99 however, the oldest water from 2022 was selected for Km 104 during low flows. A conceptual description (Figure 4.8) is provided

of how to interpret the SAS results from Figure 4.7

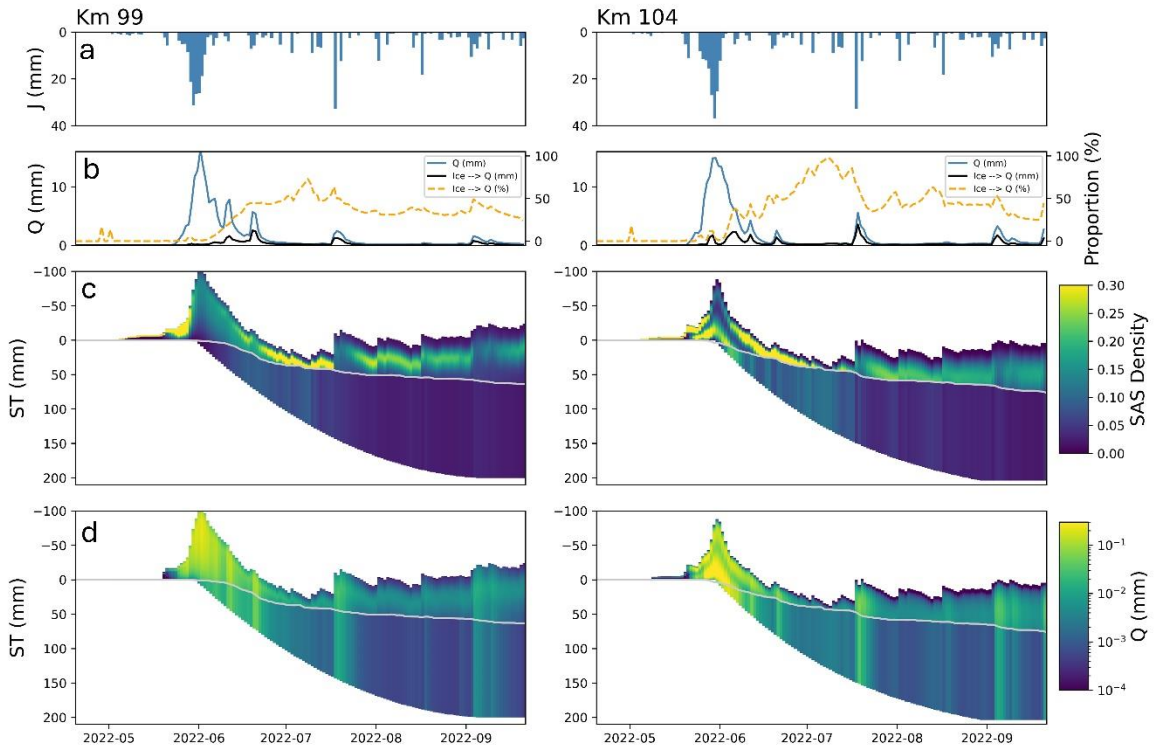

Figure 4.7. Results from SAS framework for Km 99 and Km 104 at the daily timestep. **Row a** shows snowmelt + rain for both catchments. **Row b** shows the hydrograph of both catchments overlain with the hydrograph of old water contributions (ground ice) determined from the SAS framework. The dotted yellow line indicates the proportion of old water contributions. **Row c** shows the SAS function for Q for both catchments. The height of the colour bars represents the amount of storage in the basin. Increases in storage via thaw mobilization was added to the bottom (positive number) and increases in storage via the water balance was added to the top (a negative number). The storage is age ranked where the youngest water in storage is closest to the top and the oldest water is at the bottom. The color of the bars represents the proportion of age ranked storage in the catchment contributing to flow (SAS function for Q). The grey line is the threshold below which all storage is considered old water, variability below the grey line is meaningless but the total amount of storage selected below this line has meaning. As storage from various age ranks are lost to ET and Q, the bars collapse downwards. **Row d** is the same as row c except the colors represent the amount of volume of storage contributing to discharge, which is determined by the product of SAS function for Q and Q.

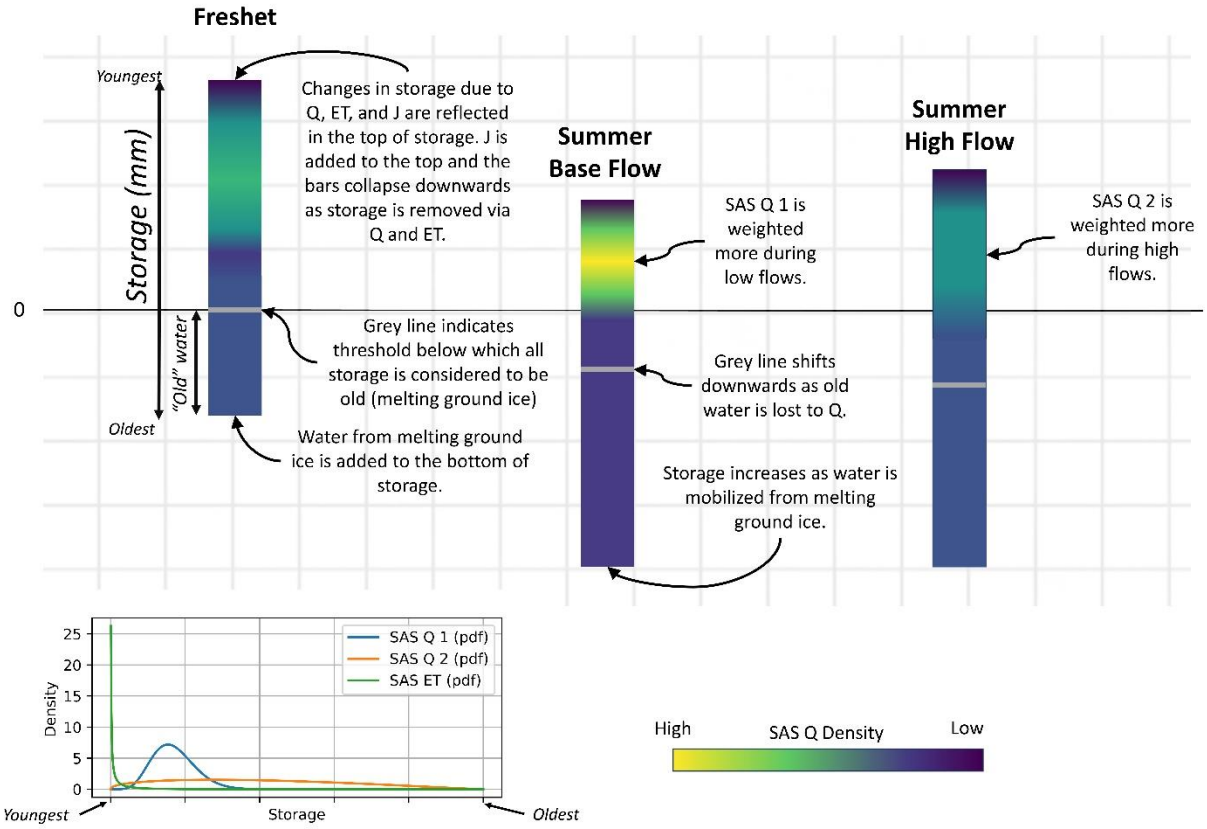

Figure 4.8. Conceptual figure as a primer for figure 4.7. Bottom left line graph displays the two SAS functions for Q along with the SAS function for ET for Km 99. The length of the bar represents total storage (mm). The water in storage is ranked by age (youngest at the top and oldest at the bottom). The colors represent the parts of storage that are contributing to discharge at a particular timestep. SAS Q 1 and SAS Q 2 represent the two weighted components of the composite SAS function for Q.

4.3.4 Fraction of Young Water

Discharge weighted and non-discharge weighted young water fractions and their respective age thresholds showed much of the streamflow was younger than 22-26 days (Table 4.3). The non-discharge weighted F_{yw} for Km 99 had the lowest fraction of young water (42%) with a threshold age of 26 days. The flow weighted young water fraction for Km 99 was the highest with 73% of the total volume of streamflow being younger than 22 days. We compared young water fractions extracted from the SAS framework and

from sine-wave fitting and found the values were within 13% of each other regardless of the basin or flow weighting. Our results suggest that F_{yw} provides an appropriate estimation of age dynamics in these northern catchments where high-quality hydrological data is often limited.

Table 4.3. F_{yw} results for Km 99 and Km 104. Both flow weighted and non-flow weighted fractions were calculated using sine-wave fitting and the SAS framework.

Site	Age Threshold	Period	Flow Weighted	F_{yw} (Sine Fitting)	Fyw (SAS)
Km 99	26 days	~170 days	No	0.42 +/- 0.04	0.55
Km 99	22 days	~170 days	Yes	0.72 +/- 0.04	0.73
Km 104	24 days	~170 days	No	0.62 +/- 0.04	0.55
Km 104	23 days	~170 days	Yes	0.6 +/- 0.04	0.71

4.4 DISCUSSION

Storage and release of water and by extension water age in permafrost underlain catchments is highly seasonal due to large annual variability in radiation and temperature that control precipitation inputs and frozen ground status. While cold region runoff processes have historically been conceptualized from globally sparse yet intense field observations, there has been limited work on water ages and sources. As the cryosphere declines, shifts in water ages and sources may provide a valuable metric to understand and evaluate future catchment hydrometric and chemical response, which are changing for large arctic rivers (Tank et al., 2016, 2023).

4.4.1 Rapid transmission of young water during freshet

Mixing results indicate much of the snowmelt water leaves the basin during freshet and does not mix with older water stored in the catchment over-winter (Figure 4.4, 4.5). As soils freeze the previous fall, ice content in the active layer is large, restricting meltwater infiltration into soils and mixing with over winter storage, and encourages rapid transmission of water to the stream through the very shallow active layer. Other mechanisms to explain this may be that extremely cold soils freeze meltwater either at the surface (Woo et al., 1982) or in the upper pores soon after infiltration (Woo and Heron, 1981) creating impeding layers to further recharge, warming the active layer through the release of latent heat, and directing meltwater to the stream. Our results are similar to Cooper *et al.* (1991) who found the majority of discharge during freshet was event water in a small arctic headwater catchment with organic soils completely frozen to the near surface and McNamara *et al.* (1997) who observed at the headwater scale, event-water predominated during all seasons yet declined in influence as scale increased. In contrast, other permafrost-underlain catchments have been found to have large quantities of pre-event water contributions to discharge that can vary as freshet progresses (Obradovic and Sklash, 1986; Carey and Quinton, 2004; Kershaw et al., 2022). In porous, coarse grained, and/or warmer soils with less frozen pore space, infiltrating meltwater may mix and as the active layer thaws, a greater old-water contribution to the stream is observed (Carey and Quinton, 2004). Significant contributions from groundwater springs have also been proposed as mechanisms for greater pre-event water during freshet in permafrost environments (Kershaw et al., 2022). Metcalfe and Buttle (2001) suggested that snowmelt

rate/timing and storage on hillslopes and in frozen soils play an important role in determining mixing and the proportion of event water during freshet. In Km 99 and 104 where soils were completely frozen, presumably there was very little mobile water in the very thin active layer as it thawed, filling pore spaces with melt water and transmitting water through porous soils quickly to the stream. Soil moisture sensor data from Km 99 suggests that soils freeze up near saturation inhibiting deep percolation during melt.

The large contribution of snowmelt water to discharge and its decline throughout the season has important implication for the concept of peak SWE as a control on late season discharge and how climate change will affect flows. In mountain environments, peak SWE can be an important driver for late season flows (Godsey et al., 2014; Jenicek et al., 2016) and are considered critical in sustaining flows under climate warming. In cold mountainous permafrost environments, there is limited mixing of snowmelt into soil storage, and the gradual decline in its importance post-freshet suggests that increases in SWE will likely result in greater freshet discharges and not increase overall storage. Thus, late season flows in catchments where over winter ice content is high, may be more influenced by summer rainfall than more temperate mountain catchments.

4.4.2 High Fraction of Young Water in Discharge

Much of the discharge for both basins was younger than 3-4 weeks (Table 4.3), particularly after volume weighting regardless of the method used (SAS vs Sine-wave fitting). This is in contrast to the findings of Jasechko *et al.* (2016) who found that ~1/3 of all water is younger than 2-3 months in most basins. The limited storage in both basins

due to a relatively thin active layer (particularly during freshet) enhances runoff and decreases transit times of water. In contrast, work in the Qinghai-Tibet Plateau showed much of the discharge to be older than 1.5 months in a continuous permafrost catchment (Song et al., 2017). However, this region has a much deeper active layer (1.3 m – 2.5 m) and negligible winter precipitation compared to our study catchments, potentially increasing transit times.

4.4.3 Ground Ice as an important source of late season flow

Our results indicate that melting ground ice from seasonal active layer thaw is an important source of water for late season discharge. Old water (ground ice) contributions to runoff exceeded 50% at times in both basins according to the SAS framework (Figure 4.7b). Additionally, the cumulative water balance showed storage was negative for much of late June and early July in both basins, even during periods of relatively high discharge (Figure 4.2, 4.3). In contrast, discharge was zero when cumulative storage change (as determined by the water balance; Figure 4.2) was zero at the start of the period (winter) in both basins. This suggests water (ice) from ground thaw contributed directly to mobile storage and discharge. A similar result was found by Piovano *et al.* (2019) who used a spatially distributed tracer based model and found water stored over-winter to be an important source of discharge post freshet in a discontinuous permafrost alpine catchment, also in Yukon, Canada. However, Piovano *et al.* (2019) suggest water in this somewhat warmer catchment was relatively old (median age of 290 days) where this work suggests Km 99 and Km 104 had very young water during freshet that rapidly got older as the open water season progressed. This highlights the large differences in age

that potentially arise as permafrost presence declines and longer and deeper flow paths emerge.

Permafrost degradation typically releases water from melting ground ice at rates and volumes too slow to drastically alter discharge (Arenson et al., 2022), yet active layer thaw releases water quickly and immobilizes considerable water over winter (Roulet and Woo, 1986; Rossi et al., 2022). Studies have shown that melting ground ice in permafrost regions can be a significant component of the water balance (Roulet and Woo, 1986; Zongxing et al., 2016). Organic soils, which are widespread in permafrost regions, have very high porosity and field capacity (Roulet and Woo, 1986) providing potential to store considerable water as ground ice. As much of the late season hydrograph is influenced by ground-ice, we believe late summer rainfall plays a particularly important role in influencing runoff processes post-freshet the following year. However, there have been few investigations to test this assertion in permafrost catchments, yet the growing importance of rainfall on arctic catchments has been documented (Beel et al., 2021).

4.4.4 Discharge drives water age selection

Although reviews of isotopic hydrograph separations have shown a rapid mobilization of pre-event water in streamflow is typical during events despite prompt streamflow response (Buttle, 1994; Kirchner, 2003; Klaus and McDonnell, 2013), the majority of studies using the SAS framework have found an inverse storage effect, where greater proportions of young water is selected from storage by discharge as antecedent storage increases (Harman, 2015, 2019; Benettin et al., 2017; Fang et al., 2019; Piovano

et al., 2020). This suggests that greater proportions of younger water are mobilized during storm events. These seemingly contradictory results arise due to the significantly larger presence of pre-event water compared to event water in storage, as suggested in Waddington et al. (1993). Thus, even in scenarios where greater amounts of younger water is mobilized, the proportion of event water available for mobilization into streamflow is typically much lower than old water. If event water completely mixes with pre-event water in storage, much of the discharge would consist of pre-event assuming the volume of water stored in the catchment is significantly greater than the volume that enters storage during the event.

We found discharge to alter age selection of water in storage, however our results do not conform to the inverse storage effect as the selection of young water does not increase during high flows. Instead, we observe the opposite during high flows, where a greater proportion of old water is selected by discharge from storage. During high flows, the SAS function selects from a larger range of ages in both basins. This suggests that there is greater mixing of storage during high flows rather than preferential selection of younger water. A rising water table along with infiltrating water during events may provide an opportunity for water stored in the previously unsaturated zone (composed of a variety of ages), to mix with the more mobile water stored below the water table. During low flows, SAS functions for discharge show the preference for selection of intermediate ages of water from storage in Km 99 whereas discharge in Km 104 selects intermediate ages and older water (presumably snowmelt) during low flows (Figure 4.7c). This suggests that some melt water enters a component of storage with very slow flow

paths in Km 99. Km 99 is slightly more mountainous, has greater dynamic storage than Km 104 as inferred from the hydrographs (Figure 4.3), and may have deeper flow paths in the upland regions, particularly on south-facing slopes with thicker active layers. The differences could also be explained by the slightly greater uncertainty in the Km 104 water balance. The youngest water in storage does not significantly contribute to runoff of either basin post freshet, likely due to the youngest water being stored near the surface where it is preferentially evaporated and only contributes to discharge if displaced by new precipitation.

4.4.5 ET Selects the Youngest Water in Storage

Our mixing analysis and the water balance indicate ~155 mm of runoff was snow water and there was ~190 mm of snow melt for Km 99. This indicates that approximately 80% of meltwater leaves the basin by late June and hence the majority of ET water is not sourced from snow but instead is sourced from rainwater. We make the assumption that the amount of snow water stored in the catchment over winter that contributes to discharge is similar to the amount of snow water from melt in 2022, which remains in storage at the end of the water year. This assumption is in addition to the ones discussed by Kirchner and Allen (2020), as we only have data for one year. Our SAS results support the claim that ET is primarily composed of rainwater. The SAS function for ET that best reproduced the tracer values in discharge had a LIFO distribution, indicating that only the youngest water in storage is evaporated. Model fit for the SAS function of discharge rapidly declined as the SAS function for ET moved away from LIFO (Table 4.2). This indicates that much of the ET flux consisted of the youngest water in storage. Evaporation

is generally younger than transpiration as much of evaporation typically restricted to the top soil (Wythers et al., 1999; Sprenger et al., 2019; Smith et al., 2020), whereas plants can transpire water of various ages from wherever plant roots can access it (Smith et al., 2020; Nehemy et al., 2021; Jia et al., 2022). For example, (Smith et al., 2020) showed that shrubs preferentially select the water in the shallowest depth during wet conditions in a Scottish headwater catchment but favor water at the 5-15 cm depth during drier conditions. This may imply that shrubs in this catchment also generally transpire younger water, assuming that the water close to the soil surface is younger than the water stored in deeper soil layers. Thus, a LIFO selection function may be a reasonable assumption in subarctic catchments that is overlain with peat and vegetation that has a very shallow root depth. An implication of our findings is that using the LIFO assumption to determine the minimum ET age of a catchment using just a water balance, as shown in Hahm *et al.* (2022), may provide a close approximation of actual ET ages in tundra environments.

4.4.6 Limitations

The SAS framework is sensitive to the uncertainty associated with the water balance, which is generally high, particularly in topographically complex snow-covered catchments. We believe that our measurements of the water balance components are reasonably as; (1) we directly measured ET, which is rare in these environments, (2) we captured pre-freshet and freshet runoff, which is rarely captured in remote permafrost environments (Shogren et al., 2024), (3) both catchments had relatively homogeneous

land cover reducing the potential spatial variability of SWE and energy fluxes, and (4) we were able to constrain the water balance in both catchments. Additionally, SWE along with its associated tracer concentrations can be highly variable across space (Noor et al., 2023), adding uncertainty to the analysis that cannot be easily quantified.

Our estimation of storage mobilization would have high uncertainty as soil moisture may have high spatial variability, we argue that the calibration of the SAS function of Q would counter our estimation to some degree. For example, if we overestimated the amount of water mobilized in our basins, the SAS function would select less water from the old water component. If we underestimated the amount of old water in storage, the SAS function would select more water from the old component. Thus, our interpretations from the SAS framework would be less sensitive to uncertainty in thaw mobilization than other components of the water and tracer mass balance.

4.5 CONCLUSION

Characterization of catchment storage and release processes provides first order information on runoff and biogeochemical processes. Enhancing our understanding of these processes informs predictions on how catchments will respond to climate change, which is of particular concern in high latitude permafrost systems that are subject to permafrost thaw. To advance our understanding, we conducted a detailed characterization of water age dynamics in two headwater permafrost-underlain catchments which to our knowledge has not previously occurred. We used end-member mixing, young water fractions, and StorAge Selection functions and the major findings of this study are:

1. There was rapid transmission of snow water due to limited mixing with immobile (frozen) storage during freshet.
2. The fraction of young water in discharge of these basins is much greater than most other catchments due to a relatively thin active layer.
3. Ground ice is a significant source of runoff post freshet.
4. We found evidence of storage mixing during high flows and did not observe the inverse storage effect. Instead, we observed a more uniform selection during high antecedent wetness.
5. Our results indicate the ET flux was likely composed of the youngest water in storage due to the presence of peat soils with high storage capacity and limited shallow rooting depth of tundra vegetation. This implies much of the snow left the basins as runoff whereas rain water was the source of ET.

The short transit times observed in these permafrost catchments has important implications for stream chemistry as rapid travel reduces contact between water and mineral/organic surfaces (Benettin et al., 2015), particularly during freshet. As permafrost thaws, we expect water sources to shift, chemistry to change, and water ages to increase. Greater supra-, intra-, and sub-permafrost connectivity along with changes to precipitation will alter water flow pathways and ages with uncertain outcomes at larger scales. We advocate for continued work on transit times and water ages, which are a critical aspect of the hydrological cycle rarely considered. Finally, we urge for sustained and expanded research at the headwater scale in remote cold environments as this is where our process understanding emerges.

ACKNOWLEDGEMENTS

We thank Calvin Newbery, Andras Szeitz, Aliana Fristensky, David Barrett, and Tyler de Jong for field assistance. We thank Amanda Harrison and Sarah Ariano for feedback and suggestions on the conceptual figure used in this manuscript.

CHAPTER 5

5.1 CONCLUSIONS

High latitude regions are rapidly warming, leading to permafrost degradation, changes in phase, timing, and magnitude of precipitation, and vegetation expansion. These changes are expected to dramatically alter hydrological and biogeochemical processes. Furthermore, there are limited field based hydrological and biogeochemical studies in these environments, largely due to logistical constraints associated with studying cold remote regions.

The overall objective of this thesis is to advance our understanding of seasonality of hydrological and biogeochemical processes to better predict how northern environments will respond to changes in precipitation regimes and permafrost extent induced by climate warming. Chapter 2 uses synoptic sampling over a variety of seasons and flow states in a mesoscale heterogeneous catchment to address how seasonality alters spatial patterns of discharge and solute export. Chapter 3 uses grab samples of chemistry across several permafrost underlain catchments to identify the drivers of seasonality of stream chemistry. Chapter 4 uses a robust hydrological and meteorological dataset to quantify water age dynamics in two headwater catchments underlain with continuous permafrost.

Results from Chapter 2 showed that despite high seasonality in discharge and chemistry, the relative contributions of subcatchments remains similar year-round in the Wolf Creek Research Basin. Spatial patterns of discharge and chemistry were highly

stable, despite strong seasonal trends in both discharge and chemistry. The high spatial variability of stream discharge and chemistry suggests that catchment biophysical heterogeneity is critical to understanding hydrological and biogeochemical processes in cold mountainous environments.

Results from Chapter 3 indicated that permafrost extent was a key driver for seasonal variability of major ions, where greater permafrost extent lead to stronger seasonal patterns of major ion concentrations in streams. However, permafrost extent was not strongly linked to the seasonal pattern of DOC concentrations. Instead, topography was more important for seasonality of DOC as freshet led to a rapid depletion of OC stores in the thinner organic layer of mountain soils. We found the seasonal decline of DOC to be driven by depletion of solute stores and a seasonal increase of major ions to be primarily driven by deepening of flow paths due to active layer thaw and decreases in discharge.

In Chapter 4, linking the water balance with the mixing analysis revealed that much of the discharge occurred over the span of 3 weeks and was primarily composed of snow water in both catchments. Most of the snowmelt water left as runoff in both basins whereas the rainfall water left the basins as ET. The SAS framework revealed that much of the post freshet hydrograph was composed of melting ground ice from the thawing active layer. Additionally, the youngest water did not leave as discharge except during very high flows, indicating that recent rainfall was disconnected from the stream and does not mix with the majority of older water in storage. During summer events, storage

became more mixed and led to a more uniform SAS function. The SAS framework revealed that the high field capacity of organic soils and/or shallow root depth of vegetation likely lead to the youngest water from storage to be selected by ET. The short and largely atypical transit times in these permafrost catchments has important implications for runoff processes and stream chemistry. The fast transit times, particularly during freshet, will limit contact time between the water and organic sources. The ground ice content during freshet may have crucial influence on recharge and thus late season flows in these basins.

Our results show that seasonal processes such as active layer thaw, precipitation phase and timing, depletion of OC stores have a strong influence on runoff and biogeochemical cycling. However, this seasonality may not override the high spatial heterogeneity often found in mountain environments. Changing precipitation patterns and permafrost degradation will alter seasonality in water storage/release, and biogeochemical cycling. Results of this thesis have provided detailed information of the seasonality of runoff and biogeochemical processes in high latitude systems. This thesis was the first attempt at characterizing spatial patterns of stream chemistry and discharge across multiple seasons in a high latitude catchment. This thesis also makes one of the first attempts to disentangle multiple drivers of seasonal stream chemistry, and it identifies the catchment characteristics which drive these patterns. Lastly, this work presents the first detailed characterization of water age dynamics, and thus water storage, mixing, and release processes in catchments underlain by continuous permafrost.

These results highlight the need for more long term and intensive field-based studies in permafrost environments, particularly in mountainous regions. Although synoptic campaigns incorporated all four seasons, surveys were largely restricted to low flows. Conducting synoptic sampling in Wolf Creek (or other similar catchments) during freshet is logistically challenging, however the characterization of spatial patterns during this period is crucial to understanding arguably the most important hydrological season. In this thesis, we were only able to access the late periods of freshet due to the limited accessibility of Wolf Creek during early and peak freshet. Consistent long-term sampling of stream chemistry, particularly continuous sampling, is severely lacking in permafrost environments. Incorporating techniques such as GAMs with long term sampling may reveal long term changes in biogeochemical processes caused by changes in climate and/or permafrost degradation. Additionally, conducting event based CQ analysis during freshet and incorporating melt rates is a next step to better understand biogeochemical processes in high latitude catchments. Ample opportunities exist to better characterize water age dynamics in cold regions, as our current understanding of water storage and release processes is severely limited in permafrost environments. Long term monitoring with a robust dataset, similar to one presented in this thesis but for multiple years, would markedly improve our understanding of water cycling and potentially biogeochemical cycling. The results presented in Chapter 4 of this thesis were from a single year and we were unable to assess other drivers of water age dynamics such as, peak SWE, melt intensity, catchment wetness before freeze up, and antecedent wetness. A longer-term

dataset similar to the one collected in TWO in 2022 would allow for a deeper understanding of water storage, mixing, and release processes in high latitude catchments.

REFERENCES

Abbott, B.W. et al., 2018, Unexpected spatial stability of water chemistry in headwater stream networks: Ecology Letters, v. 21, p. 296–308, doi:10.1111/ele.12897.

Ala-aho, P., Tetzlaff, D., McNamara, J.P., Laudon, H., Kormos, P., and Soulsby, C., 2017a, Modeling the isotopic evolution of snowpack and snowmelt: Testing a spatially distributed parsimonious approach: Water Resources Research, v. 53, p. 5813–5830, doi:10.1002/2017WR020650.

Ala-aho, P., Tetzlaff, D., McNamara, J.P., Laudon, H., and Soulsby, C., 2017b, Using isotopes to constrain water flux and age estimates in snow-influenced catchments using the STARR (Spatially distributed Tracer-Aided Rainfall–Runoff) model: Hydrology and Earth System Sciences, v. 21, p. 5089–5110, doi:10.5194/hess-21-5089-2017.

Ali, G., Tetzlaff, D., Soulsby, C., and McDonnell, J.J., 2012, Topographic, pedologic and climatic interactions influencing streamflow generation at multiple catchment scales: Hydrological Processes, v. 26, p. 3858–3874, doi:10.1002/hyp.8416.

Arenson, L.U., Harrington, J.S., Koenig, C.E.M., and Wainstein, P.A., 2022, Mountain Permafrost Hydrology—A Practical Review Following Studies from the Andes: Geosciences (Switzerland), v. 12, doi:10.3390/geosciences12020048.

Beel, C.R., Heslop, J.K., Orwin, J.F., Pope, M.A., Schevers, A.J., Hung, J.K.Y., Lafrenière, M.J., and Lamoureux, S.F., 2021, Emerging dominance of summer rainfall driving High Arctic terrestrial-aquatic connectivity: Nature Communications, v. 12, p. 1448, doi:10.1038/s41467-021-21759-3.

Bekryaev, R. V., Polyakov, I. V., and Alexeev, V.A., 2010, Role of polar amplification in long-term surface air temperature variations and modern arctic warming: Journal of Climate, v. 23, p. 3888–3906, doi:10.1175/2010JCLI3297.1.

Benettin, P., Bailey, S.W., Campbell, J.L., Green, M.B., Rinaldo, A., Likens, G.E., McGuire, K.J., and Botter, G., 2015, Linking water age and solute dynamics in streamflow at the Hubbard Brook Experimental Forest, NH, USA: Water Resources Research, v. 51, p. 9256–9272, doi:10.1002/2015WR017552.

Benettin, P., Soulsby, C., Birkel, C., Tetzlaff, D., Botter, G., and Rinaldo, A., 2017, Using SAS functions and high-resolution isotope data to unravel travel time distributions in headwater catchments: Water Resources Research, v. 53, p. 1864–1878, doi:10.1002/2016WR020117.

Biagi, K.M., Ross, C.A., Oswald, C.J., Sorichetti, R.J., Thomas, J.L., and Wellen, C.C., 2022, Novel predictors related to hysteresis and baseflow improve predictions of watershed nutrient loads: An example from Ontario's lower Great Lakes basin: Science of the Total Environment, v. 826, p. 154023, doi:10.1016/j.scitotenv.2022.154023.

Birch, A.L., Stallard, R.F., Bush, S.A., and Barnard, H.R., 2021, The influence of land cover and storm magnitude on hydrologic flowpath activation and runoff generation in steep tropical catchments of central Panama: Journal of Hydrology, v. 596, p. 126138, doi:10.1016/j.jhydrol.2021.126138.

Birkel, C. et al., 2020, Headwaters drive streamflow and lowland tracer export in a large-scale humid tropical catchment: Hydrological Processes, v. 34, p. 3824–3841,

doi:10.1002/hyp.13841.

Birkel, C., Correa Barahona, A., Duvert, C., Granados Bolaños, S., Chavarría Palma, A., Durán Quesada, A.M., Sánchez Murillo, R., and Biester, H., 2021, End member and Bayesian mixing models consistently indicate near-surface flowpath dominance in a pristine humid tropical rainforest: Hydrological Processes, v. 35, p. 1–15, doi:10.1002/hyp.14153.

Bonnaventure, P.P., Lewkowicz, A.G., Kremer, M., and Sawada, M.C., 2012, A Permafrost Probability Model for the Southern Yukon and Northern British Columbia, Canada: Permafrost and Periglacial Processes, v. 23, p. 52–68, doi:10.1002/ppp.1733.

Botter, G., Bertuzzo, E., and Rinaldo, A., 2011, Catchment residence and travel time distributions: The master equation: Geophysical Research Letters, v. 38, p. n/a-n/a, doi:10.1029/2011GL047666.

Boucher, J.L., and Carey, S.K., 2010, Exploring runoff processes using chemical, isotopic and hydrometric data in a discontinuous permafrost catchment: Hydrology Research, v. 41, p. 508–519, doi:10.2166/nh.2010.146.

Boyer, E.W., Hornberger, G.M., Bencala, K.E., and McKnight, D.M., 1997, Response characteristics of DOC flushing in an alpine catchment: Hydrological Processes, v. 11, p. 1635–1647, doi:10.1002/(SICI)1099-1085(19971015)11:12<1635::AID-HYP494>3.0.CO;2-H.

Buttle, J.M., 1994, Isotope hydrograph separations and rapid delivery of pre-event water from drainage basins: Progress in Physical Geography, v. 18, p. 16–41,

doi:10.1177/030913339401800102.

Carey, S.K., 2003, Dissolved organic carbon fluxes in a discontinuous permafrost subarctic alpine catchment: Permafrost and Periglacial Processes, v. 14, p. 161–171, doi:10.1002/ppp.444.

Carey, S., and DeBeer, C., 2008, Rainfall-runoff hydrograph characteristics in a discontinuous permafrost watershed and their relation to ground thaw: Proc., Ninth Int. Conf. on Permafrost. Fairbanks, …, p. 233–238, http://www.usask.ca/hydrology/papers/Carey_DeBeer_2008.pdf.

Carey, S.K., and Quinton, W.L., 2005, Evaluating runoff generation during summer using hydrometric, stable isotope and hydrochemical methods in a discontinuous permafrost alpine catchment: Hydrological Processes, v. 19, p. 95–114, doi:10.1002/hyp.5764.

Carey, S.K., and Quinton, W.L., 2004, Evaluating snowmelt runoff generation in a discontinuous permafrost catchment using stable isotope, hydrochemical and hydrometric data: Nordic Hydrology, v. 35, p. 309–324, doi:10.2166/nh.2004.0023.

Carey, S.K., and Woo, M.-K., 1999, Hydrology of two slopes in subarctic Yukon, Canada: Hydrological Processes, v. 13, p. 2549–2562, doi:10.1002/(SICI)1099-1085(199911)13:16<2549::AID-HYP938>3.0.CO;2-H.

Carey, S.K., and Woo, M., 2001a, Slope runoff processes and flow generation in a subarctic, subalpine catchment: Journal of Hydrology, v. 253, p. 110–129, doi:10.1016/S0022-1694(01)00478-4.

Carey, S.K., and Woo, M., 2001b, Spatial variability of hillslope water balance, wolf

creek basin, subarctic yukon: Hydrological Processes, v. 15, p. 3113–3132, doi:10.1002/hyp.319.

Carey, S.K., and Woo, M.K., 2000, The role of soil pipes as a slope runoff mechanism, Subarctic Yukon, Canada: Journal of Hydrology, v. 233, p. 206–222, doi:10.1016/S0022-1694(00)00234-1.

Carroll, R.W.H., Bearup, L.A., Brown, W., Dong, W., Bill, M., and Willlams, K.H., 2018, Factors controlling seasonal groundwater and solute flux from snow-dominated basins: Hydrological Processes, v. 32, p. 2187–2202, doi:10.1002/hyp.13151.

Cohen, J. et al., 2014, Recent Arctic amplification and extreme mid-latitude weather: Nature Geoscience, v. 7, p. 627–637, doi:10.1038/ngeo2234.

Colpron, M., 2022, The Yukon Digital Bedrock Geology compilation, *in* Yukon Exploration and Geology 2021, K.E. MacFarlane (ed.), Yukon Geological Survey, p. 143–159.

Cooper, L.W., Olsen, C.R., Solomon, D.K., Larsen, I.L., Cook, R.B., and Grebmeier, J.M., 1991, Stable Isotopes of Oxygen and Natural and Fallout Radionuclides Used for Tracing Runoff During Snowmelt in an Arctic Watershed: Water Resources Research, v. 27, p. 2171–2179, doi:10.1029/91WR01243.

Creed, I.F. et al., 2015, The river as a chemostat: fresh perspectives on dissolved organic matter flowing down the river continuum (R. Smith, Ed.): Canadian Journal of Fisheries and Aquatic Sciences, v. 72, p. 1272–1285, doi:10.1139/cjfas-2014-0400.

Dinçer, T., Payne, B.R., Florkowski, T., Martinec, J., and Tongiorgi, E., 1970, Snowmelt

runoff from measurements of tritium and oxygen-18: Water Resources Research, v. 6, p. 110–124, doi:10.1029/WR006i001p00110.

Ellehoj, M.D., Steen-Larsen, H.C., Johnsen, S.J., and Madsen, M.B., 2013, Ice-vapor equilibrium fractionation factor of hydrogen and oxygen isotopes: Experimental investigations and implications for stable water isotope studies: Rapid Communications in Mass Spectrometry, v. 27, p. 2149–2158, doi:10.1002/rcm.6668.

Environmental Protection Agency (EPA), 1974, Method 415.1: Organic Carbon, Total (Combustion Or Oxidation).:

Fang, Z., Carroll, R.W.H., Schumer, R., Harman, C., Wilusz, D., and Williams, K.H., 2019, Streamflow partitioning and transit time distribution in snow-dominated basins as a function of climate: Journal of Hydrology, v. 570, p. 726–738, doi:10.1016/j.jhydrol.2019.01.029.

Floriancic, M.G., Fischer, B.M.C., Molnar, P., Kirchner, J.W., and Meerveld, H.J., 2019, Spatial variability in specific discharge and streamwater chemistry during low flows: results from snapshot sampling campaigns in eleven Swiss catchments: Hydrological Processes, p. 1–20, doi:10.1002/hyp.13532.

Fork, M.L., Sponseller, R.A., and Laudon, H., 2020, Changing Source-Transport Dynamics Drive Differential Browning Trends in a Boreal Stream Network: Water Resources Research, v. 56, doi:10.1029/2019WR026336.

Frey, K.E., and McClelland, J.W., 2009, Impacts of permafrost degradation on arctic river biogeochemistry: Hydrological Processes, v. 23, p. 169–182, doi:10.1002/hyp.7196.

Frey, K.E., and Smith, L.C., 2005, Amplified carbon release from vast West Siberian

peatlands by 2100: Geophysical Research Letters, v. 32, p. 1–4, doi:10.1029/2004GL022025.

Godsey, S.E., Kirchner, J.W., and Clow, D.W., 2009, Concentration-discharge relationships reflect chemostatic characteristics of US catchments: Hydrological Processes, v. 23, p. 1844–1864, doi:10.1002/hyp.7315.

Godsey, S.E., Kirchner, J.W., and Tague, C.L., 2014, Effects of changes in winter snowpacks on summer low flows: Case studies in the Sierra Nevada, California, USA: Hydrological Processes, v. 28, p. 5048–5064, doi:10.1002/hyp.9943.

Gu, S., Casquin, A., Dupas, R., Abbott, B.W., Petitjean, P., Durand, P., and Gruau, G., 2021, Spatial Persistence of Water Chemistry Patterns Across Flow Conditions in a Mesoscale Agricultural Catchment: Water Resources Research, v. 57, p. 1–15, doi:10.1029/2020WR029053.

Gu, B., Schmitt, J., Chen, Z., Liang, L., and McCarthy, J.F., 1994, Adsorption and Desorption of Natural Organic Matter on Iron Oxide: Mechanisms and Models: Environmental Science and Technology, v. 28, p. 38–46, doi:10.1021/es00050a007.

Hahm, W.J., Lapides, D.A., Rempe, D.M., McCormick, E.L., and Dralle, D.N., 2022, The Age of Evapotranspiration: Lower-Bound Constraints From Distributed Water Fluxes Across the Continental United States: Water Resources Research, v. 58, p. 1–11, doi:10.1029/2022WR032961.

Hall, F.R., 1971, Dissolved Solids-Discharge Relationships: 2. Applications to Field Data: Water Resources Research, v. 7, p. 591–601, doi:10.1029/WR007i003p00591.

Harman, C.J., 2019, Age-Ranked Storage-Discharge Relations: A Unified Description of

Spatially Lumped Flow and Water Age in Hydrologic Systems: Water Resources Research, v. 55, p. 7143–7165, doi:10.1029/2017WR022304.

Harman, C.J., 2015, Time-variable transit time distributions and transport: Theory and application to storage-dependent transport of chloride in a watershed: Water Resources Research, v. 51, p. 1–30, doi:10.1002/2014WR015707.

Harman, C.J., and Xu Fei, E., 2024, mesas.py v1.0: a flexible Python package for modeling solute transport and transit times using StorAge Selection functions: Geoscientific Model Development, v. 17, p. 477–495, doi:10.5194/gmd-17-477-2024.

Hastie, T., and Tibshirani, R., 1986, Generalized Additive Models: Statistical Science, v. 1, p. 409–435, doi:10.1214/ss/1177013604.

Hinzman, A.M., Sjöberg, Y., Lyon, S.W., Ploum, S.W., and Velde, Y., 2020, Increasing non-linearity of the storage-discharge relationship in sub-Arctic catchments: Hydrological Processes, v. 34, p. 3894–3909, doi:10.1002/hyp.13860.

Hinzman, A.M., Sjöberg, Y., Lyon, S., Schaap, P., and van der Velde, Y., 2022, Using a mechanistic model to explain the rising non-linearity in storage discharge relationships as the extent of permafrost decreases in Arctic catchments: Journal of Hydrology, v. 612, p. 128162, doi:10.1016/j.jhydrol.2022.128162.

Hooper, R.P., 2003, Diagnostic tools for mixing models of stream water chemistry: Water Resources Research, v. 39, p. 1–13, doi:10.1029/2002WR001528.

Hornberger, G.M., Bencala, K.E., and McKnight, D.M., 1994, Hydrological controls on dissolved organic carbon during snowmelt in the Snake River near Montezuma,

Colorado: Biogeochemistry, v. 25, p. 147–165, doi:10.1007/BF00024390.

Jasechko, S., Kirchner, J.W., Welker, J.M., and McDonnell, J.J., 2016, Substantial proportion of global streamflow less than three months old: Nature Geoscience, v. 9, p. 126–129, doi:10.1038/ngeo2636.

Jenicek, M., Seibert, J., Zappa, M., Staudinger, M., and Jonas, T., 2016, Importance of maximum snow accumulation for summer low flows in humid catchments: Hydrology and Earth System Sciences, v. 20, p. 859–874, doi:10.5194/hess-20-859-2016.

Jia, G., Nehemy, M.F., Chen, L., Yu, X., and Liu, Z., 2022, Ephemeral connectivity between trees and groundwater in a temperate forest in China: Journal of Hydrology, v. 610, p. 127887, doi:10.1016/j.jhydrol.2022.127887.

Kaplan, J.O., and New, M., 2006, Arctic climate change with a 2°C global warming: Timing, climate patterns and vegetation change: Climatic Change, v. 79, p. 213–241, doi:10.1007/s10584-006-9113-7.

Karlsen, R.H., Grabs, T., Bishop, K., Buffam, I., Laudon, H., and Seibert, J., 2016a, Landscape controls on spatiotemporal discharge variability in a boreal catchment: Water Resources Research, v. 52, p. 6541–6556, doi:10.1002/2016WR019186.

Karlsen, R.H., Seibert, J., Grabs, T., Laudon, H., Blomkvist, P., and Bishop, K., 2016b, The assumption of uniform specific discharge: unsafe at any time? Hydrological Processes, v. 30, p. 3978–3988, doi:10.1002/hyp.10877.

Kershaw, G.G.L., Wolfe, B.B., and English, M.C., 2022, Characterizing seasonal differences in hydrological flow paths and source water contributions to alpine

tundra streamflow: Hydrological Processes, v. 36, p. 1–15, doi:10.1002/hyp.14775.

Killick, R., Fearnhead, P., and Eckley, I.A., 2012, Optimal detection of changepoints with a linear computational cost: Journal of the American Statistical Association, v. 107, p. 1590–1598, doi:10.1080/01621459.2012.737745.

Killick, R., Haynes, K., and IA, E., 2022, changepoint: An R package for changepoint analysis:, https://cran.r-project.org/package=changepoint.

Kim, M., Pangle, L.A., Cardoso, C., Lora, M., Volkmann, T.H.M., Wang, Y., Harman, C.J., and Troch, P.A., 2016, Transit time distributions and StorAge Selection functions in a sloping soil lysimeter with time-varying flow paths: Direct observation of internal and external transport variability: Water Resources Research, v. 52, p. 7105–7129, doi:10.1002/2016WR018620.

Kim, M., Volkmann, T.H.M., Wang, Y., Meira Neto, A.A., Matos, K., Harman, C.J., and Troch, P.A., 2022, Direct Observation of Hillslope Scale StorAge Selection Functions in Experimental Hydrologic Systems: Geomorphologic Structure and Preferential Discharge of Old Water: Water Resources Research, v. 58, p. 1–27, doi:10.1029/2020WR028959.

Kirchner, J.W., 2003, A double paradox in catchment hydrology and geochemistry: Hydrological Processes, v. 17, p. 871–874, doi:10.1002/hyp.5108.

Kirchner, J.W., 2016, Aggregation in environmental systems-Part 1: Seasonal tracer cycles quantify young water fractions, but not mean transit times, in spatially heterogeneous catchments: Hydrology and Earth System Sciences, v. 20, p. 279–297, doi:10.5194/hess-20-279-2016.

Kirchner, J.W., and Allen, S.T., 2020, Seasonal partitioning of precipitation between streamflow and evapotranspiration, inferred from end-member splitting analysis: Hydrology and Earth System Sciences, v. 24, p. 17–39, doi:10.5194/hess-24-17-2020.

Klaus, J., and McDonnell, J.J., 2013, Hydrograph separation using stable isotopes: Review and evaluation: Journal of Hydrology, v. 505, p. 47–64, doi:10.1016/j.jhydrol.2013.09.006.

Koch, J.C., Dornblaser, M.M., and Striegl, R.G., 2021, Storm-Scale and Seasonal Dynamics of Carbon Export From a Nested Subarctic Watershed Underlain by Permafrost: Journal of Geophysical Research: Biogeosciences, v. 126, doi:10.1029/2021JG006268.

Kusunoki, S., Mizuta, R., and Hosaka, M., 2015, Future changes in precipitation intensity over the Arctic projected by a global atmospheric model with a 60-km grid size: Polar Science, v. 9, p. 277–292, doi:10.1016/j.polar.2015.08.001.

Laudon, H., Spence, C., Buttle, J., Carey, S.K., McDonnell, J.J., McNamara, J.P., Soulsby, C., and Tetzlaff, D., 2017, Save northern high-latitude catchments: Nature Geoscience, v. 10, p. 324–325, doi:10.1038/ngeo2947.

Lehn, G.O., Jacobson, A.D., Douglas, T.A., McClelland, J.W., Barker, A.J., and Khosh, M.S., 2017, Constraining seasonal active layer dynamics and chemical weathering reactions occurring in North Slope Alaskan watersheds with major ion and isotope (δ34SSO4, δ13CDIC, 87Sr/86Sr, δ44/40Ca, and δ44/42Ca) measurements: Geochimica et Cosmochimica Acta, v. 217, p. 399–420,

doi:10.1016/j.gca.2017.07.042.

Leipe, S.C., and Carey, S.K., 2021, Rapid shrub expansion in a subarctic mountain basin revealed by repeat airborne LiDAR: Environmental Research Communications, v. 3, p. 071001, doi:10.1088/2515-7620/ac0e0c.

Leutner, B., Horning, N., and Schwalb-Willmann, J., 2023, RStoolbox: Tools for Remote Sensing Data Analysis:, https://bleutner.github.io/RStoolbox/.

Lewkowicz, A.G., and Ednie, M., 2004, Probability mapping of mountain permafrost using the BTS method, Wolf Creek, Yukon Territory, Canada: Permafrost and Periglacial Processes, v. 15, p. 67–80, doi:10.1002/ppp.480.

Li, L., Knapp, J.L.A., Lintern, A., Ng, G.H.C., Perdrial, J., Sullivan, P.L., and Zhi, W., 2024, River water quality shaped by land–river connectivity in a changing climate: Nature Climate Change, v. 14, doi:10.1038/s41558-023-01923-x.

Lyon, S.W., and Destouni, G., 2010, Changes in Catchment-Scale Recession Flow Properties in Response to Permafrost Thawing in the Yukon River Basin: International Journal of Climatology, v. 30, p. 2138–2145, doi:10.1002/joc.1993.

MacLean, R., Oswood, M.W., Irons, J.G., and McDowell, W.H., 1999, The effect of permafrost on stream biogeochemistry: A case study of two streams in the Alaskan (U.S.A.) taiga: Biogeochemistry, v. 47, p. 239–267, doi:10.1007/BF00992909.

Maloszewski, P., Rauert, W., Trimborn, P., Herrmann, A., and Rau, R., 1992, Isotope hydrological study of mean transit times in an alpine basin (Wimbachtal, Germany): Journal of Hydrology, v. 140, p. 343–360, doi:10.1016/0022-1694(92)90247-S.

McCrystall, M.R., Stroeve, J., Serreze, M., Forbes, B.C., and Screen, J.A., 2021, New

climate models reveal faster and larger increases in Arctic precipitation than previously projected: Nature Communications, v. 12, p. 1–12, doi:10.1038/s41467-021-27031-y.

McGuire, K.J., and McDonnell, J.J., 2006, A review and evaluation of catchment transit time modeling: Journal of Hydrology, v. 330, p. 543–563, doi:10.1016/j.jhydrol.2006.04.020.

McKenzie, J.M., Kurylyk, B.L., Walvoord, M.A., Bense, V.F., Fortier, D., Spence, C., and Grenier, C., 2021, Invited perspective: What lies beneath a changing arctic? Cryosphere, v. 15, p. 479–484, doi:10.5194/tc-15-479-2021.

McKnight, D.M., and Duren, S.M., 2004, Biogeochemical processes controlling midday ferrous iron maxima in stream waters affected by acid rock drainage: Applied Geochemistry, v. 19, p. 1075–1084, doi:10.1016/j.apgeochem.2004.01.007.

McNamara, J.P., Kane, D.L., and Hinzman, L.D., 1998, An analysis of streamflow hydrology in the Kuparuk River Basin, Arctic Alaska: A nested watershed approach: Journal of Hydrology, v. 206, p. 39–57, doi:10.1016/S0022-1694(98)00083-3.

McNamara, J.P., Kane, D.L., and Hinzman, L.D., 1997, Hydrograph separations in an Arctic watershed using mixing model and graphical techniques: Water Resources Research, v. 33, p. 1707–1719, doi:10.1029/97WR01033.

McNamara, J.P., Tetzlaff, D., Bishop, K., Soulsby, C., Seyfried, M., Peters, N.E., Aulenbach, B.T., and Hooper, R., 2011, Storage as a Metric of Catchment Comparison: Hydrological Processes, v. 25, p. 3364–3371, doi:10.1002/hyp.8113.

Metcalfe, R.A., and Buttle, J.M., 2001, Soil partitioning and surface store controls on

spring runoff from a boreal forest peatland basin in North-Central Manitoba, Canada: Hydrological Processes, v. 15, p. 2305–2324, doi:10.1002/hyp.262.

Moncrieff, J., Clement, R., Finnigan, J., and Meyers, T., 2004, Averaging, Detrending, and Filtering of Eddy Covariance Time Series, *in* Handbook of Micrometeorology, p. 7–31.

Moncrieff, J.B., Massheder, J.M., de Bruin, H., Elbers, J., Friborg, T., Heusinkveld, B., Kabat, P., Scott, S., Soegaard, H., and Verhoef, A., 1997, A system to measure surface fluxes of momentum, sensible heat, water vapour and carbon dioxide: Journal of Hydrology, v. 188–189, p. 589–611, doi:10.1016/S0022-1694(96)03194-0.

Morales, K., and Oswald, C., 2020, Water age in stormwater management ponds and stormwater management pond-treated catchments: Hydrological Processes, v. 34, p. 1854–1867, doi:10.1002/hyp.13697.

Musolff, A., Schmidt, C., Selle, B., and Fleckenstein, J.H., 2015, Catchment controls on solute export: Advances in Water Resources, v. 86, p. 133–146, doi:10.1016/j.advwatres.2015.09.026.

Nehemy, M.F., Benettin, P., Asadollahi, M., Pratt, D., Rinaldo, A., and McDonnell, J.J., 2021, Tree water deficit and dynamic source water partitioning: Hydrological Processes, v. 35, doi:10.1002/hyp.14004.

Nicholls, E.M., and Carey, S.K., 2021, Evapotranspiration and energy partitioning across a forest-shrub vegetation gradient in a subarctic, alpine catchment: Journal of Hydrology, v. 602, p. 126790, doi:10.1016/j.jhydrol.2021.126790.

Nicholls, E.M., Clark, M.G., and Carey, S.K., 2023, Transpiration and evaporative partitioning at a boreal forest and shrub taiga site in a subarctic alpine catchment, Yukon territory, Canada: Hydrological Processes, v. 37, p. 1–18, doi:10.1002/hyp.14900.

Noor, K., Marttila, H., Klöve, B., Welker, J.M., and Ala-aho, P., 2023, The Spatiotemporal Variability of Snowpack and Snowmelt Water 18O and 2H Isotopes in a Subarctic Catchment: Water Resources Research, v. 59, p. 1–19, doi:10.1029/2022WR033101.

Obradovic, M.M., and Sklash, M.G., 1986, An isotopic and geochemical study of snowmelt runoff in a small arctic watershed: Hydrological Processes, v. 1, p. 15–30, doi:10.1002/hyp.3360010104.

Obu, J. et al., 2019, Northern Hemisphere permafrost map based on TTOP modelling for 2000–2016 at 1 km2 scale: Earth-Science Reviews, v. 193, p. 299–316, doi:10.1016/j.earscirev.2019.04.023.

Parnell, A.C., Phillips, D.L., Bearhop, S., Semmens, B.X., Ward, E.J., Moore, J.W., Jackson, A.L., Grey, J., Kelly, D.J., and Inger, R., 2013, Bayesian stable isotope mixing models: Environmetrics, v. 24, p. 387–399, doi:10.1002/env.2221.

Pastore, M., and Calcagnì, A., 2019, Measuring distribution similarities between samples: A distribution-free overlapping index: Frontiers in Psychology, v. 10, p. 1–8, doi:10.3389/fpsyg.2019.01089.

Pastore, M., Loro, P., Mingione, M., and Calcagni', A., 2022, overlapping: Estimation of Overlapping in Empirical Distributions:, https://cran.r-

project.org/package=overlapping.

Petrone, K.C., Jones, J.B., Hinzman, L.D., and Boone, R.D., 2006, Seasonal export of carbon, nitrogen, and major solutes from Alaskan catchments with discontinuous permafrost: Journal of Geophysical Research: Biogeosciences, v. 111, p. n/a-n/a, doi:10.1029/2005JG000055.

Piovano, T.I., Tetzlaff, D., Carey, S.K., Shatilla, N.J., Smith, A., and Soulsby, C., 2019, Spatially distributed tracer-aided runoff modelling and dynamics of storage and water ages in a permafrost-influenced catchment: Hydrology and Earth System Sciences, v. 23, p. 2507–2523, doi:10.5194/hess-23-2507-2019.

Piovano, T., Tetzlaff, D., Maneta, M., Buttle, J.M., Carey, S.K., Laudon, H., McNamara, J., and Soulsby, C., 2020, Contrasting storage-flux-age interactions revealed by catchment inter-comparison using a tracer-aided runoff model: Journal of Hydrology, v. 590, doi:10.1016/j.jhydrol.2020.125226.

Pomeroy, J.W., Gray, D.M., Brown, T., Hedstrom, N.R., Quinton, W.L., Granger, R.J., and Carey, S.K., 2007, The cold regions hydrological model: a platform for basing process representation and model structure on physical evidence: Hydrological Processes, v. 21, p. 2650–2667, doi:10.1002/hyp.6787.

Quinton, W.L., and Marsh, P., 1999, A conceptual framework for runoff generation in a permafrost environment: Hydrological Processes, v. 13, p. 2563–2581, doi:10.1002/(SICI)1099-1085(199911)13:16<2563::AID-HYP942>3.0.CO;2-D.

R Core Team, 2022, R: A Language and Environment for Statistical Computing:, https://www.r-project.org/.

Ran, Y. et al., 2022, New high-resolution estimates of the permafrost thermal state and hydrothermal conditions over the Northern Hemisphere: Earth System Science Data, v. 14, p. 865–884, doi:10.5194/essd-14-865-2022.

Rasouli, K., Pomeroy, J.W., Janowicz, J.R., Carey, S.K., and Williams, T.J., 2014, Hydrological sensitivity of a northern mountain basin to climate change: Hydrological Processes, v. 28, p. 4191–4208, doi:10.1002/hyp.10244.

Rasouli, K., Pomeroy, J.W., Janowicz, J.R., Williams, T.J., and Carey, S.K., 2019, A long-term hydrometeorological dataset (1993–2014) of a northern mountain basin: Wolf Creek Research Basin, Yukon Territory, Canada: Earth System Science Data, v. 11, p. 89–100, doi:10.5194/essd-11-89-2019.

Rinaldo, A., Benettin, P., Harman, C.J., Hrachowitz, M., McGuire, K.J., van der Velde, Y., Bertuzzo, E., and Botter, G., 2015, Storage selection functions: A coherent framework for quantifying how catchments store and release water and solutes: Water Resources Research, v. 51, p. 4840–4847, doi:10.1002/2015WR017273.

Rodriguez, N.B., and Klaus, J., 2019, Catchment Travel Times From Composite StorAge Selection Functions Representing the Superposition of Streamflow Generation Processes: Water Resources Research, v. 55, p. 9292–9314, doi:10.1029/2019WR024973.

Ross, C.A., Moslenko, L.L., Biagi, K.M., Oswald, C.J., Wellen, C.C., Thomas, J.L., Raby, M., and Sorichetti, R.J., 2022, Total and dissolved phosphorus losses from agricultural headwater streams during extreme runoff events: Science of the Total Environment, v. 848, p. 157736, doi:10.1016/j.scitotenv.2022.157736.

Rossi, M. et al., 2022, Active Layer and Permafrost Investigations Using Geophysical and Geocryological Methods—A Case Study of the Khanovey Area, Near Vorkuta, in the NE European Russian Arctic: Frontiers in Earth Science, v. 10, p. 1–22, doi:10.3389/feart.2022.910078.

Roulet, N.T., and Woo, M.-K., 1986, Hydrology of a wetland in the continuous permafrost region: Journal of Hydrology, v. 89, p. 73–91, doi:10.1016/0022-1694(86)90144-7.

Seybold, E.C., Fork, M.L., Braswell, A.E., Blaszczak, J.R., Fuller, M.R., Kaiser, K.E., Mallard, J.M., and Zimmer, M.A., 2022, A Classification Framework to Assess Ecological, Biogeochemical, and Hydrologic Synchrony and Asynchrony: Ecosystems, v. 25, p. 989–1005, doi:10.1007/s10021-021-00700-1.

Shatilla, N., and Carey, S., 2019, Assessing inter-annual and seasonal patterns of DOC and DOM quality across a complex alpine watershed underlain by discontinuous permafrost in Yukon, Canada: Hydrology and Earth System Sciences, v. 23, p. 3571–3591, doi:10.5194/hess-23-3571-2019.

Shatilla, N.J., Tang, W., and Carey, S.K., 2023, Multi-year high-frequency sampling provides new runoff and biogeochemical insights in a discontinuous permafrost watershed: Hydrological Processes, v. 37, doi:10.1002/hyp.14898.

Sheng, Y., Smith, L.C., MacDonald, G.M., Kremenetski, K. V., Frey, K.E., Velichko, A.A., Lee, M., Beilman, D.W., and Dubinin, P., 2004, A high-resolution GIS-based inventory of the west Siberian peat carbon pool: Global Biogeochemical Cycles, v. 18, doi:10.1029/2003GB002190.

Shogren, A. et al., 2021a, Multi-year, spatially extensive, watershed scale synoptic stream chemistry and water quality conditions for six permafrost-underlain Arctic watersheds: Earth System Science Data Discussions, p. 1–39, doi:10.5194/essd-2021-155.

Shogren, A.J., Zarnetske, J.P., Abbott, B.W., Grose, A.L., Rec, A.F., Nipko, J., Song, C., O'Donnell, J.A., and Bowden, W.B., 2024, Hydrology Controls Dissolved Organic Carbon and Nitrogen Export and Post-Storm Recovery in Two Arctic Headwaters: Journal of Geophysical Research: Biogeosciences, v. 129, doi:10.1029/2023JG007583.

Shogren, A.J., Zarnetske, J.P., Abbott, B.W., Iannucci, F., Frei, R.J., Griffin, N.A., and Bowden, W.B., 2019, Revealing biogeochemical signatures of Arctic landscapes with river chemistry: Scientific Reports, v. 9, p. 1–11, doi:10.1038/s41598-019-49296-6.

Shogren, A.J., Zarnetske, J.P., Abbott, B.W., Iannucci, F., Medvedeff, A., Cairns, S., Duda, M.J., and Bowden, W.B., 2021b, Arctic concentration–discharge relationships for dissolved organic carbon and nitrate vary with landscape and season: Limnology and Oceanography, v. 66, p. S197–S215, doi:10.1002/lno.11682.

Sillmann, J., Kharin, V. V., Zwiers, F.W., Zhang, X., and Bronaugh, D., 2013, Climate extremes indices in the CMIP5 multimodel ensemble: Part 2. Future climate projections: Journal of Geophysical Research Atmospheres, v. 118, p. 2473–2493, doi:10.1002/jgrd.50188.

Skierszkan, E.K., Carey, S.K., Jackson, S.I., Fellwock, M., Fraser, C., and Lindsay,

M.B.J., 2024, Seasonal controls on stream metal(loid) signatures in mountainous discontinuous permafrost: Science of the Total Environment, v. 908, p. 167999, doi:10.1016/j.scitotenv.2023.167999.

Smith, A.A., Tetzlaff, D., and Soulsby, C., 2020, Using storage selection functions to assess mixing patterns and water ages of soil water, evaporation and transpiration: Advances in Water Resources, v. 141, p. 103586, doi:10.1016/j.advwatres.2020.103586.

Song, C., Wang, G., Liu, G., Mao, T., Sun, X., and Chen, X., 2017, Stable isotope variations of precipitation and streamflow reveal the young water fraction of a permafrost watershed: Hydrological Processes, v. 31, p. 935–947, doi:10.1002/hyp.11077.

Spence, C., Ali, G., Oswald, C.J., and Wellen, C., 2019, An Application of the T-TEL Assessment Method to Evaluate Connectivity in a Lake-Dominated Watershed after Drought: JAWRA Journal of the American Water Resources Association, v. 55, p. 318–333, doi:10.1111/1752-1688.12702.

Spence, C., Kokelj, S.A., Kokelj, S. V, and Hedstrom, N., 2014, The process of winter streamflow generation in a subarctic Precambrian Shield catchment: Hydrological Processes, v. 28, p. 4179–4190, doi:10.1002/hyp.10119.

Sprenger, M. et al., 2019, The Demographics of Water: A Review of Water Ages in the Critical Zone: Reviews of Geophysics, v. 57, p. 800–834, doi:10.1029/2018RG000633.

Staudinger, M., Stoelzle, M., Seeger, S., Seibert, J., Weiler, M., and Stahl, K., 2017,

Catchment water storage variation with elevation: Hydrological Processes, v. 31, p. 2000–2015, doi:10.1002/hyp.11158.

Steer, P., and Woo, M., 1983, Measurement of slope runoff in a permafrost region: Canadian Geotechnical Journal, v. 20, p. 361–365, doi:10.1139/t83-039.

Van Stempvoort, D.R., Spoelstra, J., Bickerton, G., Koehler, G., Mayer, B., Nightingale, M., and Miller, J., 2023, Sulfate in streams and groundwater in a cold region (Yukon Territory, Canada): Evidence of weathering processes in a changing climate: Chemical Geology, v. 631, p. 121510, doi:10.1016/j.chemgeo.2023.121510.

Stewart, B. et al., 2022, Streams as Mirrors: Reading Subsurface Water Chemistry From Stream Chemistry: Water Resources Research, v. 58, p. 1–20, doi:10.1029/2021WR029931.

Stock, B.C., Jackson, A.L., Ward, E.J., Parnell, A.C., Phillips, D.L., and Semmens, B.X., 2018, Analyzing mixing systems using a new generation of Bayesian tracer mixing models: PeerJ, v. 6, p. e5096, doi:10.7717/peerj.5096.

Stockinger, M.P., Bogena, H.R., Lücke, A., Diekkrüger, B., Cornelissen, T., and Vereecken, H., 2016, Tracer sampling frequency influences estimates of young water fraction and streamwater transit time distribution: Journal of Hydrology, v. 541, p. 952–964, doi:10.1016/j.jhydrol.2016.08.007.

Tank, S.E. et al., 2023, Recent trends in the chemistry of major northern rivers signal widespread Arctic change: Nature Geoscience, v. 16, p. 789–796, doi:10.1038/s41561-023-01247-7.

Tank, S.E., Striegl, R.G., McClelland, J.W., and Kokelj, S. V., 2016, Multi-decadal

increases in dissolved organic carbon and alkalinity flux from the Mackenzie drainage basin to the Arctic Ocean: Environmental Research Letters, v. 11, p. 054015, doi:10.1088/1748-9326/11/5/054015.

Tetzlaff, D., Piovano, T., Ala-Aho, P., Smith, A., Carey, S.K., Marsh, P., Wookey, P.A., Street, L.E., and Soulsby, C., 2018, Using stable isotopes to estimate travel times in a data-sparse Arctic catchment: Challenges and possible solutions: Hydrological Processes, v. 32, p. 1936–1952, doi:10.1002/hyp.13146.

Thomas, R.D., and Rampton, V.N., 1982a, Surficial Geology and Geomorphology, Engineer Creek, Yukon Territory:, doi:10.4095/119068.

Thomas, R.D., and Rampton, V.N., 1982b, Surficial Geology and Geomorphology, North Klondike River, Yukon Territory:, doi:10.4095/119397.

Thompson, S.E., Basu, N.B., Lascurain, J., Aubeneau, A., and Rao, P.S.C., 2011, Relative dominance of hydrologic versus biogeochemical factors on solute export across impact gradients: Water Resources Research, v. 47, p. 1–20, doi:10.1029/2010WR009605.

Townsend-Small, A., McClelland, J.W., Max Holmes, R., and Peterson, B.J., 2011, Seasonal and hydrologic drivers of dissolved organic matter and nutrients in the upper Kuparuk River, Alaskan Arctic: Biogeochemistry, v. 103, p. 109–124, doi:10.1007/s10533-010-9451-4.

Van Der Velde, Y., Torfs, P.J.J.F., Van Der Zee, S.E.A.T.M., and Uijlenhoet, R., 2012, Quantifying catchment-scale mixing and its effect on time-varying travel time distributions: Water Resources Research, v. 48, p. 1–13,

doi:10.1029/2011WR011310.

Vickers, D., and Mahrt, L., 1997, Quality Control and Flux Sampling Problems for Tower and Aircraft Data: Journal of Atmospheric and Oceanic Technology, v. 14, p. 512–526, doi:10.1175/1520-0426(1997)014<0512:QCAFSP>2.0.CO;2.

Waddington, J.M., Roulet, N.T., and Hill, A.R., 1993, Runoff mechanisms in a forested groundwater discharge wetland: Journal of Hydrology, v. 147, p. 37–60, doi:10.1016/0022-1694(93)90074-J.

Walvoord, M.A., and Kurylyk, B.L., 2016, Hydrologic Impacts of Thawing Permafrost-A Review: Vadose Zone Journal, v. 15, p. vzj2016.01.0010, doi:10.2136/vzj2016.01.0010.

Wang, S., He, X., Kang, S., Hong, X., Fu, H., Xue, Y., Feng, Z., and Guo, H., 2023, Assessment of streamwater age using water stable isotopes in a headwater catchment of the central Tibetan Plateau: Journal of Hydrology, v. 618, p. 129175, doi:10.1016/j.jhydrol.2023.129175.

Wang, G., Hu, H., and Li, T., 2009, The influence of freeze-thaw cycles of active soil layer on surface runoff in a permafrost watershed: Journal of Hydrology, v. 375, p. 438–449, doi:10.1016/j.jhydrol.2009.06.046.

Webb, E.K., Pearman, G.I., and Leuning, R., 1980, Correction of flux measurements for density effects due to heat and water vapour transfer: Quarterly Journal of the Royal Meteorological Society, v. 106, p. 85–100, doi:10.1002/qj.49710644707.

Webster, A.J., Douglas, T.A., Regier, P., Scheuerell, M.D., and Harms, T.K., 2022, Multi-Scale Temporal Patterns in Stream Biogeochemistry Indicate Linked

Permafrost and Ecological Dynamics of Boreal Catchments: Ecosystems, v. 25, p. 1189–1206, doi:10.1007/s10021-021-00709-6.

Woo, M., and Heron, R., 1981, Occurrence of Ice Layers at the Base of High Arctic Snowpacks: Arctic and Alpine Research, v. 13, p. 225, doi:10.2307/1551198.

Woo, M., Heron, R., and Marsh, P., 1982, Basal Ice in High Arctic Snowpacks: Arctic and Alpine Research, v. 14, p. 251, doi:10.2307/1551157.

Woo, M.-K., and Steer, P., 1986, Runoff Regime of Slopes in Continuous Permafrost Areas: Canadian Water Resources Journal, v. 11, p. 58–68, doi:10.4296/cwrj1101058.

Woo, M.K., and Winter, T.C., 1993, The role of permafrost and seasonal frost in the hydrology of northern wetlands in North America: Journal of Hydrology, v. 141, p. 5–31, doi:10.1016/0022-1694(93)90043-9.

Wood, S.N., 2023, Mixed GAM Computation Vehicle with Automatic Smoothness Estimation:

Wood, E.F., Sivapalan, M., Beven, K., and Band, L., 1988, Effects of spatial variability and scale with implications to hydrologic modeling: Journal of Hydrology, v. 102, p. 29–47, doi:10.1016/0022-1694(88)90090-X.

Wymore, A.S., Larsen, W., Kincaid, D.W., Underwood, K.L., Fazekas, H.M., McDowell, W.H., Murray, D.S., Shogren, A.J., Speir, S.L., and Webster, A.J., 2023, Revisiting the Origins of the Power-Law Analysis for the Assessment of Concentration-Discharge Relationships: Water Resources Research, v. 59, doi:10.1029/2023WR034910.

Wythers, K.R., Lauenroth, W.K., and Paruelo, J.M., 1999, Bare-Soil Evaporation Under Semiarid Field Conditions: Soil Science Society of America Journal, v. 63, p. 1341–1349, doi:10.2136/sssaj1999.6351341x.

Yukon Geological Survey, 2023, Surficial Geology dataset:, https://data.geology.gov.yk.ca/Compilation/33 (accessed January 2024).

Zhi, W., and Li, L., 2020, The Shallow and Deep Hypothesis: Subsurface Vertical Chemical Contrasts Shape Nitrate Export Patterns from Different Land Uses: Environmental Science and Technology, v. 54, p. 11915–11928, doi:10.1021/acs.est.0c01340.

Zhi, W., Li, L., Dong, W., Brown, W., Kaye, J., Steefel, C., and Williams, K.H., 2019, Distinct Source Water Chemistry Shapes Contrasting Concentration-Discharge Patterns: Water Resources Research, v. 55, p. 4233–4251, doi:10.1029/2018WR024257.

Zongxing, L., Qi, F., Wang, Q.J., Song, Y., Aifang, C., and Jianguo, L., 2016, Contribution from frozen soil meltwater to runoff in an in-land river basin under water scarcity by isotopic tracing in northwestern China: Global and Planetary Change, v. 136, p. 41–51, doi:10.1016/j.gloplacha.2015.12.002.

APPENDICIES

APPENDIX A- – Supplementary information for Chapter 2

A.1 Supplementary Figures and Tables

Table A1. Table of catchment characteristics of subcatchments in WCRB. Cluster assignment was determined from k-means cluster analysis of catchment.

Site	Topography				Landcover					Surficial Geology				Cluster
	Mean Elevation (m)	Slope Mean (Deg)	Area (Km^2)	Aspect Mean (Cos Trans)	Forest (%)	Water (%)	Shrub (%)	Tundra (%)	Bare (%)	Fluvial (%)	Lacustrine (%)	Moraine Till (%)	Bedrock (%)	
BB	1678.02	17.8	5.43	-0.23	0	0	29.74	22.99	46.84	0.26	0	59.52	40.22	Alpine Catchments
BB1	1528.55	18.3	19.19	-0.17	0.05	0.14	52.27	22.13	25.26	7.12	0.21	47.51	44.19	Wetland Influenced Catchments
BB2	1631.39	23.5	2.85	-0.37	0	0	33.59	33.65	32.6	0.31	0	33.39	66.3	Alpine Catchments
BB3	1681.47	24.6	2.26	-0.38	0	0	25.19	35.45	39.14	0	0	21.69	78.31	Alpine Catchments
BB4	1769.61	22.3	0.78	0.51	0	0	0.8	7.62	91.44	0	0	25.13	74.87	Alpine Catchments
CL	1463.95	15.5	67.78	-0.01	0.44	2.36	55.42	29.66	11.81	6.12	6.32	62.91	23.78	Downstream Catchment
CL1	1450.04	15.5	72.86	0	1.47	2.2	56.3	28.75	10.99	6.7	6.76	62.37	23.37	Downstream Catchment
GB1	1435.97	12.0	22.93	-0.22	8.03	0.17	54.93	26.64	9.58	6.55	0.13	67.56	25.77	Wetland Influenced Catchments
GB2	1593.99	11.5	8.11	-0.01	0.03	0.41	44.97	29.91	23.86	0.08	0	67.41	32.51	Alpine Catchments
GB3	1855.93	15.5	1.13	0.64	0	0	0.13	5.71	93.73	0	0	4.49	95.51	Alpine Catchments
GC	1618.67	10.9	7.25	0.03	0	0.46	40.54	31.5	26.6	0	0	64.68	35.32	Alpine Catchments
Mary_L	830.32	6.3	16.22	0.09	91.88	3.45	0.5	0.04	3.93	15.98	0	84.02	0	Lowland Lakes and Wetlands
Murray_L	827.43	5.2	5.44	0	89.93	5.09	1.26	0.04	3.43	16.03	0	83.97	0	Lowland Lakes and Wetlands
UCL2	1496.57	14.3	28.76	0.08	0.17	0.58	48.97	40.84	8.88	9.19	4.87	71.66	14.28	Downstream Catchment
UCL3	1511.08	18.9	3.13	-0.03	0	0.44	30.43	60.29	8.07	0	0	83.9	16.08	Wetland Influenced Catchments
UCL4	1677.02	25.2	1.42	-0.55	0	0	35.2	25.52	38.48	0	0	25.91	74.09	Alpine Catchments
UCL6	1552.15	9.2	10.94	0.13	0.01	1.31	29.2	60.38	8.12	11.22	0	83.09	5.69	Wetland Influenced Catchments
UCL7	1504.98	19.5	0.24	-0.58	0	1.21	58.81	39.7	0.27	11.01	0	53.54	35.45	Wetland Influenced Catchments
WC1	1365.88	13.2	150.1	0	16.85	1.41	51.82	21.78	7.8	6.57	6.34	69.12	17.12	Downstream Catchment
WC2	1367.84	13.2	149.6	0	16.6	1.42	51.99	21.86	7.82	6.44	6.37	69.17	17.17	Downstream Catchment
WC3	1382.26	13.2	145.42	0	14.42	1.45	53.47	22.48	7.88	6.01	6.55	68.9	17.67	Downstream Catchment
WC4	1389.02	13.2	142.77	0	12.96	1.48	54.39	22.86	8.02	5.98	6.43	68.81	17.88	Downstream Catchment
WC6	1435.44	13.8	107.37	-0.04	4.87	1.56	55.91	27.29	10.04	7.53	5.74	64.18	22	Downstream Catchment
WC7	1436.03	14.9	84.23	0.01	3.79	1.94	56.29	27.54	10.18	7.82	7.16	63.29	21.03	Downstream Catchment
WCO	1303.65	12.0	169.39	0.02	25.34	1.6	45.96	19.31	7.46	8	5.62	70.46	15.17	Downstream Catchment
WCT1	828.08	6.3	16.93	0.1	91.81	3.51	0.51	0.04	3.95	17.93	0	82.07	0	Downstream Catchment
WCT2	1058.58	8.6	3.12	0.09	78.58	6.75	13.3	1.01	0.05	0.34	0.78	98.88	0	Lowland Lakes and Wetlands
WCT2_1	1106.3	7.4	1.26	0.02	68.84	0.01	29.71	0.85	0	0.85	0	99.15	0	Lowland Lakes and Wetlands
WCT3	1449.76	13.8	2.03	0.57	0	8.13	65.44	12.46	13.98	0	0	58.59	41.41	Wetland Influenced Catchments
WLC1_1	1399.46	10.9	8.33	-0.03	5.76	0.38	62.67	24.43	6.75	20.51	1.35	69.84	8.3	Wetland Influenced Catchments
WLC1_3	1596.68	12.0	1.98	0.2	0	0	35.01	39.16	25.83	0	0	76.79	23.21	Alpine Catchments
WLC1_4	1383.22	10.9	2.12	-0.11	0	0.59	79.1	18.6	1.71	35.67	0	55.77	8.57	Wetland Influenced Catchments
WLO	1425.24	11.5	7.25	0.02	0.23	0.44	64.7	26.87	7.76	23.57	0	66.95	9.49	Wetland Influenced Catchments

Table A2. Table of mean and standard deviation of concentration of solutes for each source group for each survey.

		Mean						SD					
Source	Survey	2H	SpC	DOC	Ca	Sulphate	Mg	2H	SpC	DOC	Ca	Sulphate	Mg
Alpine Catchments	August 26, 2020	-157.4	106.5	1.7	15.1	14.8	3.2	3.1	86.3	0.3	13.4	17.7	3.0
	August 3, 2020	-159.9	129.1	2.0	19.4	18.4	4.6	1.8	94.9	0.2	14.6	16.7	3.8
	September 15, 2021	-162.0	116.3	1.6	17.0	20.0	4.0	1.9	102.0	0.8	15.8	24.2	4.2
	June 29, 2021	-169.6	73.5	1.8	11.4	10.4	2.5	1.7	67.4	0.4	10.6	12.3	2.9
	July 3, 2022	-167.7	76.4	1.5	9.8	10.5	1.8	1.3	63.7	0.5	9.9	11.6	2.2
Lowland Lakes and Wetlands	August 26, 2020	-136.5	398.0	13.9	47.5	60.9	23.6	19.3	110.1	5.7	9.2	50.6	11.3
	August 3, 2020	-132.7	386.7	14.0	42.7	65.1	23.5	12.8	123.7	7.0	7.8	44.8	11.3
	September 15, 2021	-145.9	439.2	12.9	59.0	69.6	24.0	13.8	107.4	5.4	12.8	44.5	9.2
	June 29, 2021	-148.1	403.3	12.8	52.3	63.4	21.8	10.5	83.5	4.7	5.6	40.7	8.3
	July 3, 2022	-154.5	363.3	14.9	43.6	54.2	15.8	8.6	110.0	3.9	9.4	36.9	7.5
Wetland Influenced Catchments	August 26, 2020	-159.6	117.8	3.6	14.7	6.4	3.6	5.6	49.7	2.6	7.6	5.3	1.4
	August 3, 2020	-159.6	108.4	3.7	16.1	6.9	3.9	4.8	45.6	2.5	7.9	6.0	1.3
	September 15, 2021	-162.6	115.4	2.4	16.7	9.0	3.9	5.3	45.1	1.5	8.3	8.2	1.4
	June 29, 2021	-167.1	95.9	3.8	14.6	6.2	3.4	3.1	38.6	2.7	7.1	5.4	1.3
	July 3, 2022	-167.4	85.7	3.9	9.0	4.6	1.6	2.4	37.5	2.4	4.7	4.2	1.0

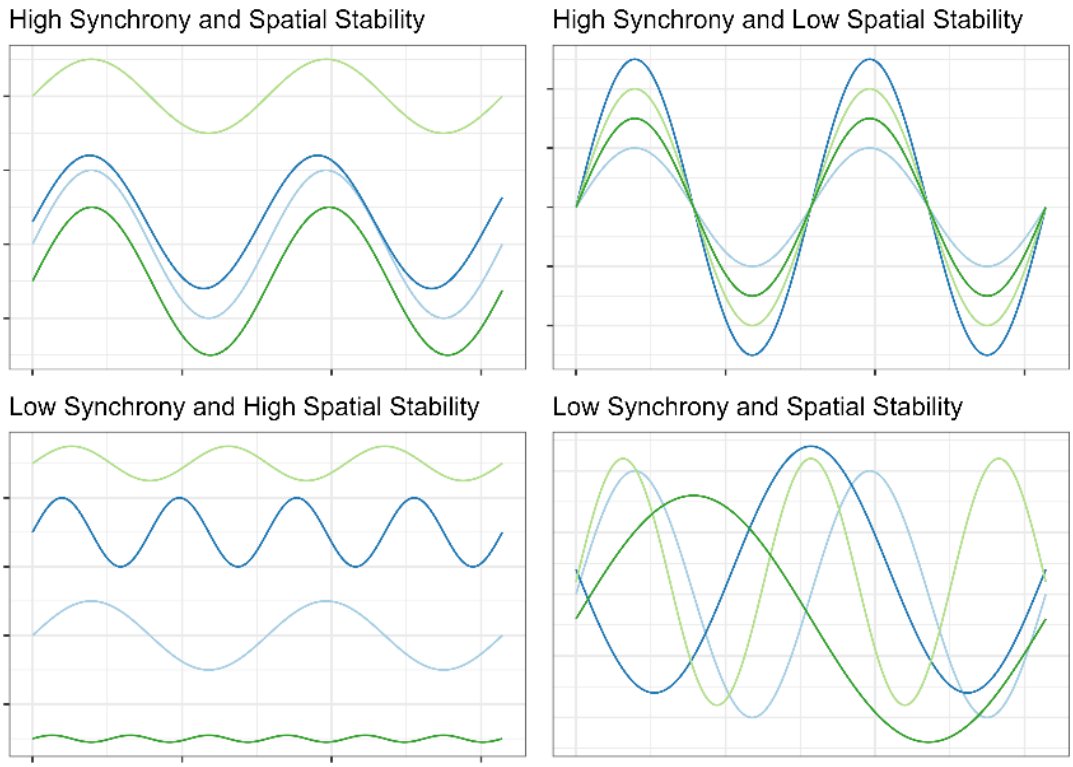

Figure A1. Four hypothetical subcatchments represented by different sine functions. Panels show hypothetical examples of differing degrees of synchrony and stability between two subcatchments. Y-axis represents concentration of solute or magnitude of flow and x-axis represents time. High synchrony and stability can be achieved with high correlation but differing mean concentrations/flow between subcatchments (top-left). High synchrony and low stability can be achieved with high correlation but similar mean or significantly different temporal variance in concentrations/flow between subcatchments (top-right). Low synchrony and high stability can be achieved with low correlation and significantly different mean concentrations/flow between subcatchments (bottom-left). Low synchrony and stability can be achieved with low correlation and similar mean concentrations/flow between subcatchments (bottom-right).

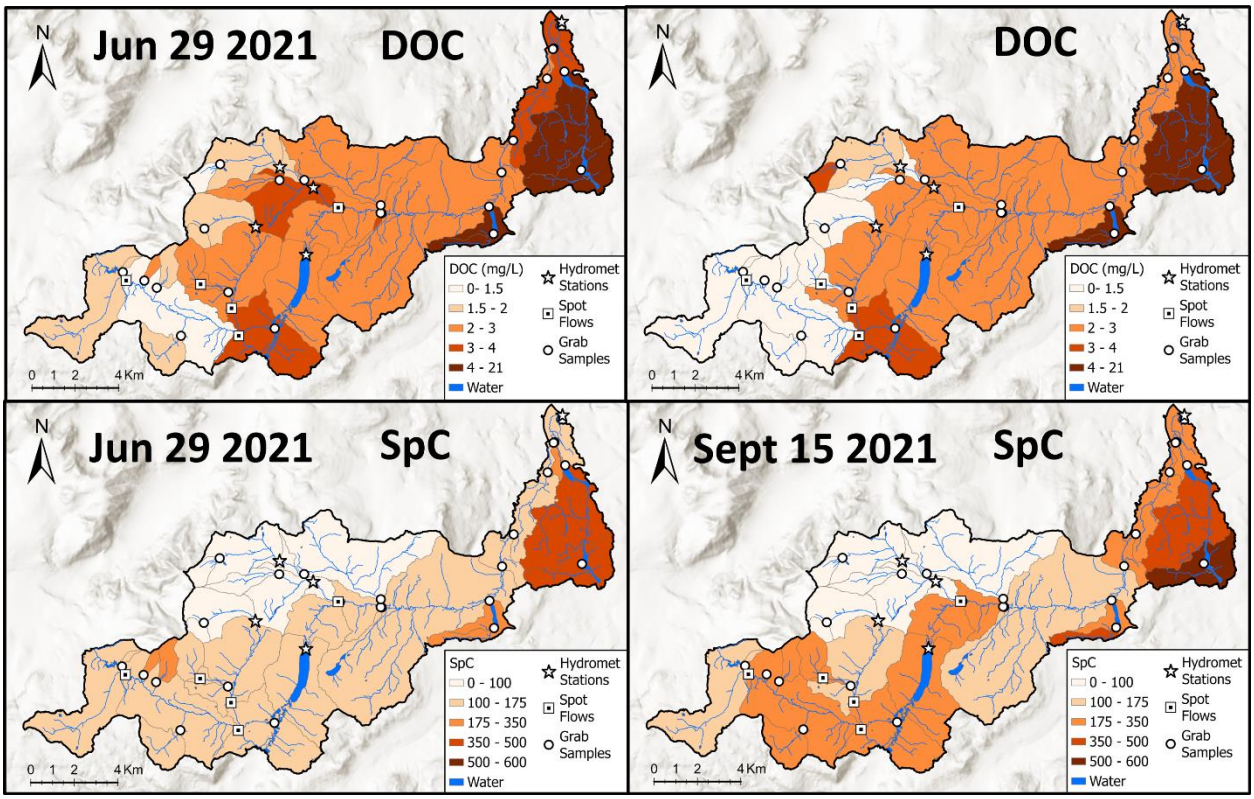

Figure A2. Map with SpC and DOC concentrations for a high (June 29 2021) and low (Sept 15 2021) flow event.

Table A3. Spatial Stability and CV from the five ice-free surveys.

Solute	Spatial Stability	Spatial CV	Spatial Stability σ	Spatial CV σ
Ca^{2+}	0.935	0.658	0.041	0.081
DOC	0.892	1.009	0.013	0.077
Mg^{2+}	0.910	1.139	0.048	0.115
SpC	0.965	0.719	0.011	0.043
Sulphate	0.951	1.422	0.014	0.083

Table A4. Synchrony and Temporal CV from the five ice-free surveys.

Solute	Synchrony	Temporal CV	Synchrony σ	Temporal CV σ
Ca^{2+}	0.600	0.205	0.178	0.093
DOC	0.375	0.156	0.162	0.069
Mg^{2+}	0.703	0.297	0.126	0.137
SpC	0.600	0.154	0.273	0.091
Sulphate	0.476	0.293	0.183	0.374

A.2 Incorporation of Winter Surveys in Analysis

A.2.1 Methods

A.2.1.1 Data Collection

Data collection for the two winter surveys was similar to the ice-free surveys dicussed in the manuscript. Due to limited daylight hours, the winter surveys were conducted over ~1 week. However, changes in discharge was relatively small over this time period. The first winter survey was conducted from February 18 2021 to February 24 2021, the second survey was conducted from March 15 2022 to March 23 2022.

A.2.1.2 Analysis

To incorporate the winter sites, we largely replicated the analysis from the manuscript except we included the sites that were accessible over winter for all surveys (n=17). We also ran the same analysis from the original manucript without the winter surveys but we removed all sites not sampled in the winter surveys. This allowed for the direct analysis of how much winter surveys influenced statistics like spatial stability and temporal synchrony. Additionally, we did not include leverage in this analysis as flows were

difficult to estimate during the winter as all channels were ice covered. For MixSIAR analysis, the same groups were kept but the sample size was lower due to the removed sites. Alpine Catchments (n=4), Lowland lakes and Wetlands (n=2), and Wetland Influenced Catchments (n=4).

A.2.2. Results and Discussion

A.2.2.1 MixSIAR with the Addition of Winter Surveys

Mixing results showed a decline in mean overlap for Lowland Lakes and Wetlands (0.59), and Wetland Influenced Catchments (0.86) after adding winter surveys. However, the lower overlap values were largely driven by greater uncertainty in the posterior distribution of some surveys. The sample size was also considerably lower for the sources when eliminating sites not present in winter surveys.

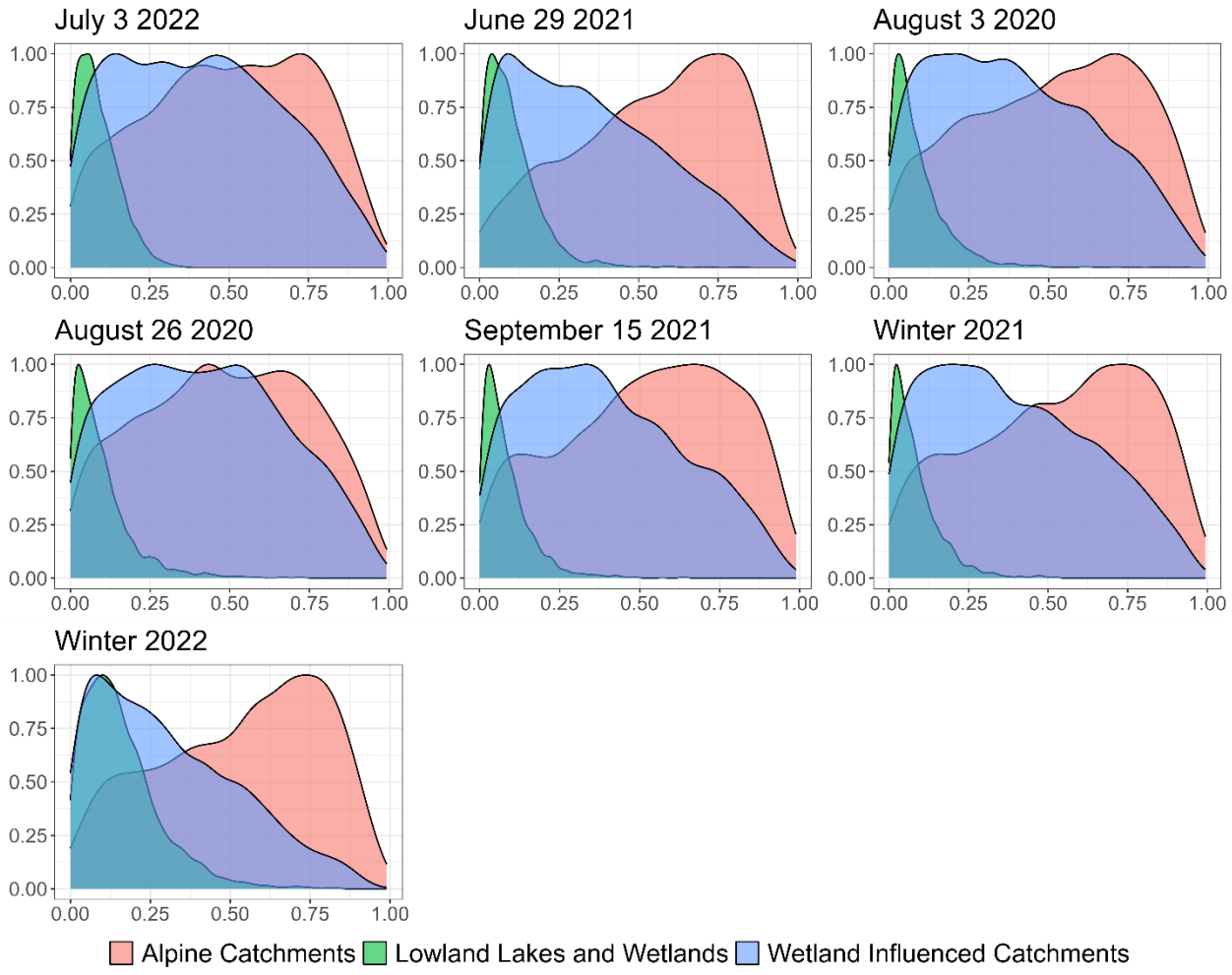

Figure A3 Scaled proportion of contribution of discharge to outlet via MixSIAR for all seven surveys.

Table A5 Overlap results of MixSIAR analysis for all possible combination for each of the three sources. Only sites available in the winter surveys were included for the analysis.

Surveys	Alpine Catchments	Lowland Lakes and Wetlands	Wetland Influenced Catchments
3 Jul 2022 – 29 Jun 2021	0.91	0.95	0.89
3 Jul 2022 - 3 Aug 2020	0.94	0.90	0.93
3 Jul 2022 - 26 Aug 2020	0.89	0.92	0.88
3 Jul 2022 - 15 Sept 2021	0.95	0.88	0.94
3 Jul 2022 - Feb 2021	0.95	0.24	0.71
3 Jul 2022 - Mar 2022	0.97	0.23	0.71
29 Jun 2021 - 3 Aug 2020	0.97	0.90	0.96
29 Jun 2021 - 26 Aug 2020	0.97	0.91	0.98
29 Jun 2021 - 15 Sept 2021	0.95	0.90	0.94
3 Jul 2022 - Feb 2021	0.94	0.20	0.81
3 Jul 2022 - Mar 2022	0.93	0.19	0.80
3 Aug 2020 - 26 Aug 2020	0.94	0.96	0.95
3 Aug 2020 - 15 Sept 2021	0.97	0.96	0.97
3 Jul 2022 - Feb 2021	0.97	0.24	0.78
3 Jul 2022 - Mar 2022	0.96	0.23	0.77
26 Aug 2020 - 15 Sept 2021	0.93	0.93	0.93
26 Aug 2020 - Feb 2021	0.91	0.25	0.81
26 Aug 2020 - Mar 2022	0.91	0.25	0.80
15 Sept 2021 - Feb 2021	0.97	0.22	0.76
15 Sept 2021 - Mar 2022	0.95	0.21	0.75
Feb 2021 - Mar 2022	0.97	0.97	0.97
Mean	0.94	0.59	0.86

A.2.2.2 Stability and Synchrony with the Addition of Winter Surveys

After adding winter surveys, spatial stability ranged from 0.8 (DOC) to 0.95 (Suphate). With SD ranging from 0.001 (Suphate) to 0.05 (DOC). Synchrony ranged from 0.29 (DOC) to 0.84 (Ca), with SD ranging from 0.06 (Mg) to 0.29 (DOC). Spatial CV ranged

from 0.76 (Ca) to 1.28 (Mg), with SD ranging from 0.05 (SpC) to 0.15 (DOC). Temporal CV ranged from 0.28 (DOC) to 0.37 (Mg).

Spatial stability remained relatively similar when winter surveys were removed from analysis, with the exception of DOC (Table A6; A8). DOC concentrations experienced a slight drop in stability, indicating potentially greater reshuffling of patterns in the winter. Indicating no major reshuffling of spatial patterns in the winter. Temporal synchrony significantly increased when winter surveys were included for all solutes except DOC (Table A7; A9). These results indicate that patterns across space were not notably altered in the winter.

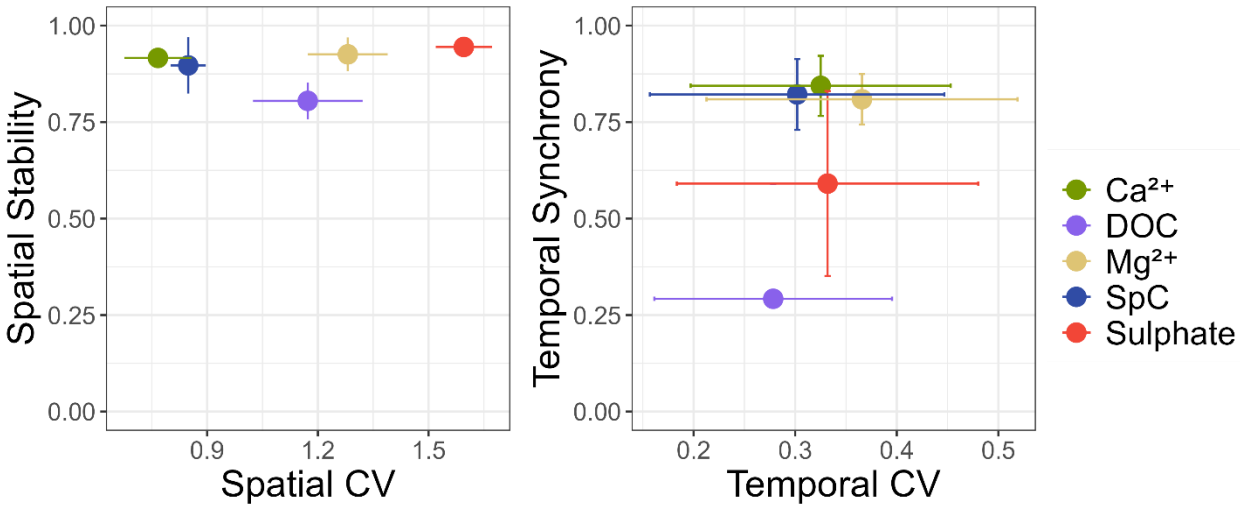

Figure A4. Left panel shows Spatial Stability plotted against Spatial CV. Right panel shows Temporal Synchrony plotted against Temporal CV. Error bars represent standard deviation. Figure includes all seven surveys.

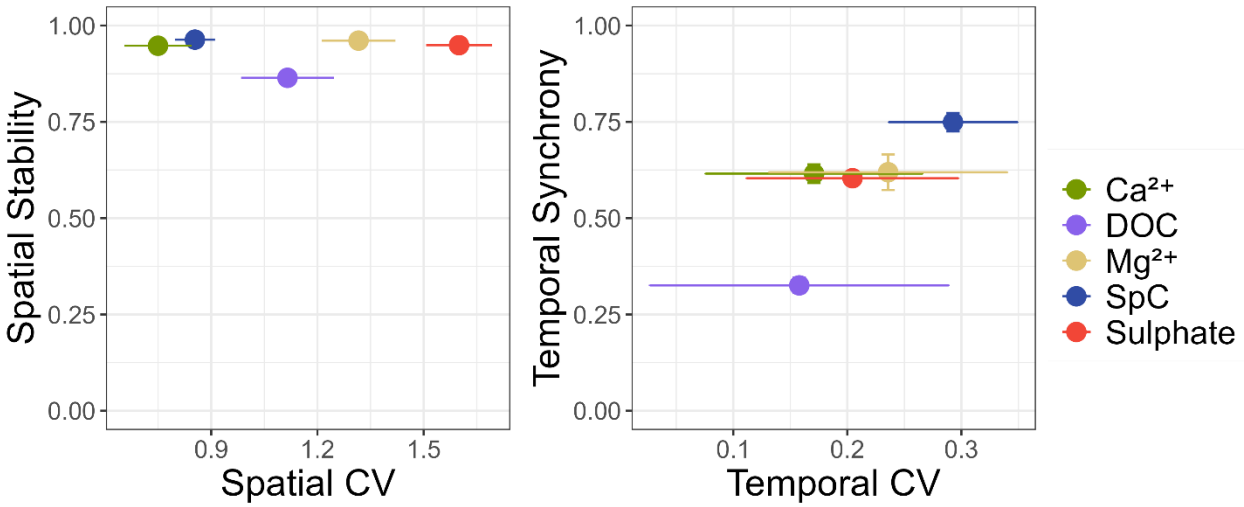

Figure A5. Left panel shows Spatial Stability plotted against Spatial CV. Right panel shows Temporal Synchrony plotted against Temporal CV. Error bars represent standard deviation. Figure includes five ice-free surveys for a subset of sites to enable comparison on the influence of winter surveys.

Table A6. Spatial Stability and CV from all seven surveys. Only the sites available in all seven surveys were used.

Solute	Spatial Stability	Spatial CV	Spatial Stability σ	Spatial CV σ
Ca^{2+}	0.916	0.767	0.025	0.091
DOC	0.805	1.173	0.047	0.148
Mg^{2+}	0.926	1.281	0.044	0.108
SpC	0.897	0.849	0.073	0.048
Sulphate	0.945	1.596	0.010	0.076

Table A7. Synchrony and Temporal CV from all seven surveys. Only the sites available in all seven surveys were used.

Solute	Synchrony	Temporal CV	Synchrony σ	Temporal CV σ
Ca^{2+}	0.844	0.325	0.078	0.128
DOC	0.292	0.278	0.298	0.117
Mg^{2+}	0.809	0.366	0.066	0.153
SpC	0.822	0.302	0.092	0.145
Sulphate	0.591	0.332	0.240	0.148

Table A8. Spatial Stability and CV from a subset of sites from the five ice-free surveys. Only the sites available in all seven surveys were used.

Solute	Spatial Stability	Spatial CV	Spatial Stability σ	Spatial CV σ
Ca^{2+}	0.948	0.750	0.024	0.095
DOC	0.864	1.115	0.020	0.131
Mg^{2+}	0.961	1.316	0.046	0.104
SpC	0.963	0.854	0.024	0.057
Sulphate	0.949	1.600	0.014	0.093

Table A9. Temporal Synchrony and CV from a subset of sites from the five ice-free surveys. Only the sites available in all seven surveys were used.

Solute	Synchrony	Temporal CV	Synchrony σ	Temporal CV σ
Ca^{2+}	0.615	0.171	0.024	0.095
DOC	0.326	0.158	0.020	0.131
Mg^{2+}	0.619	0.236	0.046	0.104
SpC	0.749	0.293	0.024	0.057
Sulphate	0.604	0.205	0.014	0.093

A.3 Estimating Discharge for Subcatchment Leverage

Discharge was estimated for all subcatchments via continuous discharge data, spot discharge menasurements, the assumption of uniform specific discharge, and mixing analysis. Figure A4 shows the decision tree used to estimate flow at all subcatchments in WCRB.

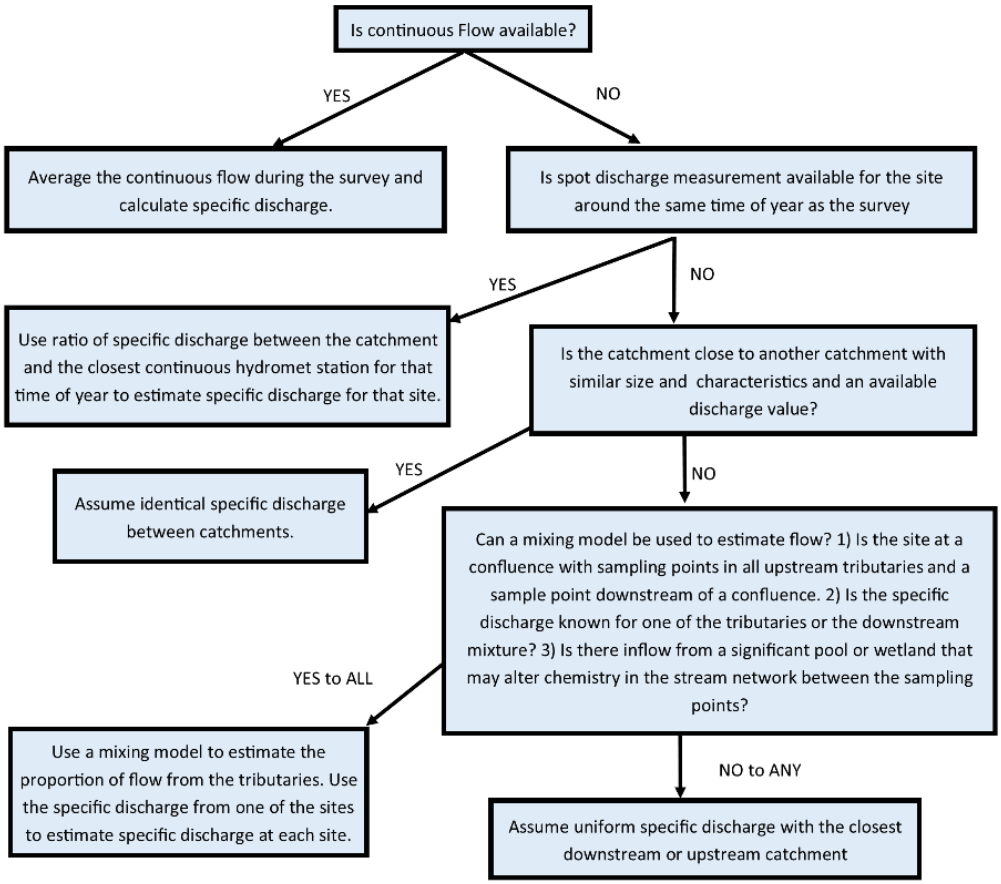

Figure A6. Decision tree used to estimate discharge for all surveys for use in the calculation of subcatchment leverage.

APPENDIX B- – Supplementary information for Chapter 3

B.1 Supplementary Table

Table B1. Summary results from all GAMs

Site	Solute	R^2	b	b SE	p-value (Q)	CV Ratio	edf	p-value (sDOY)	sDOY Range	Mean sDOY SE	n
BB	Ca	0.58	-0.31	0.04	0.00	0.40	1.00	0.003	0.49	0.09	43
CL	Ca	0.63	-0.36	0.05	0.00	0.33	2.90	0.160	0.37	0.11	34
GC	Ca	0.65	-0.37	0.05	0.00	0.36	3.40	0.011	0.40	0.16	79
Km 104	Ca	0.91	-0.10	0.03	0.00	0.33	3.69	0.000	2.14	0.16	28
Km 175	Ca	0.92	-0.26	0.03	0.00	0.33	3.55	0.000	1.22	0.08	39
Km 185	Ca	0.92	-0.17	0.02	0.00	0.29	4.92	0.000	1.70	0.09	35
Km 44	Ca	0.44	-0.12	0.03	0.00	0.23	1.67	0.009	0.39	0.09	43
Km 71	Ca	0.91	-0.33	0.04	0.00	0.53	4.11	0.000	1.36	0.11	35
Km 99	Ca	0.91	-0.30	0.03	0.00	0.31	3.42	0.000	1.41	0.13	47
WCO	Ca	0.50	-0.29	0.04	0.00	0.28	2.62	0.051	0.30	0.10	92
BB	DOC	0.53	0.12	0.06	0.04	0.39	2.82	0.002	0.52	0.17	42
CL	DOC	0.05	-0.01	0.06	0.89	0.40	1.00	0.062	0.32	0.08	34
GC	DOC	0.62	0.31	0.08	0.00	0.98	7.08	0.000	1.15	0.29	80
Km 104	DOC	0.18	-0.04	0.04	0.28	0.21	2.12	0.270	0.44	0.18	28
Km 175	DOC	0.09	0.14	0.07	0.06	0.45	1.00	0.266	0.26	0.12	38
Km 185	DOC	0.78	0.06	0.02	0.03	0.30	5.88	0.000	1.16	0.10	34
Km 44	DOC	0.52	-0.11	0.07	0.09	1.16	3.03	0.000	1.60	0.26	42
Km 71	DOC	0.47	0.10	0.17	0.56	2.04	1.00	0.000	2.35	0.22	34
Km 99	DOC	0.41	0.13	0.05	0.01	0.31	2.28	0.018	0.76	0.18	45
WCO	DOC	0.73	0.20	0.06	0.00	0.71	7.18	0.000	1.19	0.22	92
BB	Mg	0.20	-0.68	0.19	0.00	0.66	1.00	0.098	1.22	0.43	43
CL	Mg	0.66	-0.52	0.07	0.00	0.45	2.62	0.246	0.43	0.14	34
GC	Mg	0.33	-0.74	0.12	0.00	0.49	1.00	0.083	0.95	0.28	79
Km 104	Mg	0.87	-0.10	0.03	0.01	0.35	3.17	0.000	2.23	0.20	28
Km 175	Mg	0.74	-0.44	0.05	0.00	0.43	1.24	0.075	0.33	0.09	39
Km 185	Mg	0.90	-0.20	0.03	0.00	0.32	4.30	0.000	1.73	0.10	35
Km 44	Mg	0.53	-0.17	0.03	0.00	0.27	2.31	0.003	0.54	0.13	43
Km 71	Mg	0.88	-0.36	0.04	0.00	0.49	3.29	0.000	1.16	0.09	35
Km 99	Mg	0.83	-0.35	0.04	0.00	0.30	2.47	0.000	1.19	0.16	47
WCO	Mg	0.73	-0.41	0.03	0.00	0.33	2.61	0.002	0.43	0.09	92
BB	SpC	0.88	-0.23	0.03	0.00	0.33	5.64	0.000	0.59	0.11	42
CL	SpC	0.20	-0.14	0.05	0.02	0.24	1.00	0.365	0.11	0.06	24
GC	SpC	0.88	-0.30	0.03	0.00	0.30	4.69	0.000	0.32	0.09	75

Km 104	SpC	0.91	-0.08	0.02	0.00	0.29	3.66	0.000	1.69	0.15	26
Km 175	SpC	0.89	-0.27	0.02	0.00	0.29	2.05	0.000	0.67	0.06	36
Km 185	SpC	0.93	-0.15	0.02	0.00	0.27	4.78	0.000	1.48	0.08	33
Km 44	SpC	0.80	-0.11	0.01	0.00	0.18	2.07	0.000	0.54	0.05	39
Km 71	SpC	0.39	-0.31	0.10	0.00	0.52	1.00	0.000	1.06	0.12	34
Km 99	SpC	0.94	-0.29	0.02	0.00	0.29	5.30	0.000	1.07	0.13	41
WCO	SpC	0.68	-0.18	0.03	0.00	0.22	4.22	0.000	0.27	0.08	69
BB	Sulphate	0.78	-0.61	0.07	0.00	0.66	4.78	0.000	1.18	0.25	43
CL	Sulphate	0.18	-0.17	0.13	0.22	0.47	1.00	0.017	0.88	0.18	34
GC	Sulphate	0.66	-0.49	0.06	0.00	0.37	4.95	0.000	0.94	0.20	79
Km 104	Sulphate	0.40	-0.17	0.19	0.36	0.45	1.10	0.000	4.99	0.64	28
Km 175	Sulphate	0.86	-0.43	0.03	0.00	0.42	1.50	0.000	0.66	0.08	39
Km 185	Sulphate	0.90	-0.18	0.03	0.00	0.33	4.24	0.000	1.87	0.10	35
Km 44	Sulphate	0.71	-0.24	0.03	0.00	0.31	2.04	0.000	0.81	0.11	43
Km 71	Sulphate	0.86	-0.36	0.04	0.00	0.49	3.20	0.000	1.23	0.10	35
Km 99	Sulphate	0.77	-0.47	0.06	0.00	0.34	1.91	0.000	1.35	0.22	47
WCO	Sulphate	0.74	-0.31	0.03	0.00	0.36	4.24	0.000	0.42	0.11	92

APPENDIX C- – Supplementary information for Chapter 4

C.1 Isosnow

In this study, Isosnow was used to model snowmelt starting mid-April until the end of snowmelt at an hourly timestep. All inputs were assumed to be spatially uniform with the exception of the DEM, incoming solar radiation, SWE, and air temperature. Air temperature was estimated using a calibrated lapse rate (6.35ºC / km) for the two basins and incoming solar radiation was estimated using CRHM and measured incoming radiation from the met tower. Ten HRU's were created using elevation, slope, and cosine transformed aspect. The average slope and aspect were used to estimate potential incoming radiation for each HRU. We converted the potential incoming radiation to

actual incoming radiation by using the ratio of measured and potential incoming radiation at the Met tower and applying the ratio to all other HRUs. Isosnow was run for each basin separately at a 30 m resolution.

Isosnow calibration was conducted using 2,500 Monte Carlo simulations at a 300 m resolution for both basins simultaneously. Values for seven parameters were randomly selected using a uniform distribution. αpow (1 to 2; accounts for decline in albedo of old snow), TTlow (-2 to 0 °C; threshold below which all precipitation is snow), TThigh (0 to 2 °C; threshold above which all precipitation is rain), Tgrad (5 to 7°C Km^{-1}; accounts for the lapse rate of air temperature), pthresh (0.6 to 3 mm, threshold of snowfall above which the snowpack is considered to be zero days old), Efrac (-125 to 0 ‰; parameter which accounts for fractionation during sublimation for δ^2H), and Mfrac (-30 to 0 ‰; parameter which accounts for fractionation during melt for δ^2H). The Efrac and Mfrac ranges were based on ice-vapor and ice-liquid equilibrium difference (Ellehoj et al., 2013). The model was calibrated using five snow surveys measurements (SWE and δ^2H) at four transects (n=20) during melt. Mean absolute error (MAE) for SWE and the isotopic concentration of the snowpack were determined for each simulation. The 25 best runs were selected using the cumulative distribution function (CDF) of the MAE values of SWE and δ^2H concentration of the snowpack. CDF was used to determine a threshold MAE value for both SWE and δ^2H concentration of the snowpack, below which exactly 25 runs are mapped. Methods for run selection are described in detail in Ala-aho *et al.* (2017).

In addition to snow survey data, we also implemented melt lysimeters at all four transects. However, only one of the lysimeters consistently provided melt isotope data (n=5). We took the average melt isotope concentration from each model run for the same periods as the lysimeter for comparison to the observed data. Since the initial concentration of the snow directly above the lysimeter was not known and may not match the initial isotopic value of the survey transect, we subtracted the mean of all five observations from each observation to ensure a direct comparison with melt isotope concentrations simulated in Isosnow, we applied the same method to the simulated data. MAE was then calculated for each simulation. Out of the 25 best runs, the parameters from the run with the lowest MAE for melt isotope concentrations was used for Km 99 and 104 at a 30 m resolution to model snowmelt and δ^2H inputs.

C.2 Frost surveys and mobile storage estimations.

Frost surveys were conducted four-time post melt along the same four transects for which snow surveys were conducted. Additionally, soil temperature data for five depths were used to estimate active layer thickness near the met tower. Soil moisture data from the met tower from 2020 was used to estimate Volumetric Moisture Content of the entire catchment (0.63). A simple non-linear function was used to estimate daily thaw depth across the catchment (Figure C1). The daily thaw was then multiplied by 0.63 to estimate the amount of stored water that was mobilized.

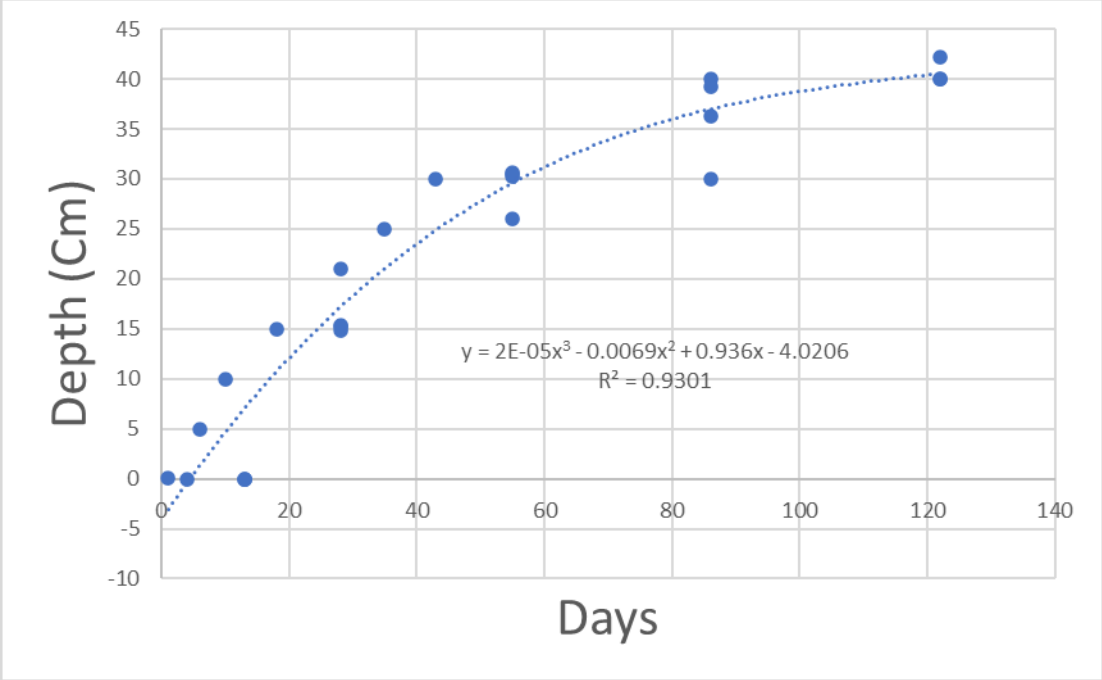

Figure C1. A simple non-linear function to estimate change in active layer thickness at Km 99 and Km 104. The observations were thaw depth estimated at one of the four transects using either the tower data or frost survey data.

C.3 Fyw Equations

Cosine and sine fitting coefficients a_p and b_p (precipitation) and, a_s and b_s (stream) were determined using IRLS (1)

$$C_p(t) = a_p \cos(2\pi f t) + b_p \sin(2\pi f t) + k_p, \qquad (1)$$

$$C_s(t) = a_s \cos(2\pi f t) + b_s \sin(2\pi f t) + k_s$$

where f is the frequency of the sine wave. The amplitudes of the sine waves (A_s and A_p) along with the phase shifts (φ_p and φ_s) were determined via equation (2).

$$A_p = \sqrt{a_p^2 + b_p^2},\ A_s = \sqrt{a_s^2 + b_s^2}, \quad (2)$$

$$\varphi_p = tan^{-1}\left(\frac{a_p}{b_p}\right), \quad \varphi_s = tan^{-1}\left(\frac{a_s}{b_s}\right)$$

The phase shift between the stream and precipitation was determined via equation 3.

$$\varphi_s - \varphi_p = tan^{-1}[(a_p b_s - a_s b_p)/(a_p a_s + b_p b_s)] \quad (3)$$

The shape parameter (α) of the gamma distribution that represents the transit time distribution was determined by iteratively solving for equation 4.

$$\varphi_s - \varphi_p = \alpha tan^{-1}\sqrt{(\frac{A_s}{A_p})^{-2/\alpha} - 1} \quad (4)$$

The scale parameter (β) for the gamma function was determined by equation 5.

$$\beta = \frac{1}{2\pi f}\sqrt{(\frac{A_s}{A_p})^{-2/\alpha} - 1} \quad (5)$$

The threshold age (τ_{yw}) was determined by equation 6 from Kirchner (2016).

$$\tau_{yw} = 0.0949 + 0.1065\alpha - 0.0126\alpha^2 \quad (6)$$

Lastly, F_{yw} was determined via equation 7 through a lower incomplete gamma function.

$$F_{yw} = \Gamma(\tau_{yw}, \alpha, \beta) \quad (7)$$